Nanomaterials for Biodiagnostic

- Nucleic Acid
  - Genetic information for identification
  - Diseases, bacterium, virus, pathogen
  - PCR with molecular fluorophore, State of the Art
  - Expansive, Non-portable, Non-multiplexing
- Proteins
  - Cancers and diseases, unusual high concentration of marker
  - ELISA (~pM) with molecular fluorophore
  - No PCR version

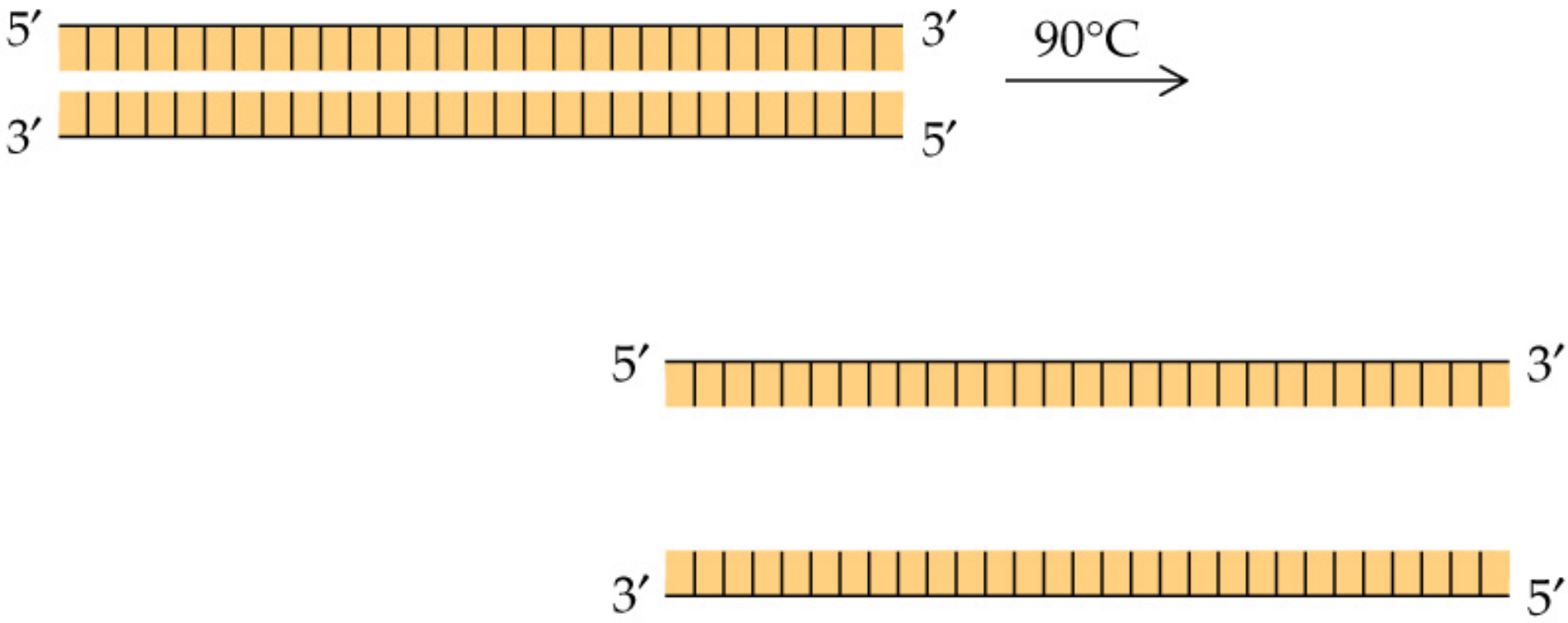

Movie http://www.youtube.com/watch?v=_YgXcJ4n-kQ

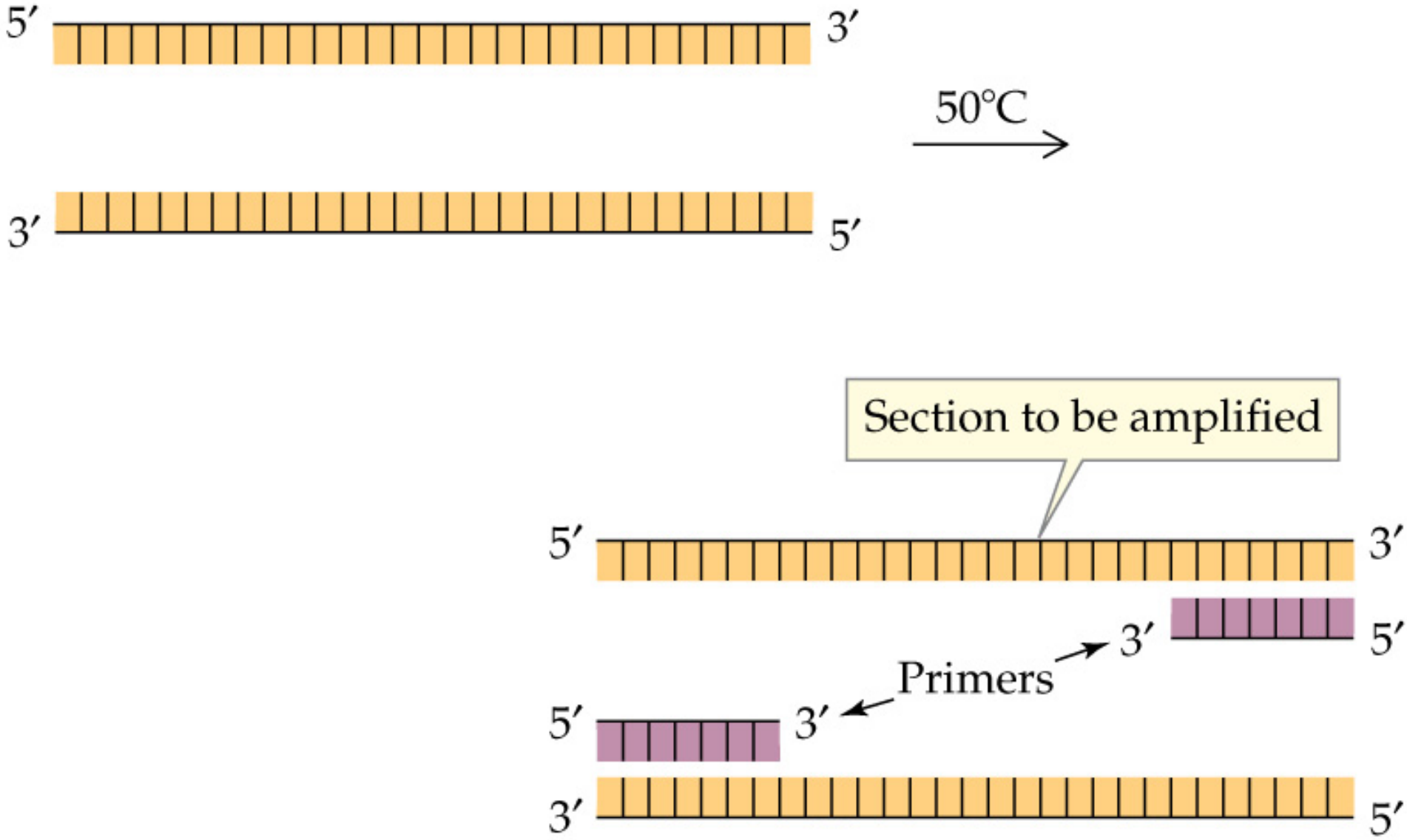
5′
3′
50°C
3′
5′
Section to be amplified
5′
3′
3′
5′
Primers
5′
3′
3′
5′

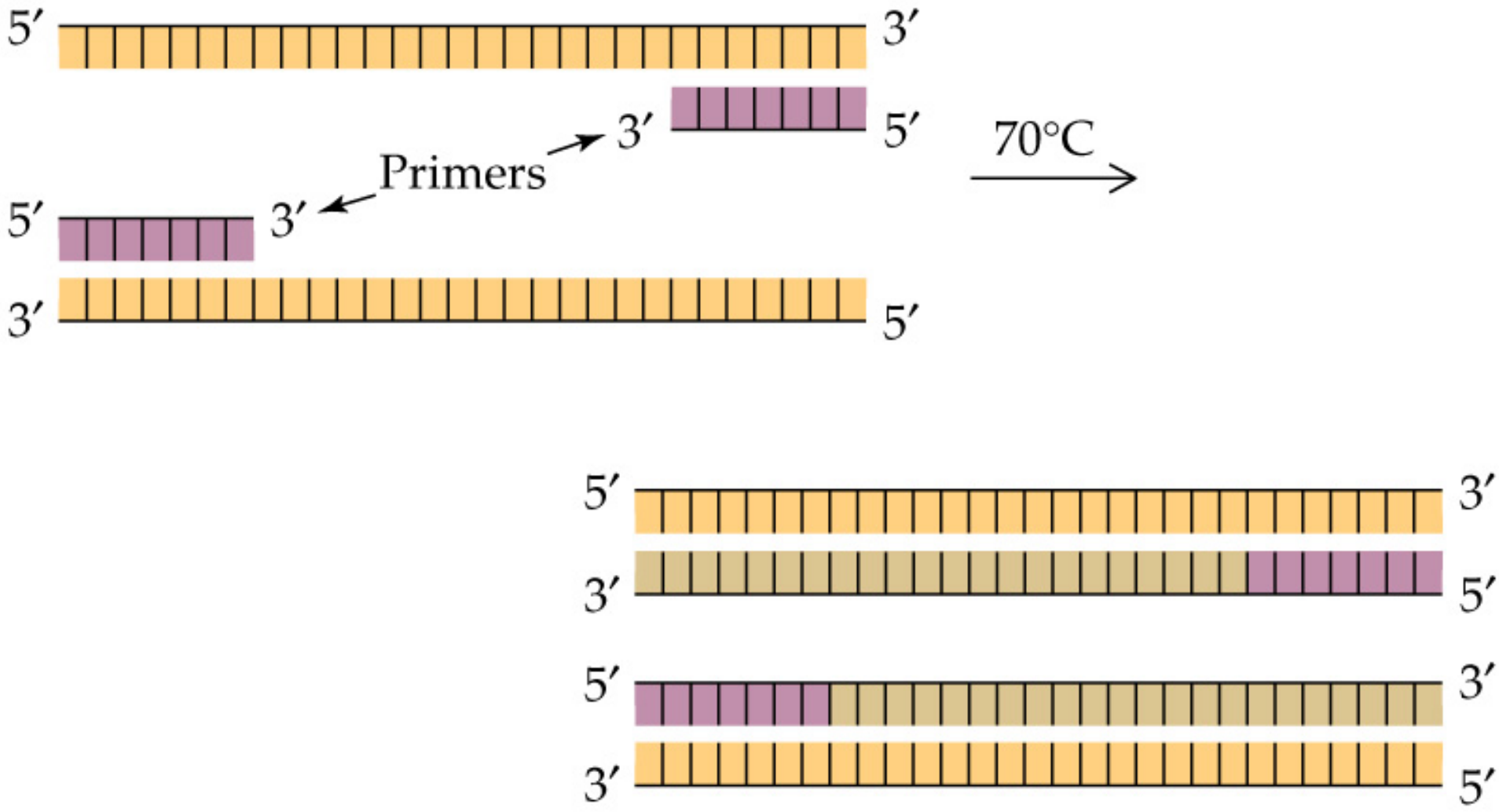
5′
3′
3′
5′
Primers
70°C
5′
3′
3′
5′
5′
3′
3′
5′
5′
3′
3′
5′

Real-time PCR

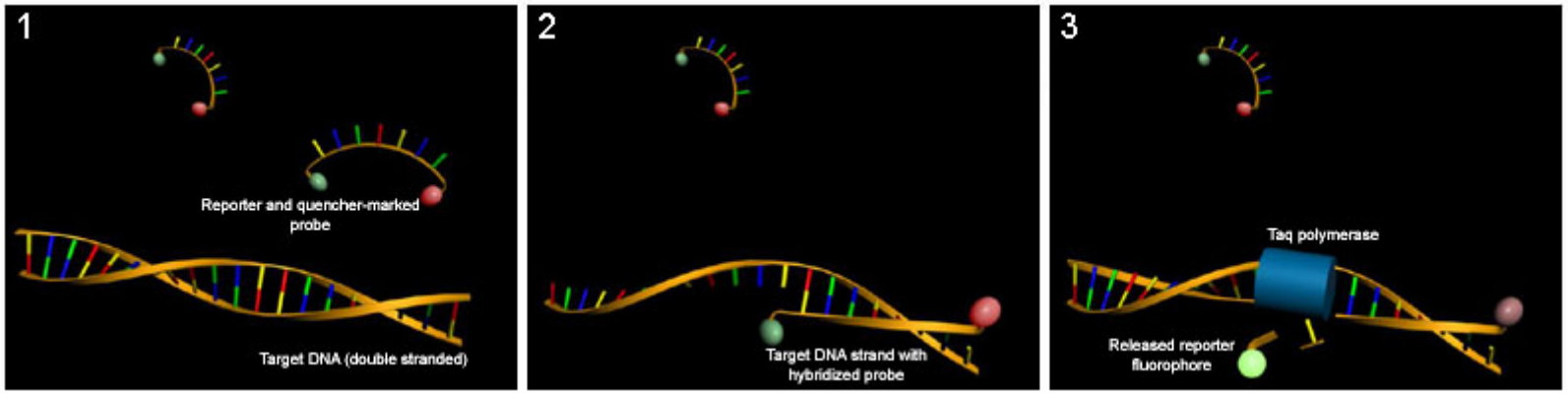

ELISA (Enzyme-Linked Immunosorbent Assay)

is a biochemical technique used mainly in immunology to detect the presence of an antibody or an antigen in a sample. It utilizes two antibodies, one of which is specific to the antigen and the other of which is coupled to an enzyme. This second antibody gives the assay its "enzyme-linked" name, and will cause a chromogenic or fluorogenic substrate to produce a signal.

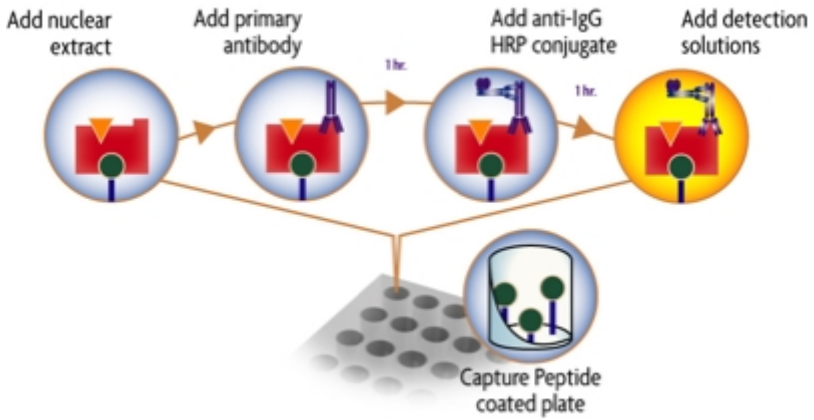

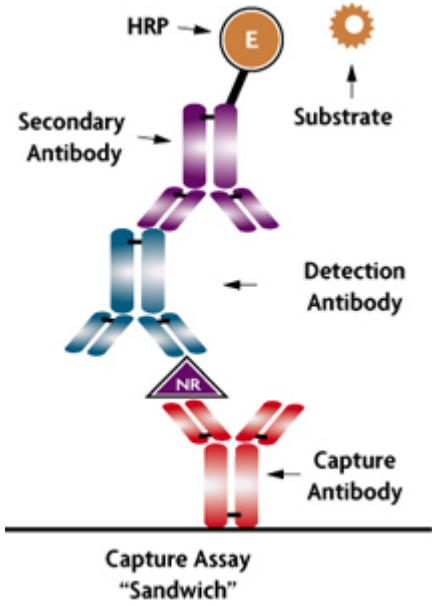

Why Nanomaterials?

- Molecular fluorophores
  - Limited spectral response
  - photostability
- Nanomaterials
  - Small size (1-100 nm)
  - Chemically tailorable physical properties
  - Unusual target binding properties
  - Structure robustness

Tailorable Physical Properties

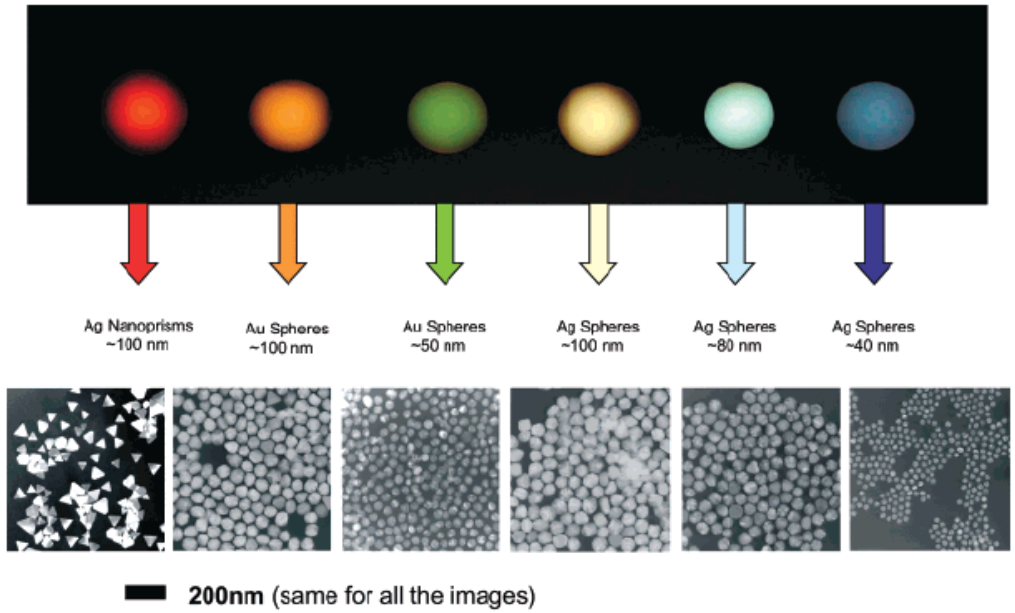

Figure 1. Sizes, shapes, and compositions of metal nanoparticles can be systematically varied to produce materials with distinct light-scattering properties.

Nanomaterial Detection

- Optical
- Electrical and electrochemical
- Magnetic
- Nanowire and Nanotubes
- Nanofabrication

Colorimetric Detection of DNA

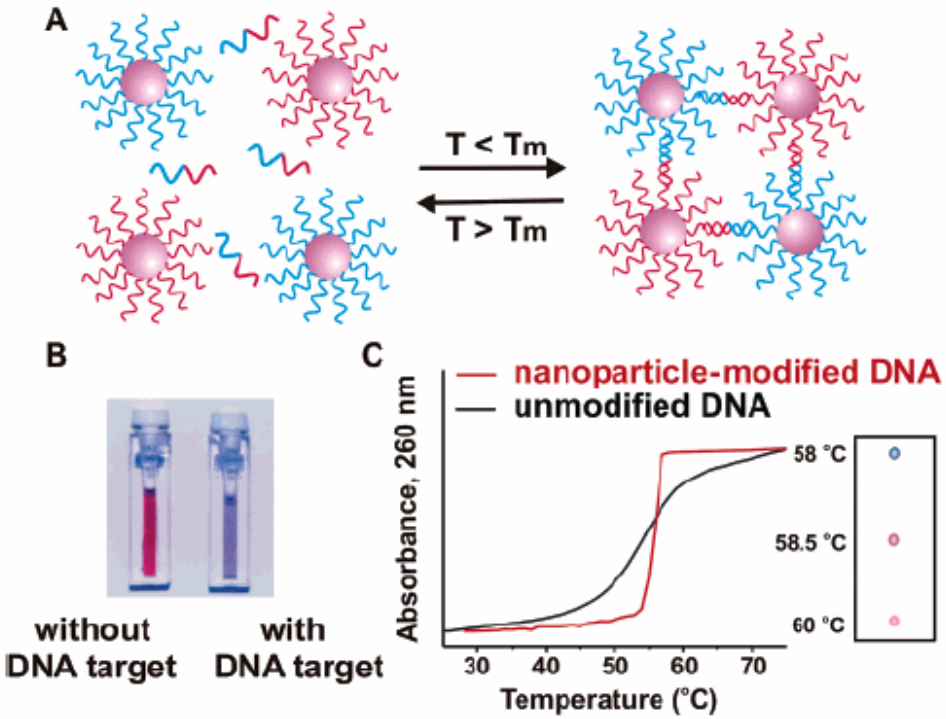

Figure 2. In the presence of complementary target DNA, oligonucleotide-functionalized gold nanoparticles will aggregate (A), resulting in a change of solution color from red to blue (B). The aggregation process can be monitored using UV−vis spectroscopy or simply by spotting the solution on a silica support (C). (Reprinted with permission from *Science* (http://www.aaas.org), ref 29. Copyright 1997 American Association for the Advancement of Science.)

A DNA-based method for rationally assembling nanoparticles into macroscopic materials

Chad A. Mirkin, Robert L. Letsinger, Robert C. Mucic & James J. Storhoff

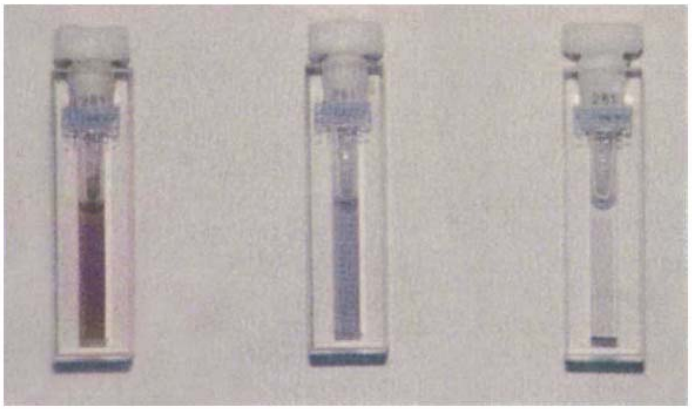

FIG. 2 Cuvettes with the Au colloids and the four DNA strands responsible for the assembly process. Left cuvette, at 80 °C with DNA-modified colloids in the unhybridized state; centre, after cooling to room temperature but before the precipitate settles; and right, after the polymeric precipitate settles to the bottom of the cuvette. Heating either of these cool solutions results in the reformation of the DNA-modified colloids in the unhybridized state (shown in the left cuvette).

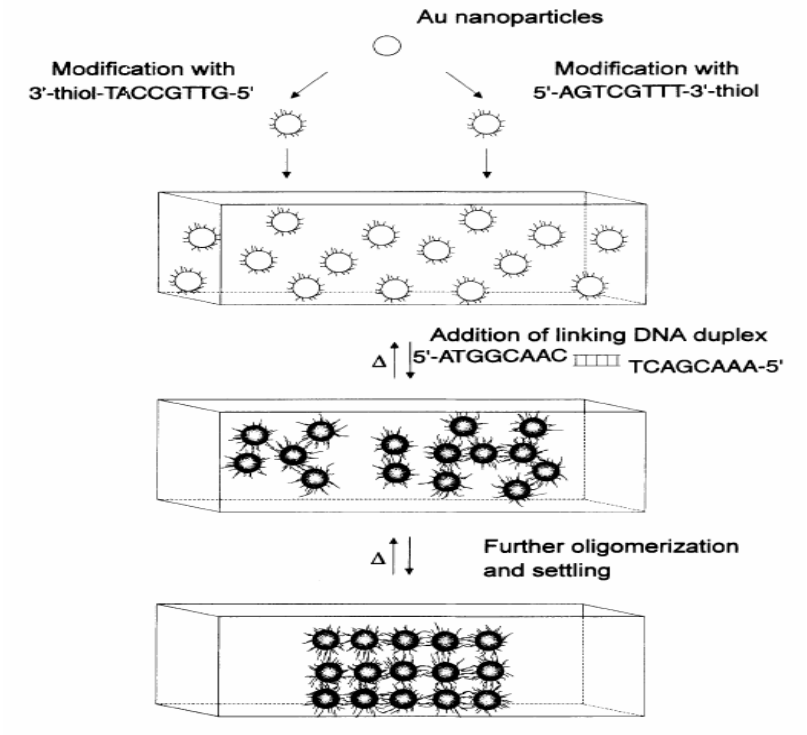

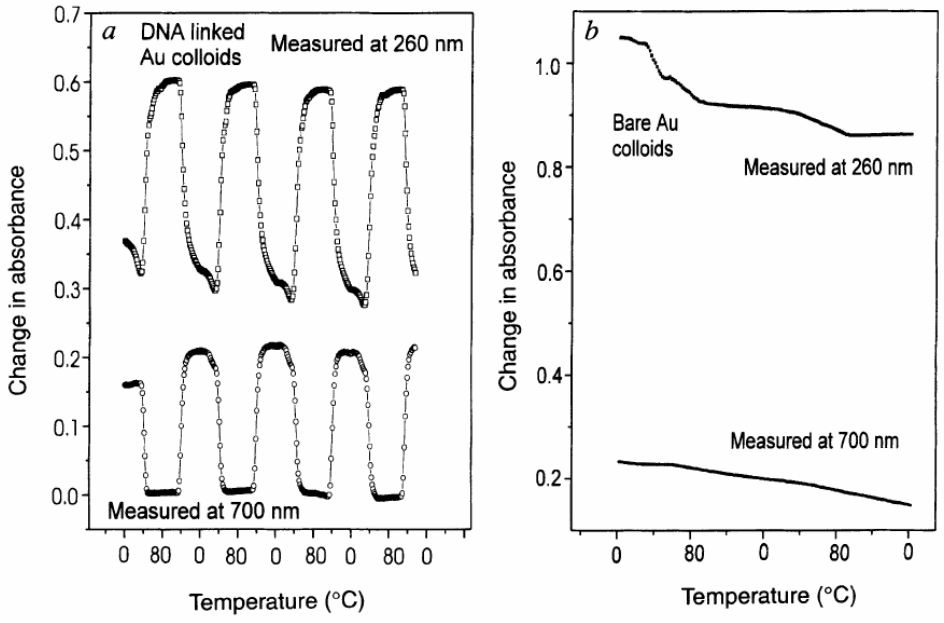

Nature, 1996, 382, 607

Selective Colorimetric Detection of Polynucleotides Based on the Distance-Dependent Optical Properties of Gold Nanoparticles

Robert Elghanian, James J. Storhoff, Robert C. Mucic,
Robert L. Letsinger,* Chad A. Mirkin*

SCIENCE • VOL. 277 • 22 AUGUST 1997

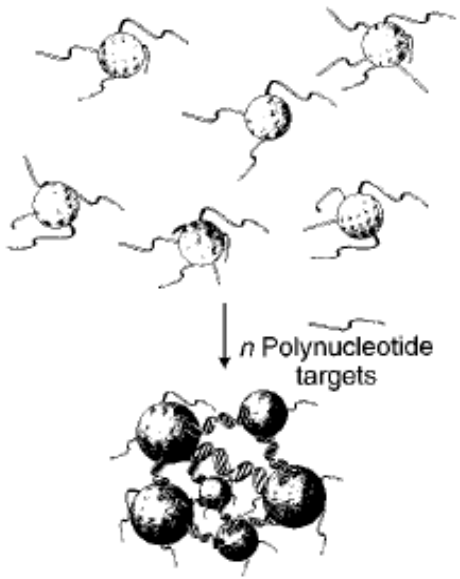

Fig. 1. Schematic representation of the concept for generating aggregates signaling hybridization of nanoparticle-oligonucleotide conjugates with oligonucleotide target molecules. The nanoparticles and the oligonucleotide interconnects are not drawn to scale, and the number of oligomers per particle is believed to be much larger than depicted.

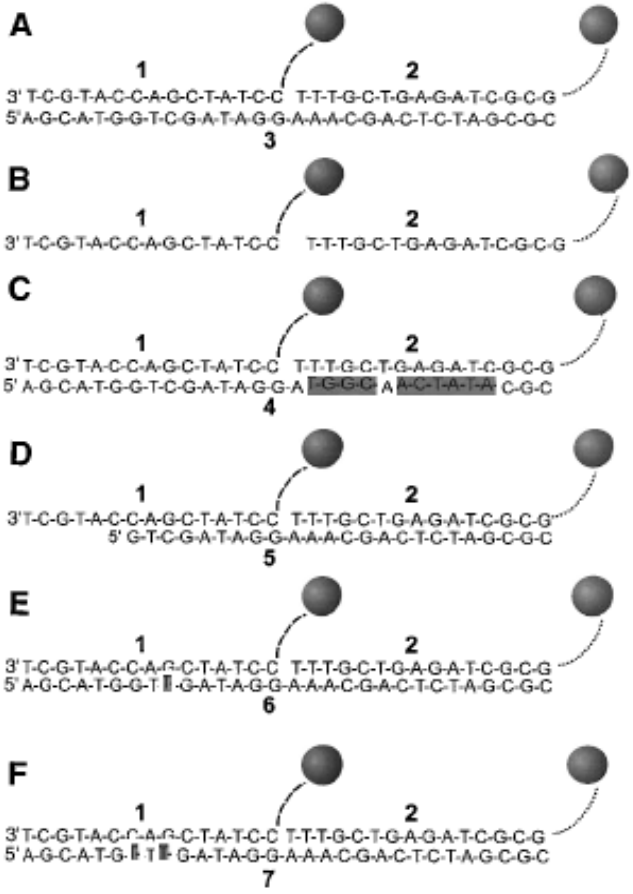

Fig. 2. Mercaptoalkyloligonucleotide-modified 13-nm Au particles and polynucleotide targets used for examining the selectivity of the nanoparticle-based colorimetric polynucleotide detection system. (**A**) Complementary target; (**B**) probes without the target; (**C**) a half-complementary target; (**D**) a 6-bp deletion; (**E**) a 1-bp mismatch; and (**F**) a 2-bp mismatch. For the sake of clarity, only two particles are shown; in reality a polymeric aggregate with many particles is formed. Dashed lines represent flexible spacer portions of the mercaptoalkyloligonucleotide strands bound to the nanoparticles; note that these spacers, because of their noncomplementary nature, do not participate in hybridization. The full sequences for the two probes, **1** and **2**, which bind to targets **3** through **7**, are

1-5′SH-$(CH_2)_6$- [CTA-ATC-CGC-ACA-G]
spacer

[CC-TAT-CGA-CCA-TGC-T]
probe

2-5′SH-$(CH_2)_6$-[ATG-GCA-ACT-ATA-C]
spacer

[GC-GCT-AGA-GTC-GTT-T]
probe

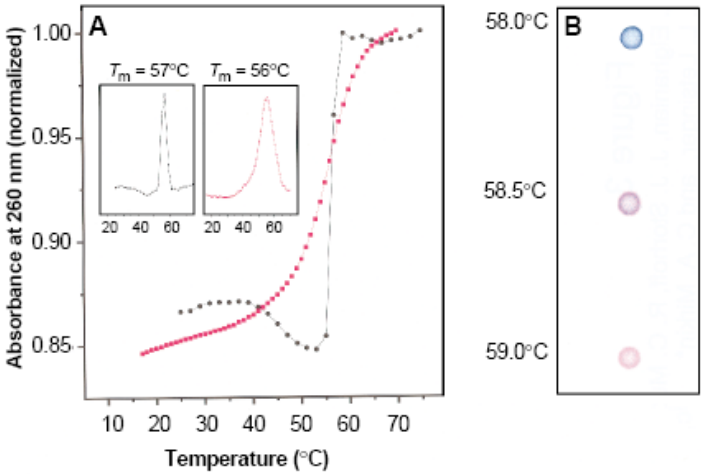

Fig. 3. (**A**) Comparison of the thermal dissociation curves for complexes of mercaptoalkyloligonucleotide-modified Au nanoparticles (black circles) and mercaptoalkyloligonucleotides without Au nanoparticles (red squares) with the complementary target, **3**, in hybridization buffer (0.1 M NaCl, 10 mM phosphate buffer, pH 7.0). For the first set (black circles), a mixture of 150 μl of each colloid conjugate and 3 μl of the target oligonucleotide in hybridization buffer (0.1 M NaCl, 10 mM phosphate, pH 7.0) was frozen at the temperature of dry ice, kept for 5 min, thawed over a period of 15 min, and diluted to 1.0 ml with buffer (final target concentration, 0.02 μM). The absorbance was measured at 1-min intervals with a temperature increase of 1°C per minute. The increase in absorption at 260 nm (A_{260}) was ~0.3 absorption units (AU). In the absence of the oligonucleotide targets, the absorbance of the nanoparticles did not increase with increasing temperature. For the second set, the mercaptoalkyloligonucleotides and complementary target (each 0.33 μM) were equilibrated at room temperature in 1 ml of buffer, and the changes in absorbance with temperature were monitored as before. The increase in A_{260} was 0.08 AU. (**Insets**) Derivative curves for each set (*15*). (**B**) Spot test showing T_c (thermal transition associated with the color change) for the Au nanoparticle probes hybridized with complementary target. A solution prepared from 150 μl of each probe and 3 μl of the target (0.06 μM final target concentration) was frozen for 5 min, allowed to thaw for 10 min, transferred to a 1-ml cuvette, and warmed at 58°C for 5 min in the thermally regulated cuvette chamber of the spectrophotometer. Samples (3 μl) were transferred to a C_{18} reverse phase plate with an Eppendorf pipette as the temperature of the solution was increased incrementally 0.5°C at 5-min intervals.

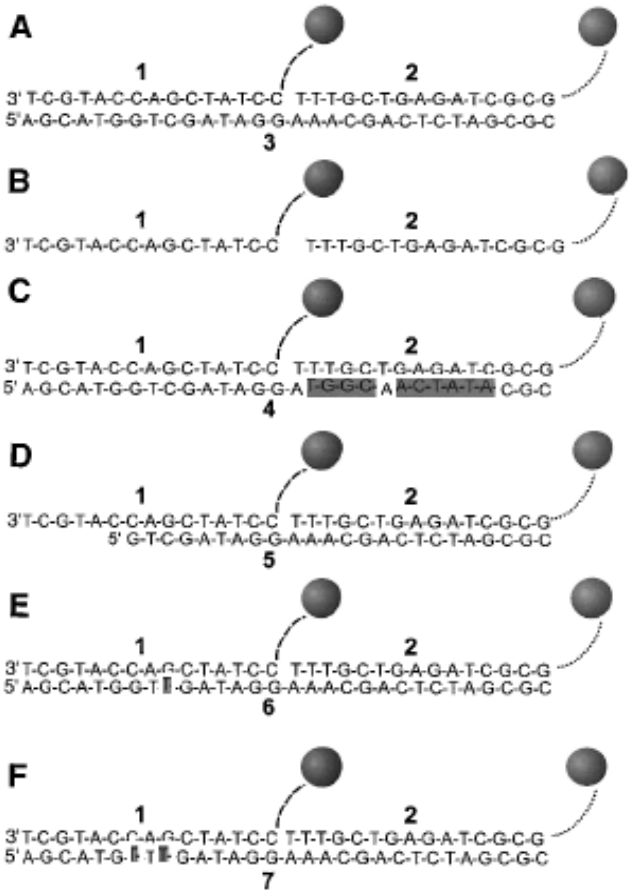

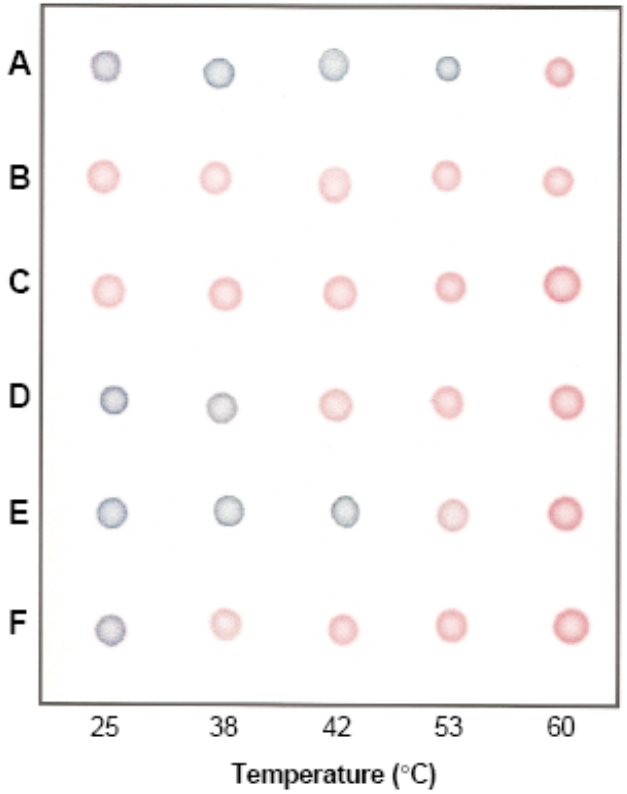

Fig. 4. Selective polynucleotide detection for the target probes shown in Fig. 2: (**A**) complementary target; (**B**) no target; (**C**) complementary to one probe; (**D**) a 6-bp deletion; (**E**) a 1-bp mismatch; and (**F**) a 2-bp mismatch. Nanoparticle aggregates were prepared in a 600-μl thin-walled Eppendorf tube by addition of 1 μl of a 6.6 μM oligonucleotide target to a mixture containing 50 μl of each probe (0.06 μM final target concentration). The mixture was frozen (5 min) in a bath of dry ice and isopropyl alcohol and allowed to warm to room temperature. Samples were then transferred to a temperature-controlled water bath, and 3-μl aliquots were removed at the indicated temperatures and spotted on a C_{18} reverse phase plate.

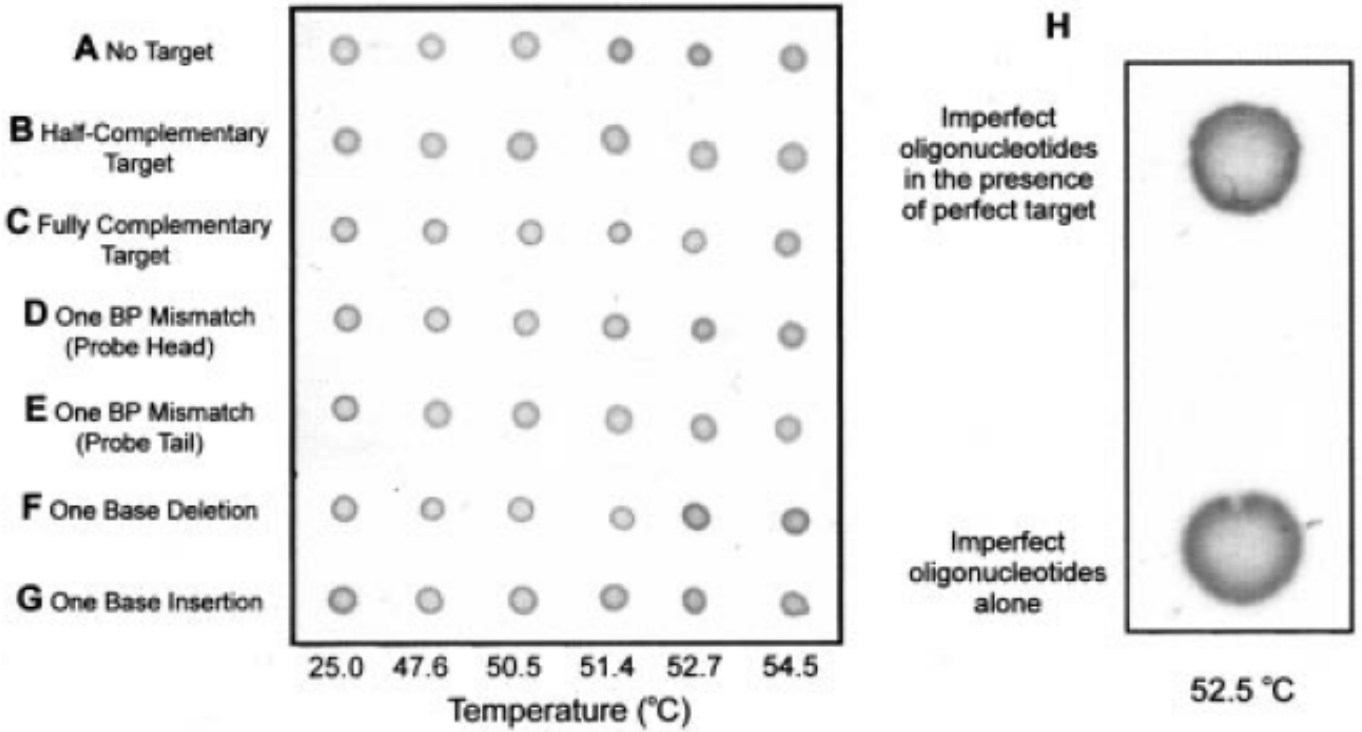

Figure 5. (A−G) The spot method for polynucleotide detection which demonstrates the selectivity of the Au nanoparticle based detection system toward single base imperfections. The probes and corresponding polynucleotide targets are listed in Figure 2. (H) Spot test demonstrating the detection and differentiation by color of a polynucleotide target in the presence of polynucleotides with single base imperfections.

1nM => 50pM

Rapid Aggregation of Gold Nanoparticles Induced by Non-Cross-Linking DNA Hybridization

Kae Sato, Kazuo Hosokawa, and Mizuo Maeda*

8102 ■ J. AM. CHEM. SOC. 2003, *125*, 8102−8103

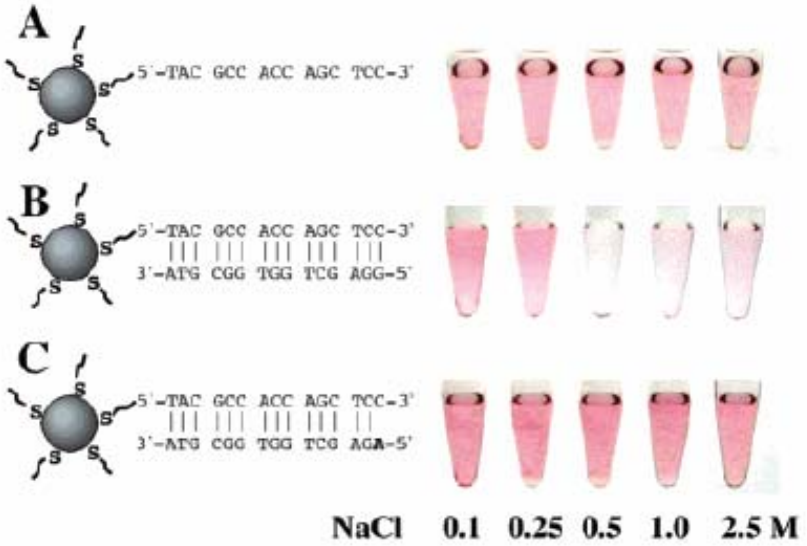

Figure 1. Aggregation behaviors of the DNA-gold nanoparticles at various NaCl concentrations at room temperature: (A) without a target DNA, (B) with the complementary target, and (C) with a target containing a single-base mismatch at its 5′ terminus. The final concentrations of the particle, the probe DNA, and the targets were 2.3, 500, and 500 nM, respectively.

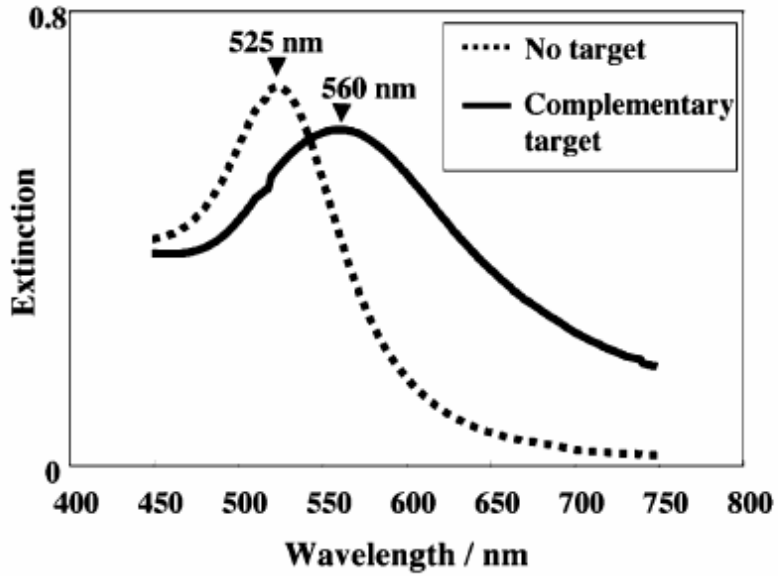

Figure 2. Visible spectra corresponding to Figure 1A (dotted line, no target) and 1B (solid line, complementary target) at 0.5 M NaCl.

60-500 nM

J. Am. Chem. Soc. **2000,** *122,* 9071−9077

Colloidal Au-Enhanced Surface Plasmon Resonance for Ultrasensitive Detection of DNA Hybridization

Lin He, Michael D. Musick, Sheila R. Nicewarner, Frank G. Salinas, Stephen J. Benkovic, Michael J. Natan, and Christine D. Keating*

Scheme 1. SPR Surface Assembly

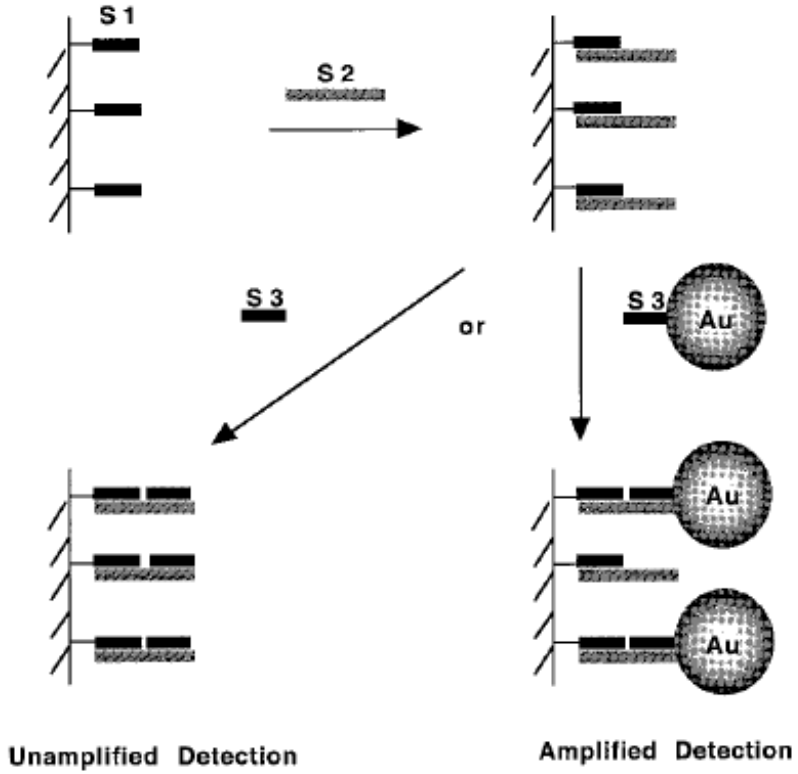

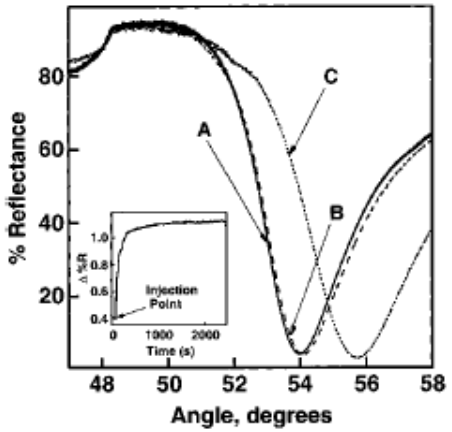

Figure 1. SPR curves of surfaces prepared in sequential steps as illustrated in Scheme 1: a MHA-coated Au film modified with a 12-mer oligonucleotide S1(A), after hybridization with its complementary 24-mer target S2 (B), and followed by introduction of S3:Au conjugate (C) to the surface. Inset: surface plasmon reflectance changes at 53.2° for the oligonucleotide-coated Au film measured during a 60-min exposure to S3:Au conjugates.

Scheme 2. SPR Surface Assembly in the Digestion Experiment

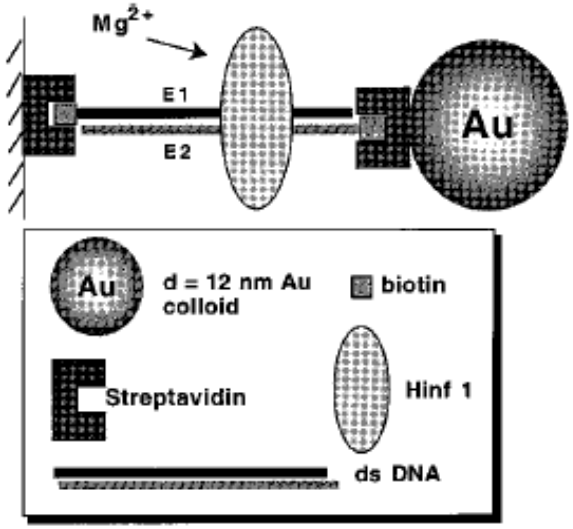

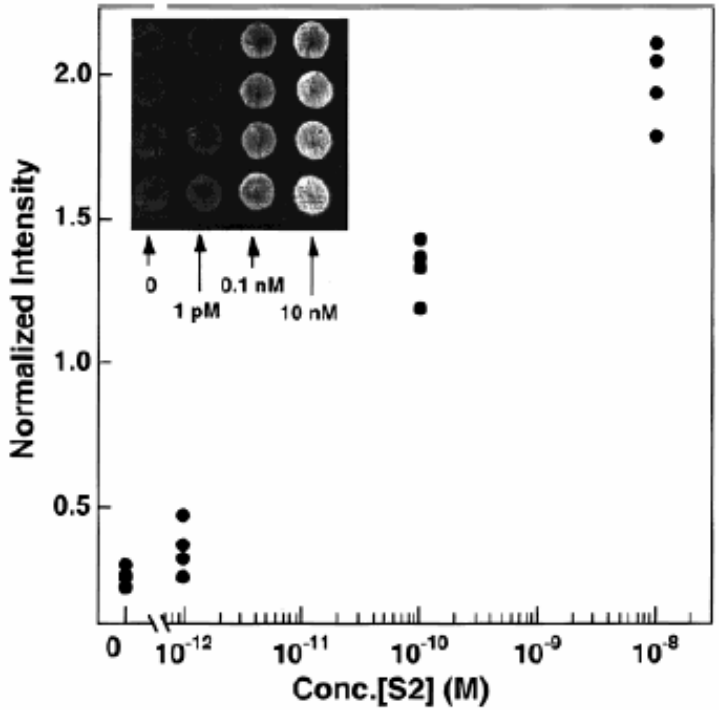

Figure 5. Plot of normalized intensity of SPR reflectance as a function of logarithmic concentration of the analyte 24-mer oligo (S2). Each spot represents one data point at the corresponding concentration. CCD parameters: exposure time = 0.3 s, 16 bit resolution, spot size = 4.5 mm in diameter. Inset: a 2-D SPR image of a Au surface derivatized with 20 μL of buffer blank, 1 pM, 0.1 nM, and 10 nM S2 oligos (from left to right, respectively).

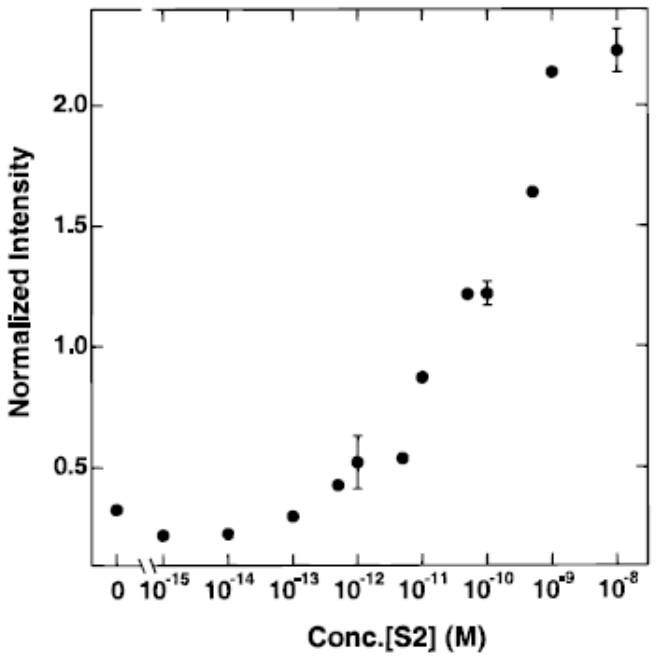

Figure 7. Plot of normalized intensity of SPR reflectance as a function of logarithmic concentration of the analyte 24-mer oligo (S2) from the image shown in Figure 6. The error bars are standard deviations from the data in Figure 5.

Table 1. Comparison of Sensitivity for Au−Amplified SPR in DNA Analysis with Other Techniques

detection method	detection limit of target DNA	refs
radiolabeling	100 fg	71
fluorescence	1.2×10^7 probes/cm^2	36
unamplified scanning SPR	100 fg/100 μm^2 for 10-mer oligos, 150 nM ~120 bp DNA	33, 35
unamplified imaging SPR	10 nM 16-mer oligos	63
Au-amplified scanning SPR	lower than 10 pM 24-mer oligos[a]	this work
Au-amplified imaging SPR	10 pM 24-mer oligos, ≤12 pg/cm^2 (≤8×10^8 oligonucleotides/cm^2)[b]	this work

[a] The spots on SPR imaging surface can be detected by scanning SPR with ease, which demonstrated a lower detection limit can be achieved with the scanning instrument. Considering an instrumental angle resolution limit of 0.005°, a theoretical detection limit of 2×10^7 particles/cm^2 can be realized.[21] [b] The oligonucleotide surface coverage reported for these experiments is an upper limit, determined by assuming 100% of the molecules in solution hybridized to the surface.

A Gold Nanoparticle Based Approach for Screening Triplex DNA Binders

Min Su Han, Abigail K. R. Lytton-Jean, and Chad A. Mirkin*

4954 ■ J. AM. CHEM. SOC. 2006, *128*, 4954−4955

Scheme 1. Representation of Structure and Color Change of Nanoassembly in the Presence of Triplex Binder at Room Temperature

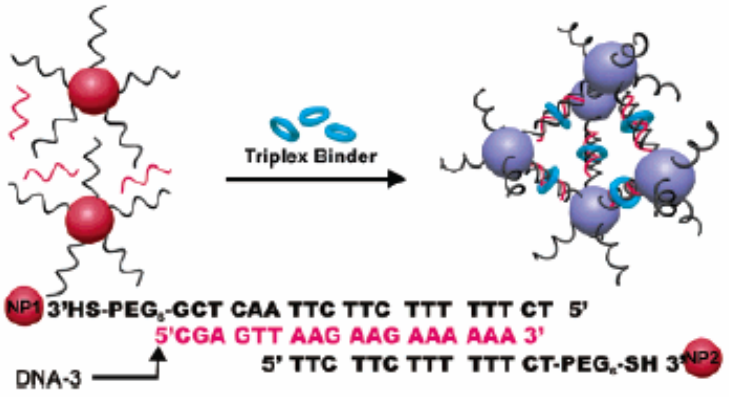

Figure 3. The color change of nanoassembly (NP-1, NP-2, and DNA-3) in the absence and presence of DNA binders at room temperature.

Sequence specific

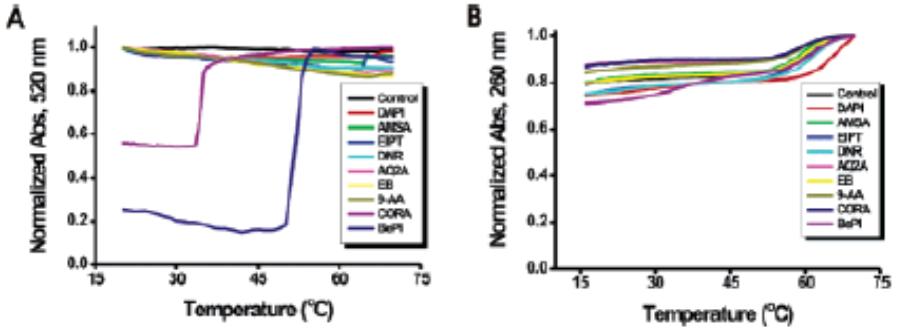

Figure 2. Melting curves of (A) NP-1, NP-2, and DNA-3 assemblies in the presence of DNA binders, (B) DNA-1, DNA-2, and DNA-3 (no nanoparticles) in the presence of DNA binders.

Self-Assembled Nanoparticle Probes for Recognition and Detection of Biomolecules

Dustin J. Maxwell, Jason R. Taylor, and Shuming Nie*,†

9606 ■ J. AM. CHEM. SOC. 2002, *124*, 9606−9612

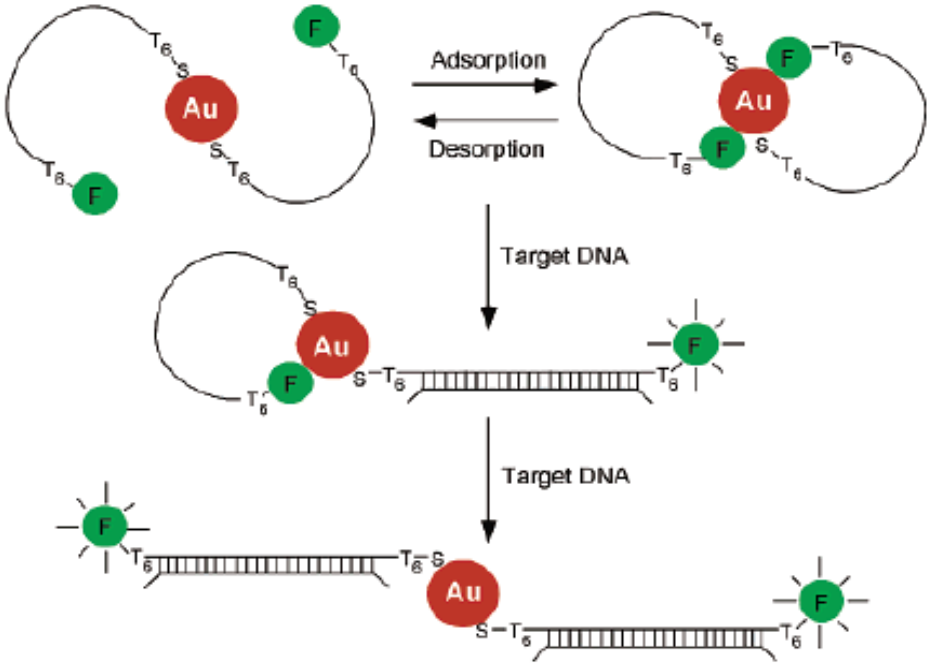

Figure 1. Nanoparticle-based probes and their operating principles. Two oligonucleotide molecules (oligos) are shown to self-assemble into a constrained conformation on each gold particle (2.5 nm diameter). A T_6 spacer (six thymines) is inserted at both the 3′- and 5′-ends to reduce steric hindrance. Single-stranded DNA is represented by a single line and double-stranded DNA by a cross-linked double line. In the assembled (closed) state, the fluorophore is quenched by the nanoparticle. Upon target binding, the constrained conformation opens, the fluorophore leaves the surface because of the structural rigidity of the hybridized DNA (double-stranded), and fluorescence is restored. In the open state, the fluorophore is separated from the particle surface by about 10 nm. See text for detailed explanation. Au, gold particle; F, fluorophore; S, sulfur atom.

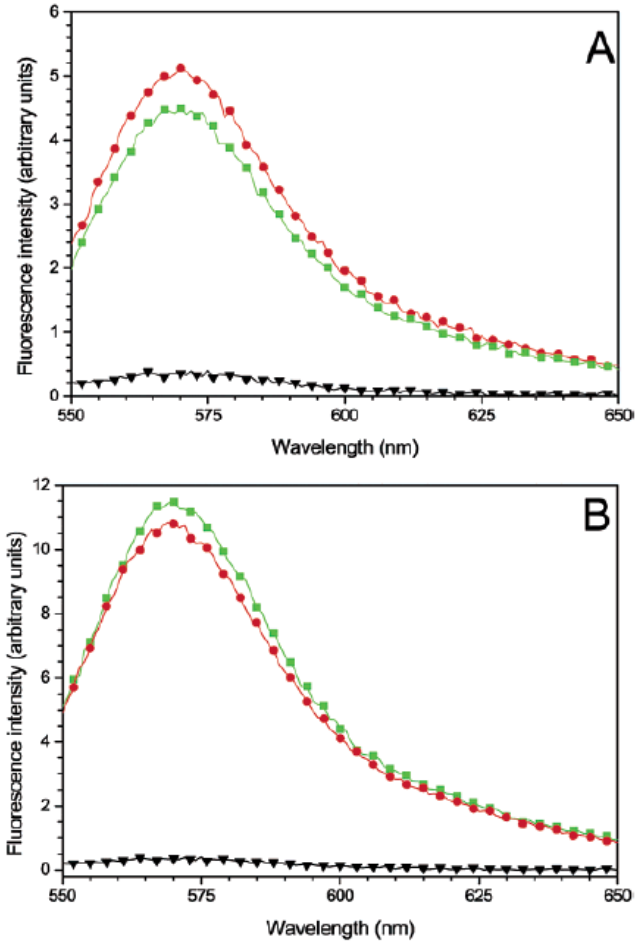

Figure 5. Fluorescence responses and the lack of sequence recognition abilities observed for nonthiolated nanoparticle probes. (A) Fluorescence spectra of nonthiolated probes generated by a complementary target (red curve), a noncomplementary target (green curve), and no target (black curve). These probes are considered nonfunctional because they do not recognize specific DNA sequences. (B) Fluorescence signals obtained from the supernatant solution when the probes were treated with a complementary target (red curve) or a noncomplementary target (green curve). The result revealed that the oligos were released into solution by nonspecific adsorption of the target on the particle surface. With a thiol group, this release was not observed (little or no signal in solution, black curve in B). The nonfunctional probes were prepared in the same way as the functional probes, except that the 3′-end thiol group was deleted. The intensity differences for the red and green curves were within experimental errors and had no particular significance.

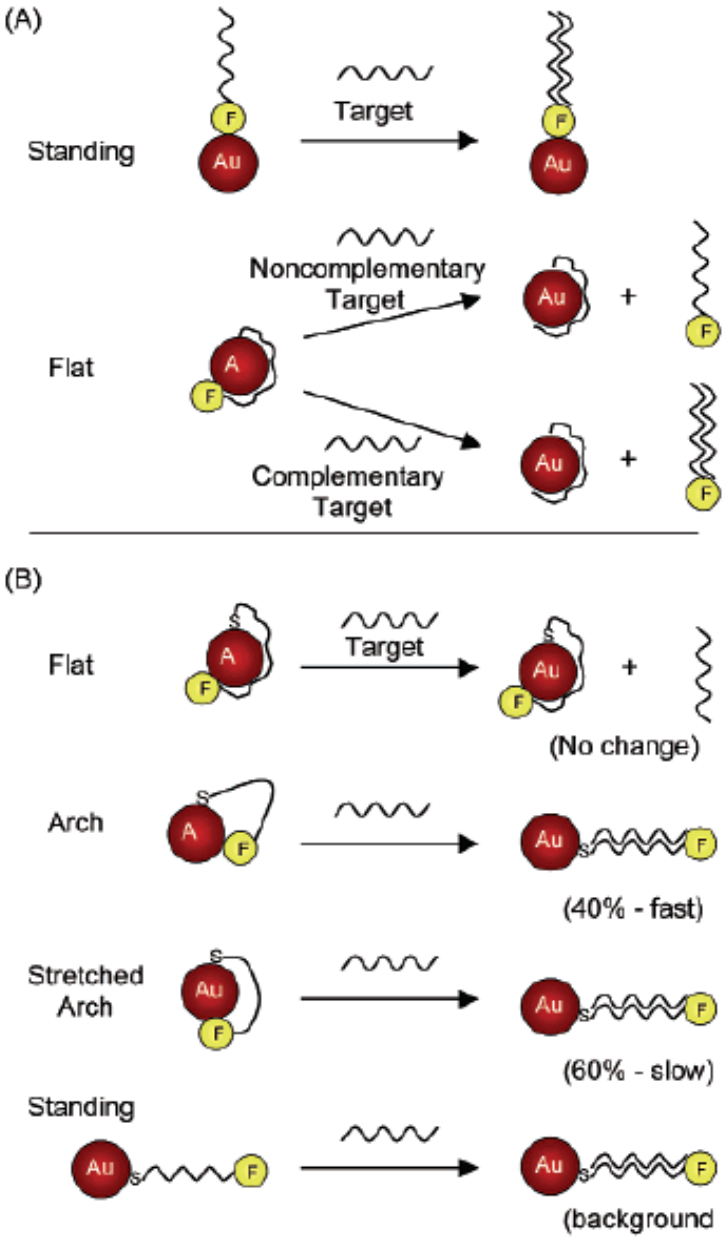

Figure 6. Schematic illustration of possible configurations for (a) nonthiolated and (b) thiolated oligonucleotides adsorbed on colloidal gold nanocrystals. Detailed discussion in text.

Silver Amplification

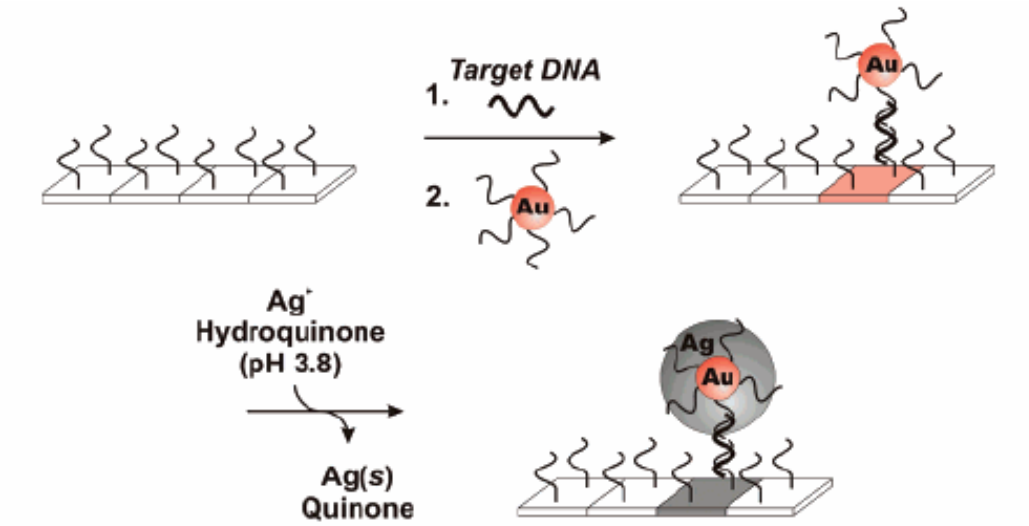

Figure 4. Scanometric DNA assay. In this assay a surface-bound capture oligonucleotide binds one-half of the target of interest, and an oligonucleotide-functionalized gold nanoparticle probe binds to the other half. Catalytic reduction of silver onto the capture/target/probe sandwich results in a signal that can be detected scanometrically. (Reprinted with permission from *Science* (http://www.aaas.org), ref 66. Copyright 2000 American Association for the Advancement of Science.)

Catalytic reduction of Ag on Au

Scanometric DNA Array Detection with Nanoparticle Probes

SCIENCE VOL 289 8 SEPTEMBER 2000

T. Andrew Taton,[1,2] Chad A. Mirkin,[1,2]* Robert L. Letsinger[1]*

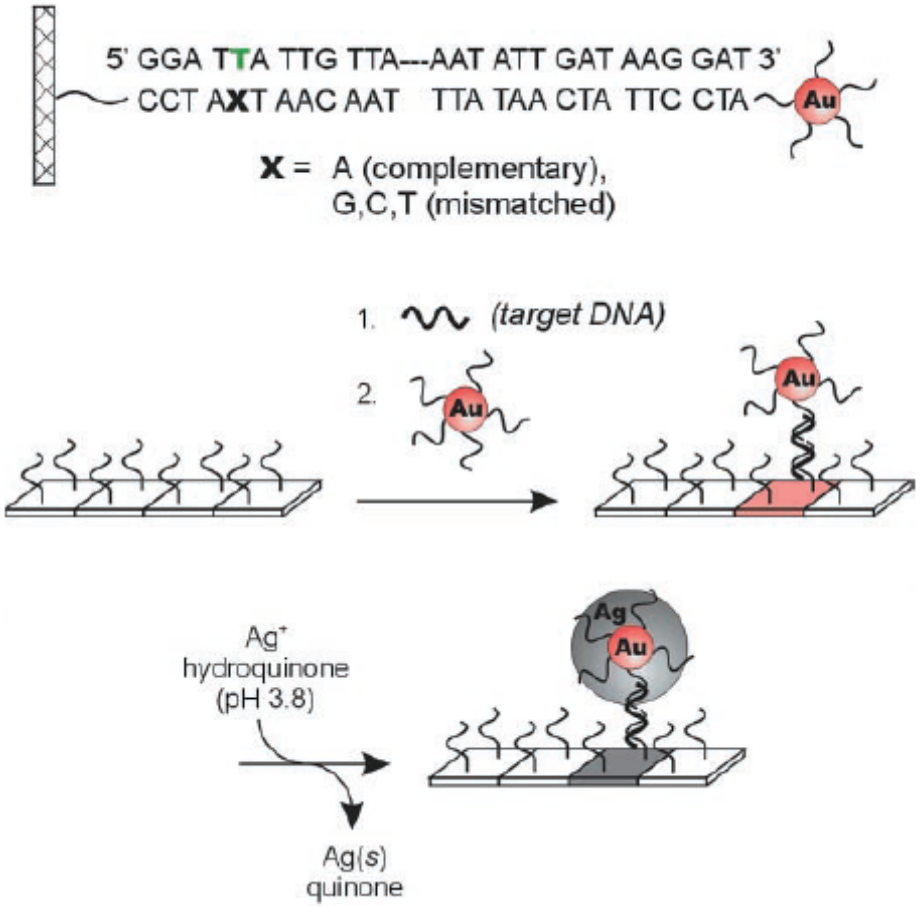

50 fM => 0.2 fM

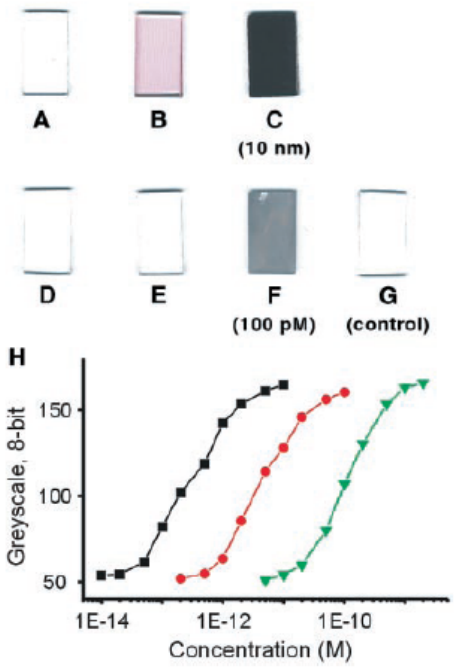

Fig. 1. Images of 7 mm by 13 mm, oligonucleotide-functionalized, float glass slides, obtained with a flatbed scanner. (**A**) Slide before hybridization of target and nanoparticle probe. (**B**) A slide identical to (A) after hybridization with oligonucleotide target (10 nM) and then nanoparticle probes (5 nM in particles). The pink color derives from the Au nanoparticle probes. (**C**) A slide identical to (B) after exposure to silver amplification solution for 5 min. (**D**) Slide before hybridization of target and nanoparticle probe. (**E**) A slide identical to (D) after hybridization with target (100 pM) and then nanoparticle probe (5 nM). The extinction of the submonolayer of nanoparticles is too low to be observed visually or with a flatbed scanner. (**F**) A slide identical to (E) after exposure to silver amplification solution for 5 min. Slide (F) is lighter than slide (C), indicating a lower concentration of target. (**G**) A control slide exposed to 5 nM nanoparticle probe and then exposed to silver amplification solution for 5 min. No darkening of the slide is observed. (**H**) Graph of 8-bit gray scale values as a function of target concentration. The gray scale values were taken from flatbed scanner images of oligonucleotide-functionalized glass surfaces that had been exposed to varying concentrations of oligonucleotide target, labeled with 5 nM oligonucleotide probe and immersed in silver amplification solution. For any given amplification time, the grayscale range is limited by surface saturation at high grayscale values and the sensitivity of the scanner at low values. Therefore, the dynamic range of this system can be adjusted by means of hybridization and amplification conditions (that is, lower target concentrations require longer amplification periods). Squares: 18-base capture-target overlap (*5*), 8× PBS hybridization buffer [1.2 M NaCl and 10 mM NaH_2PO_4/Na_2HPO_4 buffer (pH 7)], 15 min amplification time. Circles: 12-base capture-target overlap, 8× PBS hybridization buffer, 10 min amplification time. Triangles: 12-base capture-target overlap, 2× PBS hybridization buffer [0.3 M NaCl, 10 mM NaH_2PO_4/Na_2HPO_4 buffer (pH 7)], 5 min amplification time. The lowest target concentration that can be effectively distinguished from the background baseline is 50 fM.

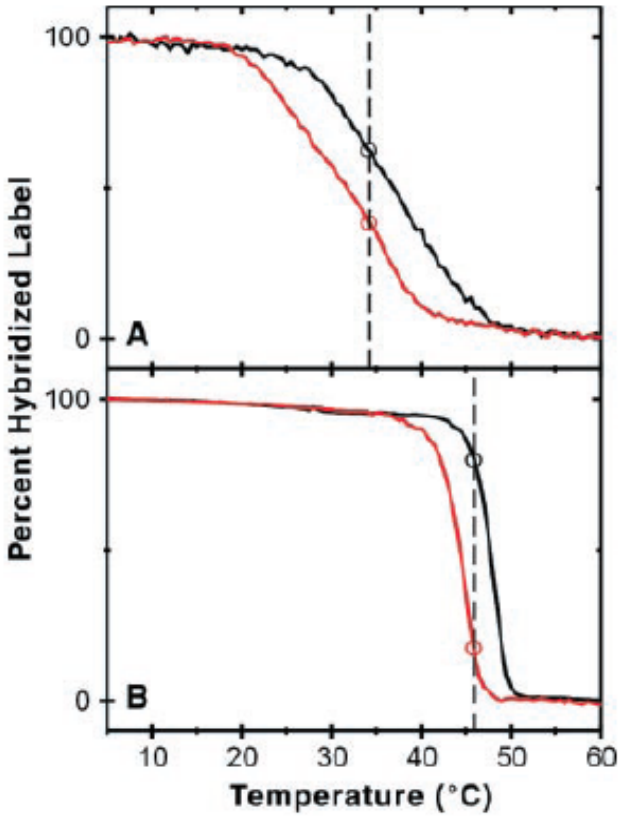

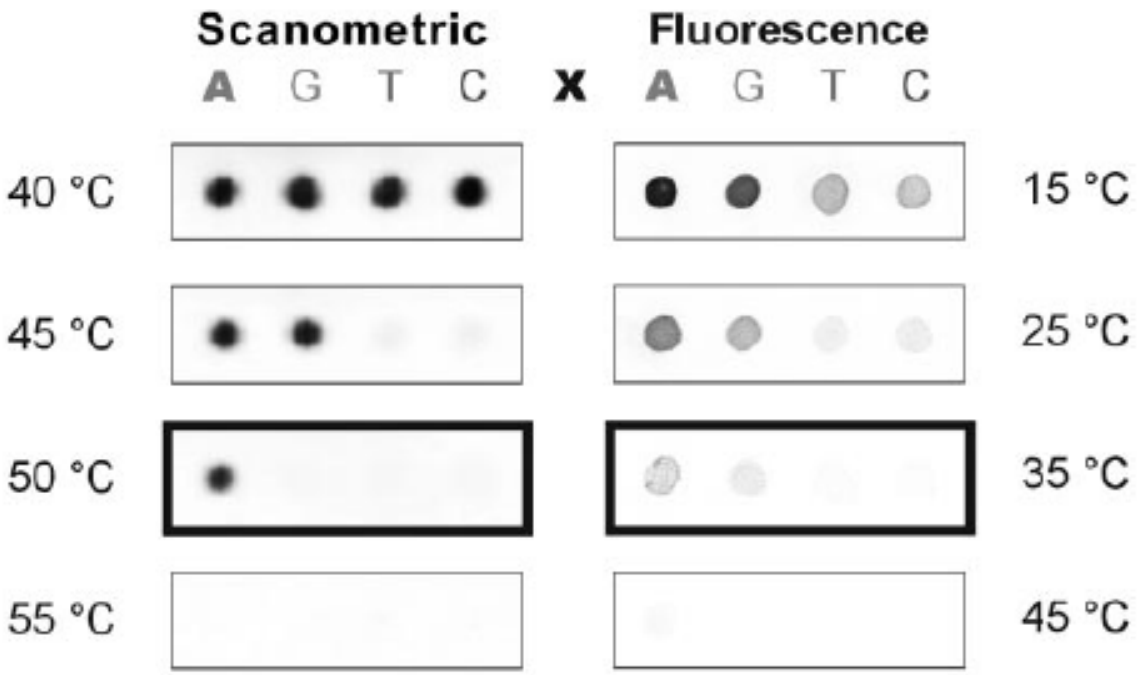

Fig. 3. (**Left**) Nanoparticle-labeled arrays developed at different stringency temperatures. Model oligonucleotide arrays (with the capture sequences shown in Scheme 1) were treated with oligonucleotide target and nanoparticle probes, followed by a 2-min buffer wash at the temperatures shown and subsequent silver amplification (*13*). Images were obtained with an Epson Expression 636 (600 dots per inch) flatbed scanner (Epson America, Long Beach, California). The darkened border indicates the array that showed optimum selectivity for the perfectly complementary target; at this temperature, the ratio of background-subtracted, 8-bit gray scale values for elements A:G:T:C, obtained from histogram averages in Adobe Photoshop (Adobe Systems, San Jose, California), is 96:9:7:6. (**Right**) Fluorophore-labeled arrays washed at different stringency temperatures. Model oligonucleotide arrays identical to those shown at left were treated with oligonucleotide target and Cy3-labeled oligonucleotide probes, followed by a 2-min buffer wash at the temperatures shown. Images were obtained with a ScanArray Confocal Microarray Scanner (GSI Lumonics, Billerica, Massachusetts). The darkened border indicates the array that showed the highest selectivity for the perfectly complementary target, as calculated by the QuantArray Analysis software package (GSI Lumonics); at this temperature, the intensity ratio (in percent, with the intensity of the X = A element at 15°C set to 100%) for elements A:G:T:C is 18:7:1:1.

Nanoparticles with Raman Spectroscopic Fingerprints for DNA and RNA Detection

YunWei Charles Cao, Rongchao Jin, Chad A. Mirkin*

30 AUGUST 2002 VOL 297 SCIENCE

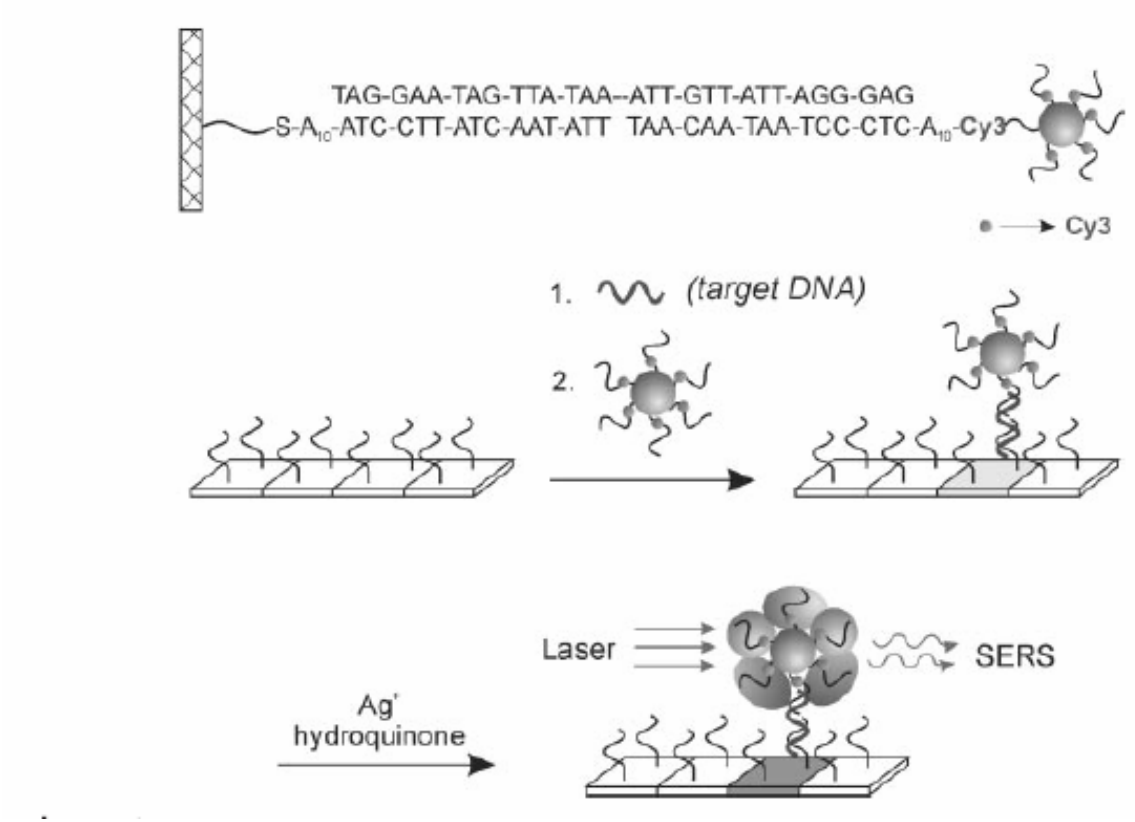

1 fM

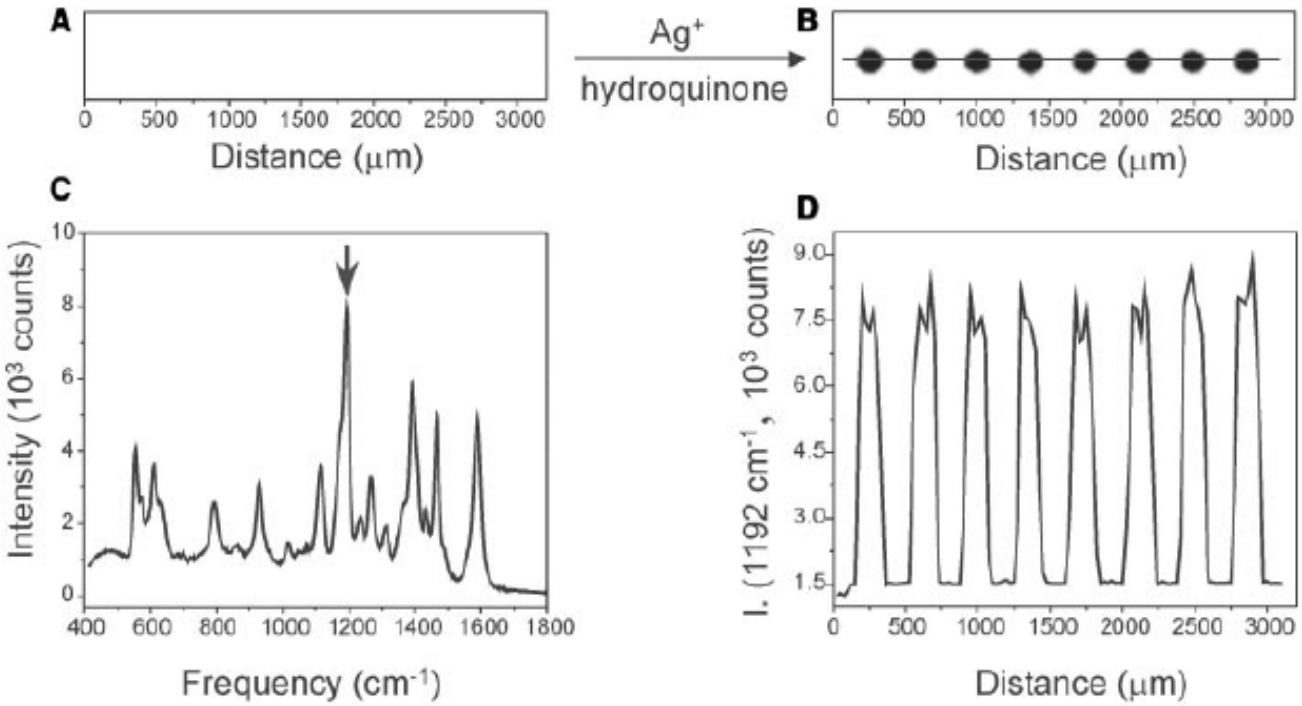

Fig. 1. Flatbed scanner images of microarrays hybridized with nanoparticles (**A**) before and (**B**) after Ag enhancing. (**C**) A typical Raman spectrum acquired from one of the Ag spots. (**D**) A profile of Raman intensity at 1192 cm^{-1} as a function of position on the chip; the laser beam from the Raman instrument is moved over the chip from left to right as defined by the line in (B).

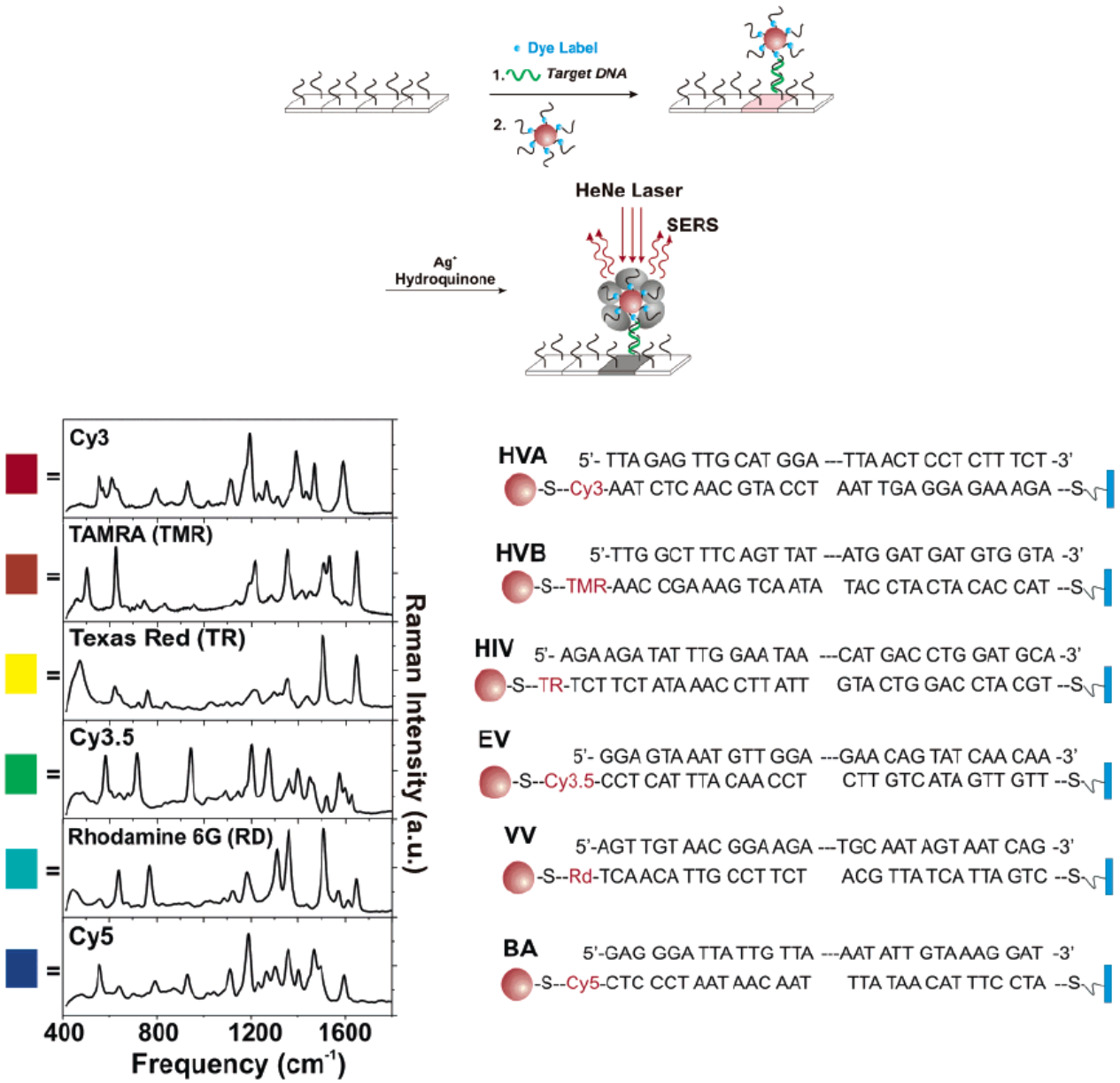

Figure 5. If Raman dyes (blue spheres) are attached to the labeling probe in the scanometric assay, the targets can be encoded and detected via the Raman signal of their labels. (Reprinted with permission from *Science* (http://www.aaas.org), ref 68. Copyright 2002 American Association for the Advancement of Science.)

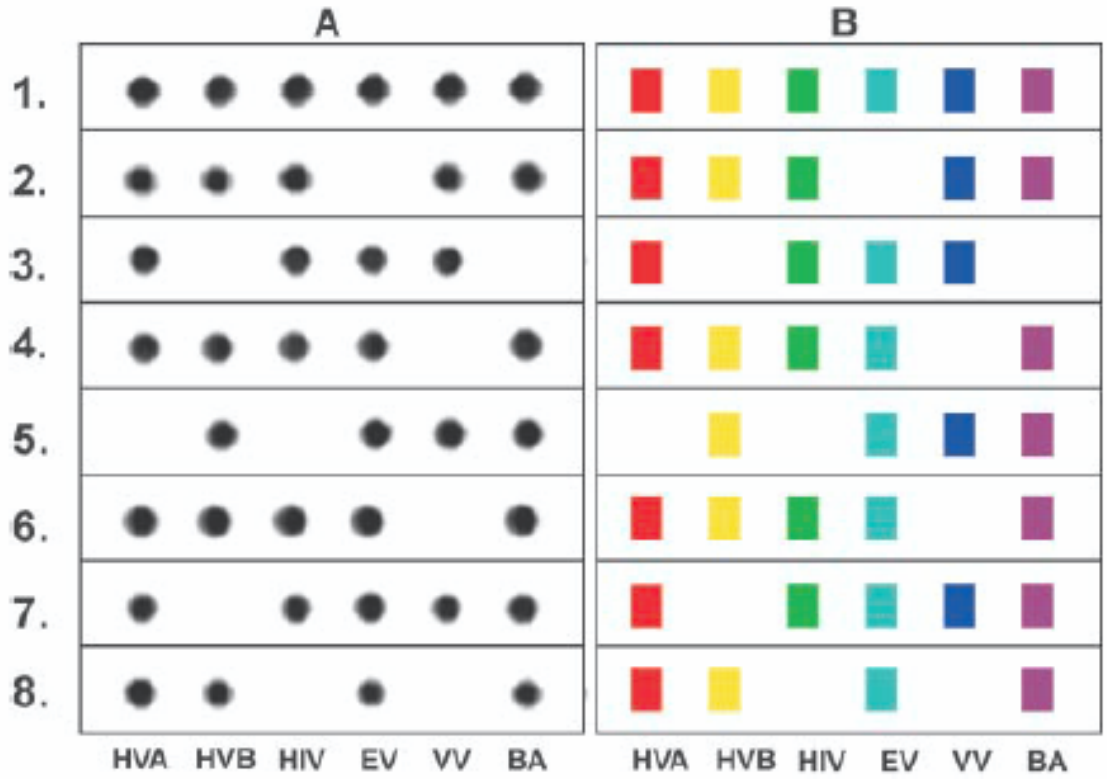

Fig. 3. (**A**) Flatbed scanner images of Ag-enhanced microarrays and (**B**) corresponding Raman spectra. The colored boxes correlate with the color-coded Raman spectra in Fig. 2. No false-positives or false-negatives were observed.

Bio-Bar-Code-Based DNA Detection with PCR-like Sensitivity

Jwa-Min Nam, Savka I. Stoeva, and Chad A. Mirkin*

J. AM. CHEM. SOC. 2004, *126*, 5932−5933

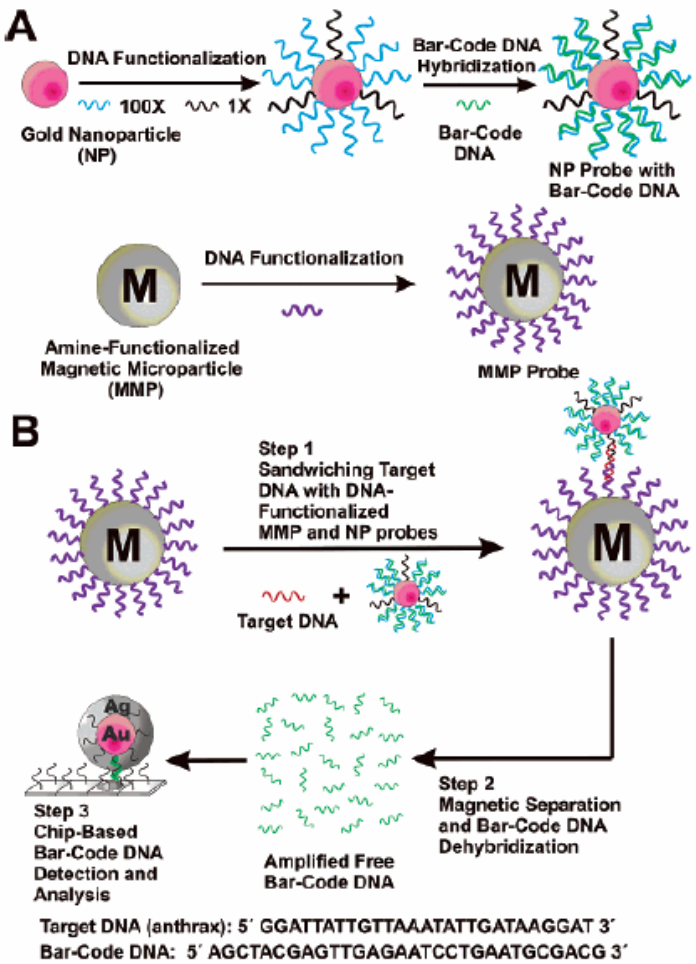

Figure 1. The DNA-BCA assay. (A) Nanoparticle and magnetic microparticle probe preparation. (B) Nanoparticle-based PCR-less DNA amplification scheme.

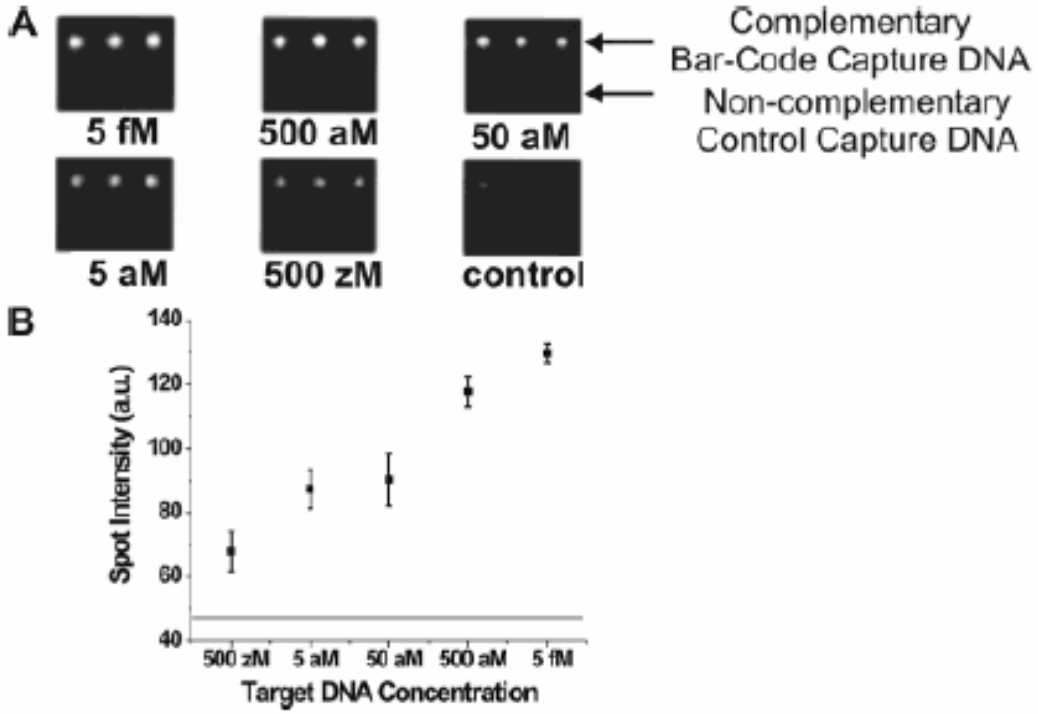

Figure 2. Amplified anthrax bar-code DNA detection with the Verigene ID system. (A) Anthrax bar-code DNA detection with 30 nm NP probes. (B) Quantitative data of spot intensities with 30 nm NP probes (Adobe Photoshop, Adobe Systems, Inc., San Jose, CA). The horizontal line represents control signal intensity (47 ± 2).

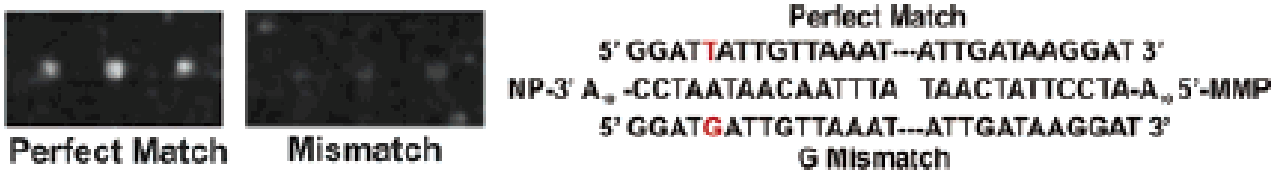

Figure 3. Single base mismatch experiment.

Nanoparticle-Based Bio–Bar Codes for the Ultrasensitive Detection of Proteins

26 SEPTEMBER 2003 VOL 301 SCIENCE

Jwa-Min Nam,* C. Shad Thaxton,* Chad A. Mirkin†

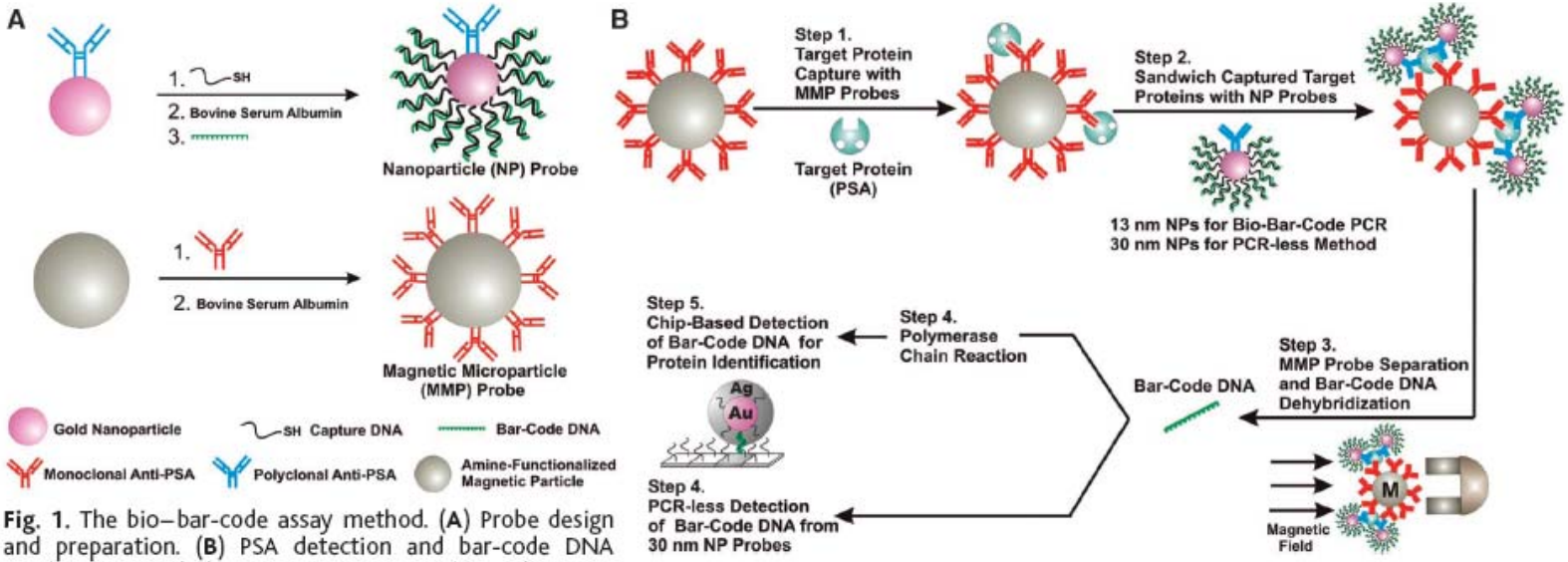

Fig. 1. The bio–bar-code assay method. (**A**) Probe design and preparation. (**B**) PSA detection and bar-code DNA amplification and identification. In a typical PSA-detection experiment, an aqueous dispersion of MMP probes functionalized with mAbs to PSA (50 μl of 3 mg/ml magnetic probe solution) was mixed with an aqueous solution of free PSA (10 μl of PSA) and stirred at 37°C for 30 min (Step 1). A 1.5-ml tube containing the assay solution was placed in a BioMag microcentrifuge tube separator (Polysciences, Incorporated, Warrington, PA) at room temperature. After 15 s, the MMP-PSA hybrids were concentrated on the wall of the tube. The supernatant (solution of unbound PSA molecules) was removed, and the MMPs were resuspended in 50 μl of 0.1 M phosphate-buffered saline (PBS) (repeated twice). The NP probes (for 13-nm NP probes, 50 μl at 1 nM; for 30-nm NP probes, 50 μl at 200 pM), functionalized with polyclonal Abs to PSA and hybridized bar-code DNA strands, were then added to the assay solution. The NPs reacted with the PSA immobilized on the MMPs and provided DNA strands for signal amplification and protein identification (Step 2). This solution was vigorously stirred at 37°C for 30 min. The MMPs were then washed with 0.1 M PBS with the magnetic separator to isolate the magnetic particles. This step was repeated four times, each time for 1 min, to remove everything but the MMPs (along with the PSA-bound NP probes). After the final wash step, the MMP probes were resuspended in NANOpure water (50 μl) for 2 min to dehybridize bar-code DNA strands from the nanoparticle probe surface. Dehybridized bar-code DNA was then easily separated and collected from the probes with the use of the magnetic separator (Step 3). For bar-code DNA amplification (Step 4), isolated bar-code DNA was added to a PCR reaction mixture (20-μl final volume) containing the appropriate primers, and the solution was then thermally cycled (*20*). The bar-code DNA amplicon was stained with ethidium bromide and mixed with gel-loading dye (*20*). Gel electrophoresis or scanometric DNA detection (*24*) was then performed to determine whether amplification had taken place. Primer amplification was ruled out with appropriate control experiments (*20*). Notice that the number of bound NP probes for each PSA is unknown and will depend upon target protein concentration.

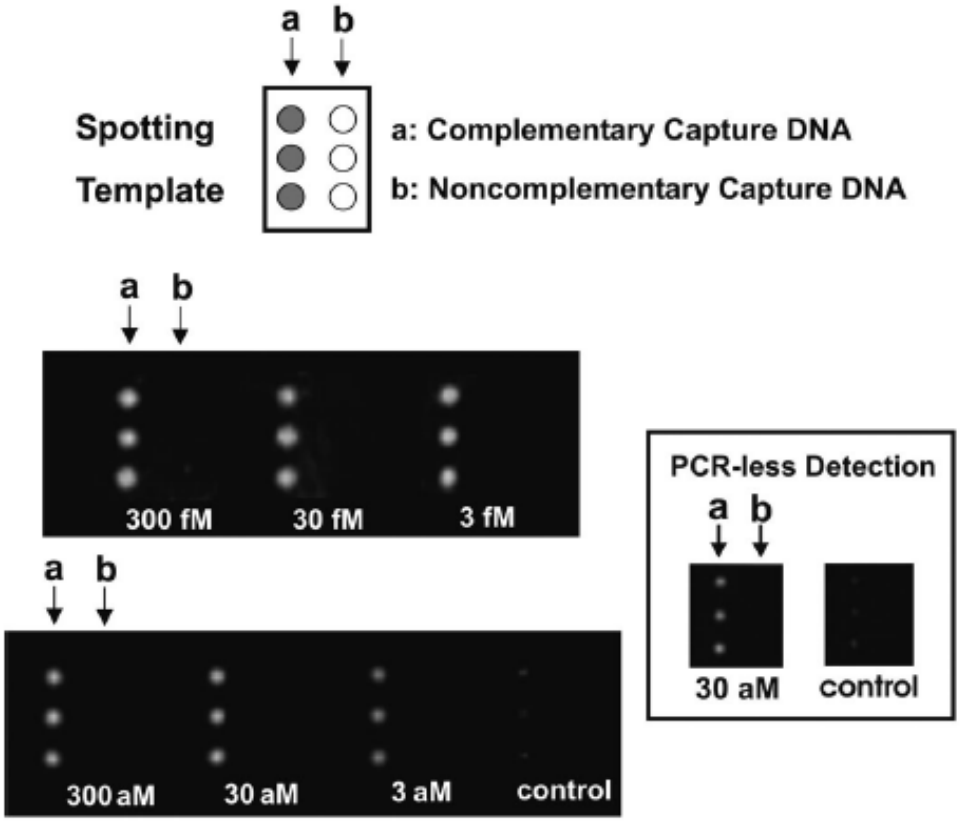

Fig. 2. Scanometric detection of PSA-specific bar-code DNA. PSA concentration (sample volume of 10 μl) was varied from 300 fM to 3 aM and a negative control sample where no PSA was added (control) is shown. For all seven samples, 2 μl of antidinitrophenyl (10 pM) and 2 μl of β-galactosidase (10 pM) were added as background proteins. Also shown is PCR-less detection of PSA (30 aM and control) with 30 nm NP probes (inset). Chips were imaged with the Verigene ID system (*20*).

Array-Based Electrical Detection of DNA with Nanoparticle Probes

So-Jung Park, T. Andrew Taton,* Chad A. Mirkin†

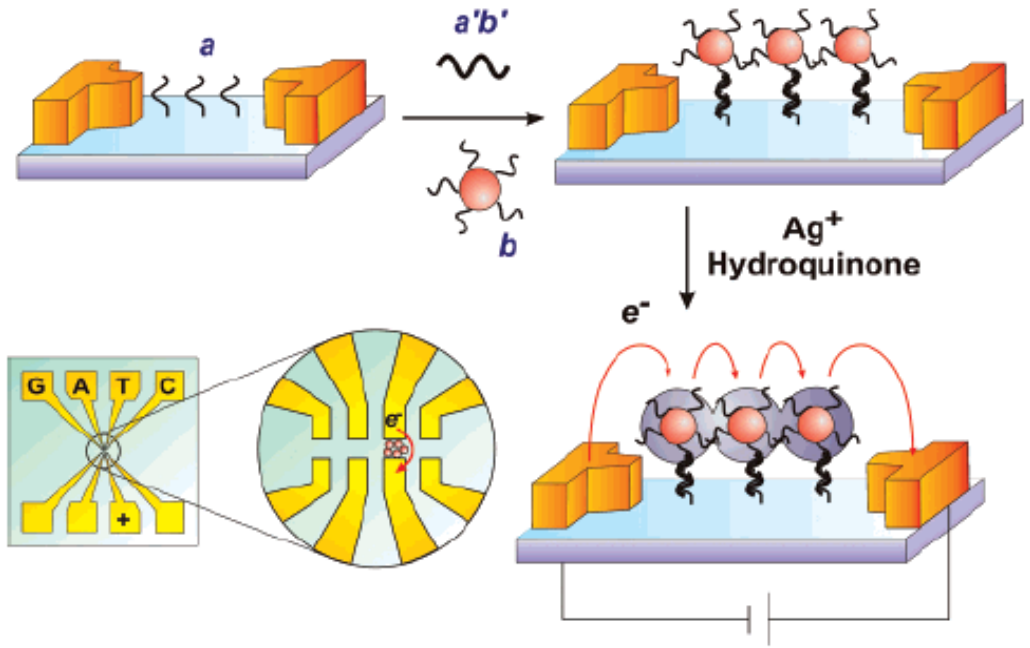

Figure 7. When the capture/target/probe sandwich is positioned in the gap between two electrodes, catalytic reduction of silver onto the sandwich system results in a signal that can be detected electrically. (Reprinted with permission from *Science* (http://www.aaas.org), ref 93. Copyright 2002 American Association for the Advancement of Science.)

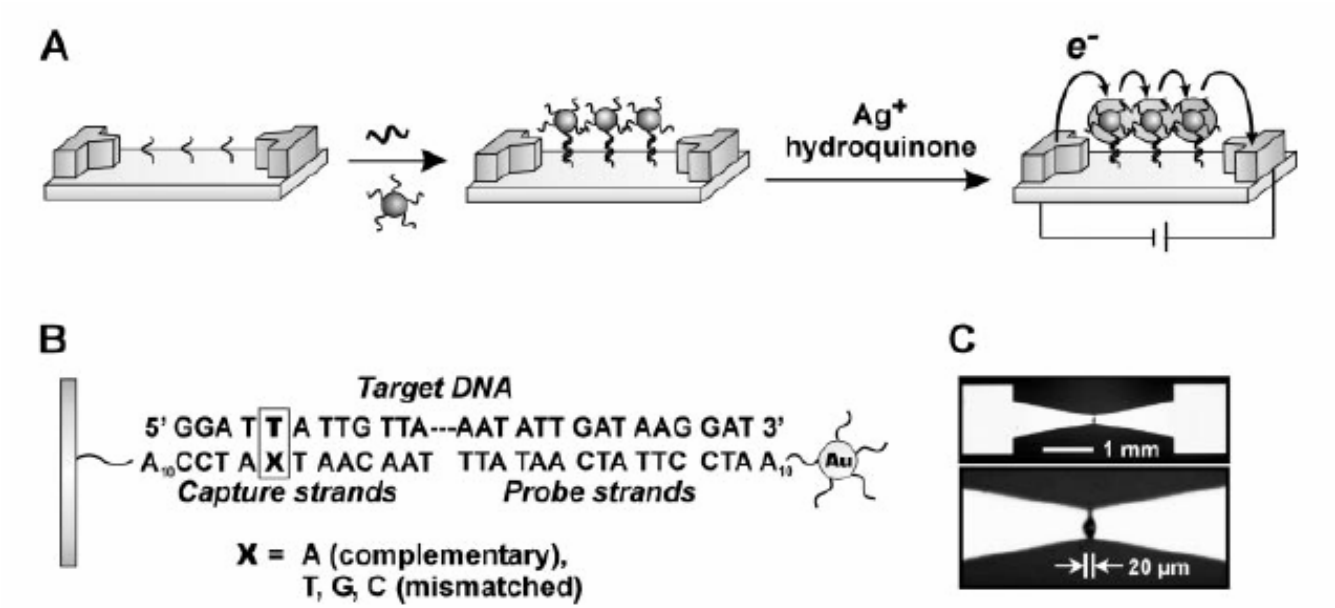

Fig. 1. (**A**) Scheme showing concept behind electrical detection of DNA. (**B**) Sequences of capture, target, and probe DNA strands. (**C**) Optical microscope images of the electrodes used in a typical detection experiment. The spot in the electrode gap in the high-magnification image is food dye spotted by a robotic arrayer (GMS 417 Microarrayer, Genetic Microsystems, Woburn, MA).

Table 1. Detection Limits of Nucleic Acid Assays[a]

	assay	ss DNA	PCR products	genomic DNA
nanostructure-based methods	colorimetric[29] (cross-linked Au nanoparticles)	~10 nM		
	colorimetric[36] (non-cross-linked Au nanoparticles)	60 nM		
	magnetic relaxation[97] (iron oxide nanoparticles)	20 pM		
	electrochemical[96] (nanoparticles)	270 pM		
	scanometric[35,66,67] (Au nanoparticles with Ag amplification)	50 fM	100 aM[b]	200 fM
	Raman spectroscopy[68] (Au nanoparticles with Ag amplification)	~1 fM		
	electrical[93] (Au nanoparticles with Ag amplification)	500 fM		
	electrical[99] (Si nanowire)	10 fM		
	electrical[103] (carbon nanotube)	54 aM		
	resonant light-scattering[61−66] (metal nanoparticles)	170 fM[b]		33 fM
	fluorescence[56] (ZnS and CdSe quantum dots)	2 nM		
	surface plasmon resonance[41] (Au nanoparticles)	10 pM		
	quartz crystal microbalance[94] (Au nanoparticles)	~1 fM		
	laser diffraction[42] (Au nanoparticles)	~50 fM		
	fluorescence[45] (fluorescent nanoparticles)	~1 fM		
	bio-bar-code amplification[71] (Au nanoparticles with Ag amplification)	500 zM		
other non-enzymatic based methods	fluorescence[35] (molecular fluorophores)		~600 fM[b]	
	fluorescence (dendrimer amplification)[134]		2.5 μg	
	electrochemical amplification[136] (electroactive reporter molecules)	100 aM		

[a] Detection limits can vary based on target length and sequence; therefore, it is difficult to compare assays without testing them using identical targets and conditions. [b] Values taken from ref 34.

Table 2. Detection Limits of Protein Assays

	assay	target	protein in saline	protein in serum
nanostructure-based methods	optical[72] (Au nanoshells)	rabbit IgG	0.88 ng/mL (~4.4 pM)[a]	0.88 ng/mL (~4.4 pM)[a]
	optical[74] (Au nanoparticles)	IgE and IgG1	~20 nM	
	magnetic relaxation[98] (iron oxide nanoparticles)	adenovirus (ADV) and herpes simplex virus (HSV)	100 ADV/ 100μL	50 HSV/ 100 μL
	scanometric[79] (Au nanoparticles with Ag amplification)	mouse IgG	200 pM	
	Raman[82] (Au nanoparticles with Raman labels)	prostate-specific antigen		30 fM
	surface plasmon resonance[83,84] (triangular Ag particles on surfaces)	streptavidin(S A) and anti-biotin (AB)	~1 pM SA and ~700 pM AB	
	electrical[110] (single-walled carbon nanotubes)	10E3 antibody to U1A RNA splicing factor	~1 nM	
	electrical[20] (Si nanowires)	streptavidin	10 pM	
	bio-bar-code amplification[75] (Au nanoparticles with Ag amplification)	prostate-specific antigen	30 aM (3 aM)[b]	(30 aM)[b]
molecular fluorophore methods	enzyme-linked immunosorbent assay	various	pM range	pM range
electrochemical methods	electrochemical amplification[137] (oligonucleotide reporter molecules)	IgG	13 fM	
enzyme-based amplification methods	immuno-PCR[76]	bovine serum albumin	2 fM	
	rolling circle amplification[77]	prostate-specific antigen	3 fM	

[a] Reported in ng/mL; authors converted to molar concentration for ease of comparison. [b] These values are the lower limits when PCR is used to amplify the bar-code DNA prior to scanometric detection of bar codes.

Cell Culture

In the remainder of this section, each step was performed using aseptic technique inside a laminar flow hood (*see* **Note 2**). Ten milliliters of medium was transferred by pipet into each labeled flask. Thawed vials were then sterilized by swabbing with alcohol. The vials were slowly opened, and the medium with the cells was transferred by pipet into the appropriately labeled flask. The flasks were next placed in a 37°C incubator at 5% CO_2, and the cells were allowed to grow until confluent.

Once confluent, the medium was aspirated off and the cells well rinsed with PBS, and then 3 mL of 0.1% trypsin was added. After approx 1 to 2 min, or when the cells began to round up and detach, 3 mL of medium was added to disperse the cells and to inhibit the trypsin (*see* **Note 3**). Cells from each flask were then transferred to an appropriately labeled 50-mL conical tube and centrifuged at 500*g* for 5 min. The supernatant was aspirated off, and the cells were resuspended in fresh medium.

Using a hemacytometer, the cells were counted and their concentration was determined (*see* **Note 4**). The cell solution was next diluted to 1×10^5 cells/mL and 150 µL was added to the glass cover slip of poly-D-lysine-coated sterile MatTek microwell dishes. The cells were incubated at 37°C with 5% CO_2 for 3 h to allow the cells to attach. Once the cells had attached, 2 mL of additional medium was added to the dish. The dishes were then returned to the incubator and allowed to grow for 3 d or until 50% confluent.

Hemacytometer

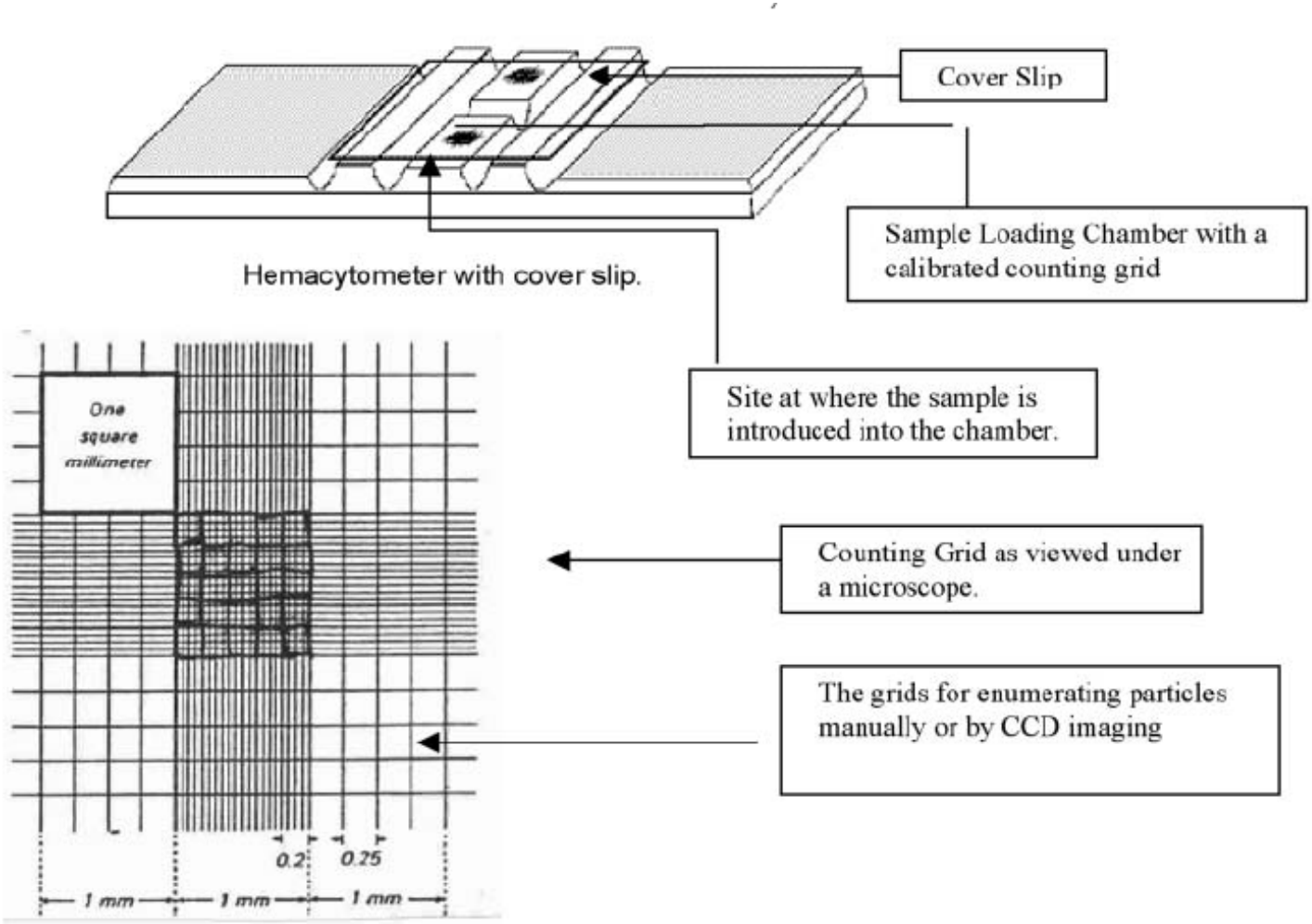

Fig. 3. Layout of hemacytometer.

Fluorescence Imaging Scheme

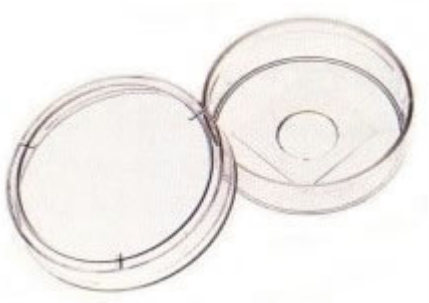

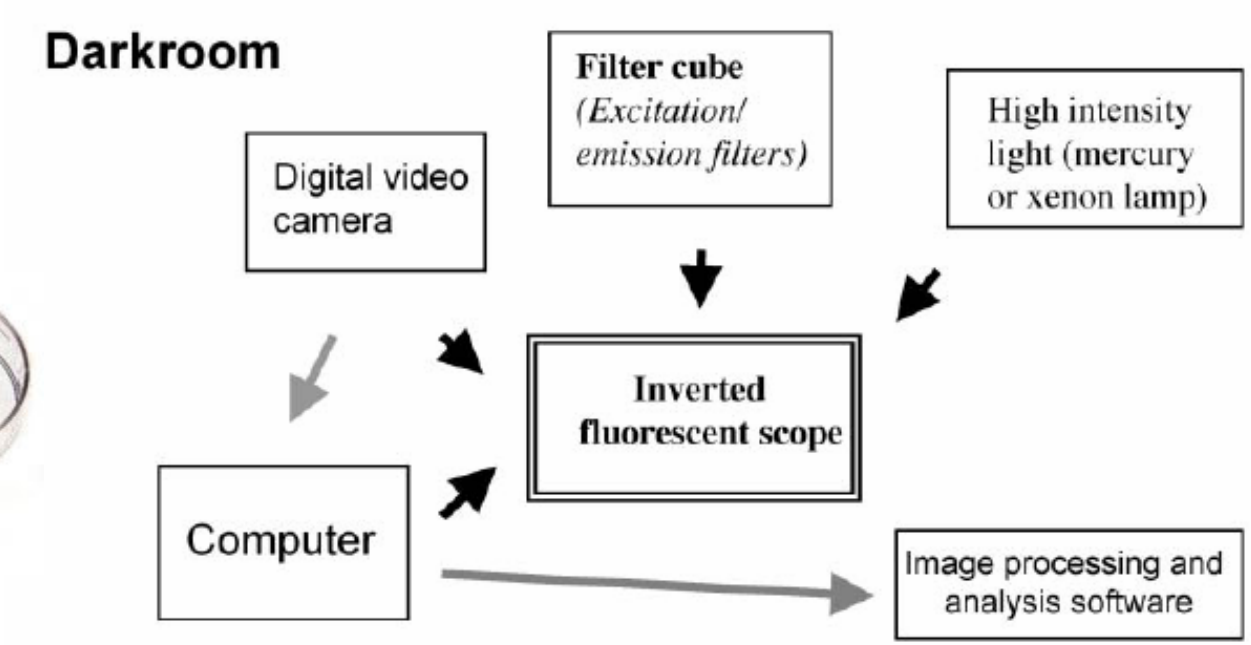

Fig. 2. Components required for fluorescent imaging. An inverted fluorescent microscope equipped with the appropriate excitation/emission filter(s) and camera insertion site also should include a mercury or xenon lamp for fluorophore excitation and a digital camera. The computer selected should have sufficient memory to process and to analyze digital images using analysis software. All equipment shown should be set up in a room in which lighting can be shut off without inconveniencing other laboratory operations.

Oligonucleotide-Modified Gold Nanoparticles for Intracellular Gene Regulation

SCIENCE VOL 312 19 MAY 2006

Nathaniel L. Rosi,* David A. Giljohann,* C. Shad Thaxton, Abigail K. R. Lytton-Jean, Min Su Han, Chad A. Mirkin†

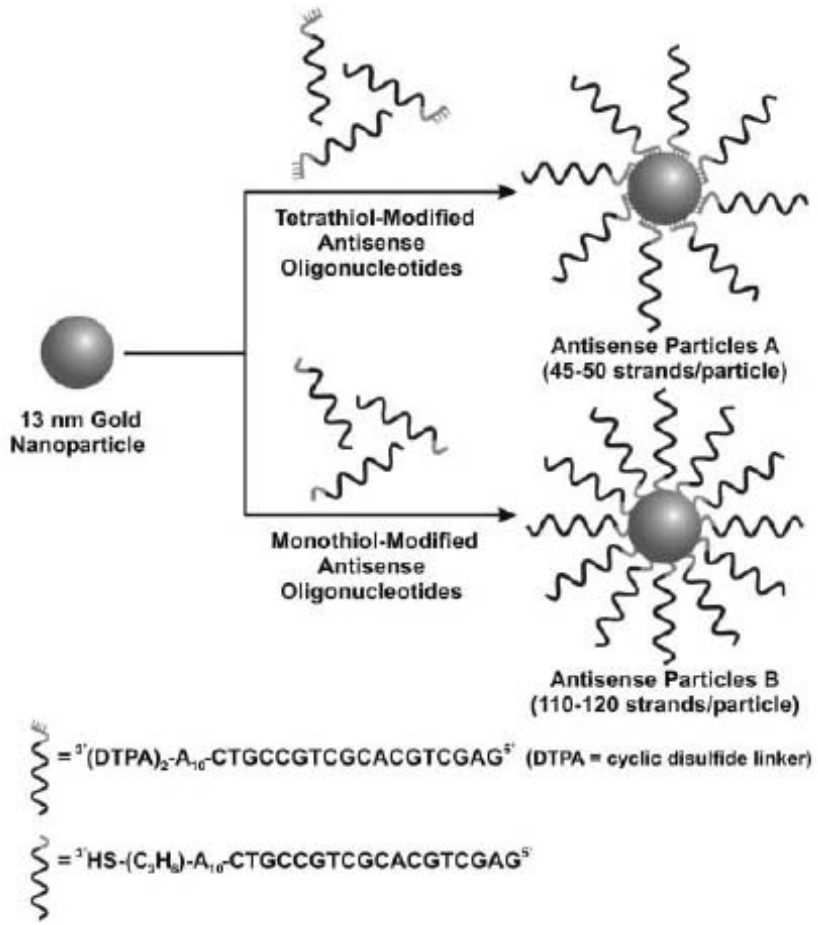

Fig 1. Preparation of antisense Au NPs. Citrate-stabilized gold nanoparticles (13 nm ± 1 nm) were functionalized with ASODNs that were premodified with an A_{10} tether and either two cyclic disulfides (DTPA) or an alkyl-thiol anchoring group to produce Antisense Particles A and B, respectively.

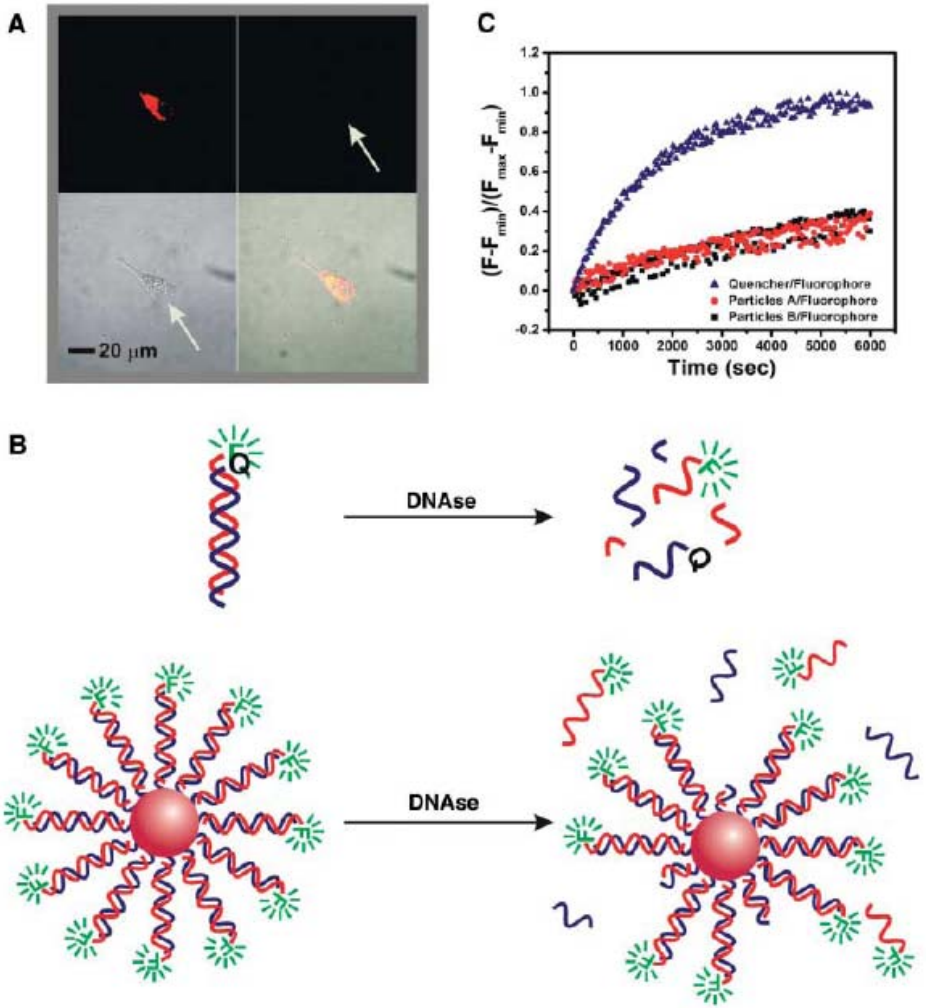

Fig. 2. Experiments aimed at understanding the intracellular stability of antisense nanoparticles. (**A**) Fluorescent microscopy images of C166-EGFP cells incubated 48 hours with antisense particle B functionalized with dual-fluorophore labeled ASODNs (3′ Cy3 and 5′ Cy5.5) only reveal fluorescence from Cy5.5 (706 to 717 nm, upper left). Negligible fluorescence is observed in the emission range of Cy3 (565 to 615 nm, upper right). Transmission and composite overlay images are shown in the lower left and lower right quadrants, respectively. The arrows indicate the location of the cell. Similar data collected from experiments using particle A are included in fig. S3 (*23*). (**B**) Duplexes composed of either quencher-modified ASODN/fluorophore-modified complement or antisense particle/fluorophore-modified complement were treated with DNase. (**C**) The ASODN duplex degraded much faster than the antisense particle duplex, as calculated using fluorescence spectroscopy, where F_{min} is the fluorescence of the mixture at its initial, fully hybridized state and F_{max} is the maximum fluorescence of the system at 80°C where all of the oligonucleotides are dehybridized.

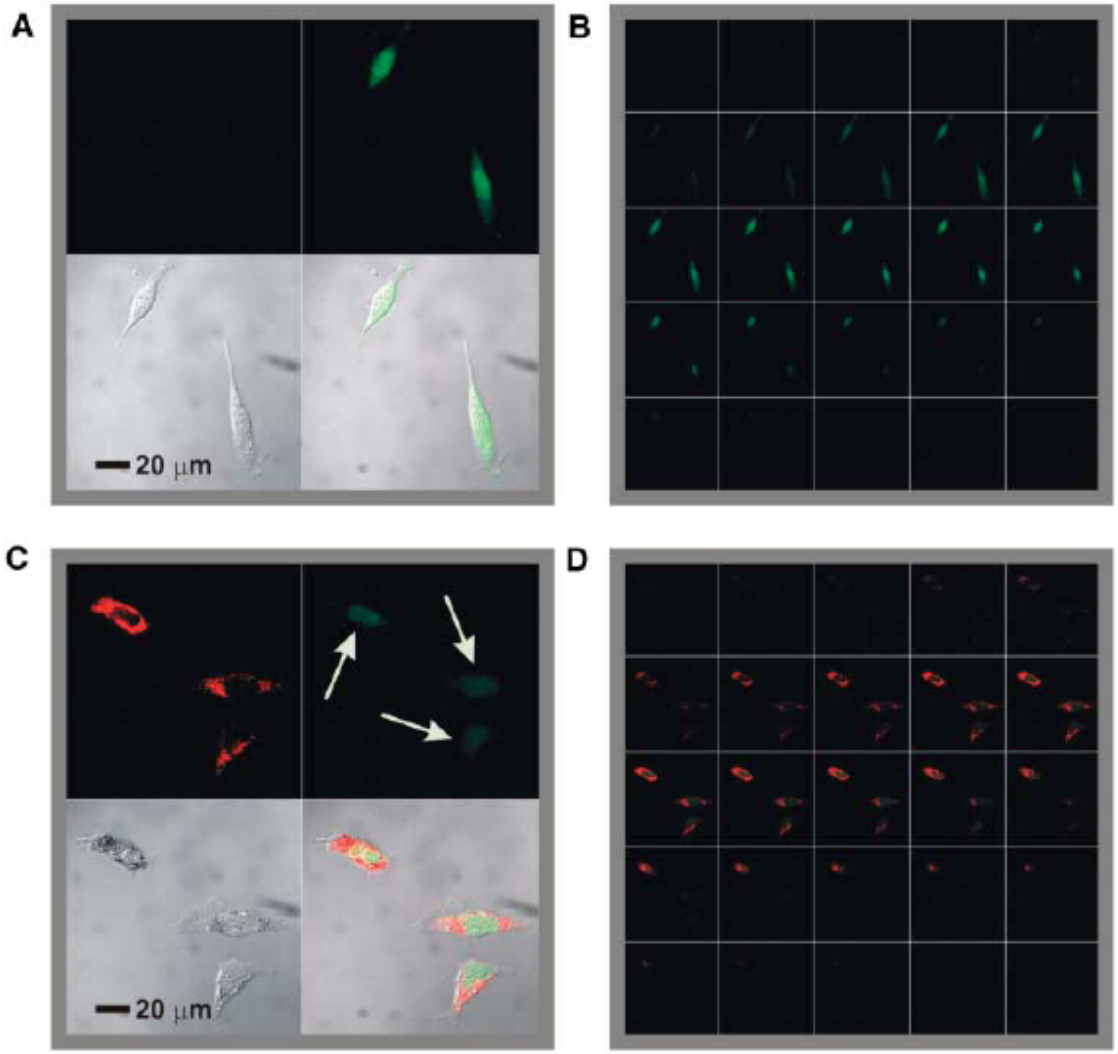

Fig. 3. Confocal fluorescence microscopy images showing EGFP knockdown. (A) Untreated control C166-EGFP cells (upper left, Cy5.5 emission, 706 to 717 nm; upper right, EGFP emission, 500 to 550 nm; lower left, transmission image of cells; lower right, composite overlay of all three channels) showed a significant amount of emission throughout the cell. (B) 1 μm sectioning images of control cells. (C and D) Cells treated with antisense particles A or B showed a decrease in the amount of EGFP emission.

Table 1. Performance characteristics of antisense nanoparticles.

Antisense experiment	Observed toxicity	Approximate binding constant	Percent decrease in EGFP expression
Antisense Particles A (0.024 nmol particles 1.08 nmol ASODN)	No	7.1×10^{20}	11 ± 2
Antisense Particles A (0.048 nmol particles 2.16 nmol ASODN)	No	7.1×10^{20}	14 ± 0.4
Antisense Particles B (0.024 nmol particles 2.64 nmol ASODN)	No	2.6×10^{22}	14 ± 1
Antisense Particles B (0.048 nmol particles 5.28 nmol ASODN)	No	2.6×10^{22}	20 ± 4
Nonsense Particles A (0.048 nmol particles)	No	N/A	0 ± 3
Nonsense Particles B (0.048 nmol particles)	No	N/A	0 ± 2
Lipofectamine 2000 (0.024 nmol ASODN)	No	6.7×10^{20}	6 ± 0.2
Lipofectamine 2000 (2.64 nmol ASODN)	Yes	6.7×10^{20}	N/A
Cytofectin (0.024 nmol ASODN)	No	6.7×10^{20}	7 ± 0.7
Cytofectin (2.64 nmol ASODN)	Yes	6.7×10^{20}	N/A

Determining the Size and Shape Dependence of Gold Nanoparticle Uptake into Mammalian Cells

B. Devika Chithrani,[†,‡] Arezou A. Ghazani,[†,‡] and Warren C. W. Chan*[,†,‡,§]

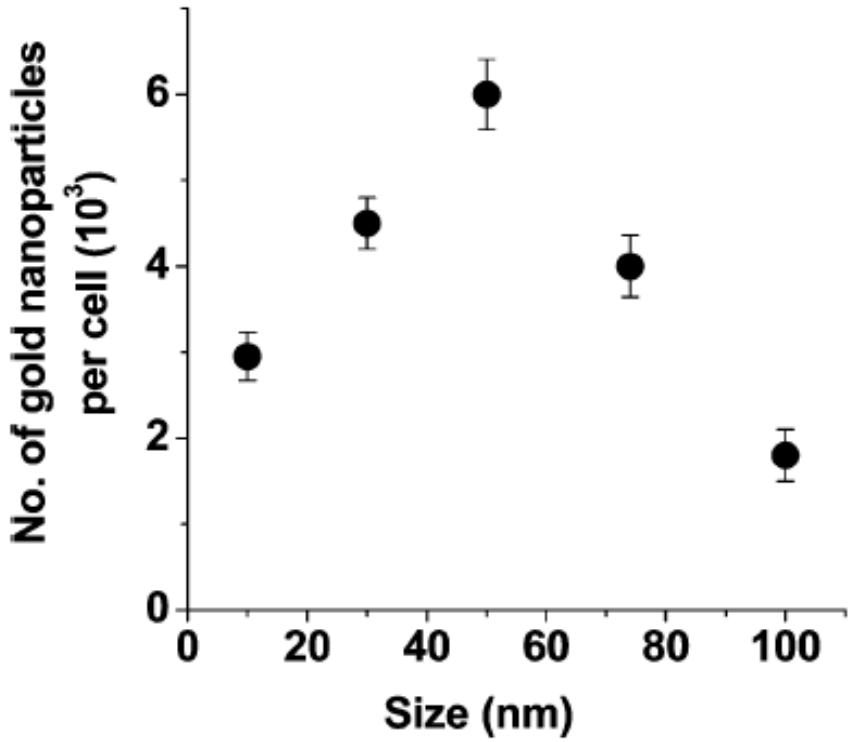

Figure 1. Dependence of cellular uptake of gold nanoparticles as a function of size.

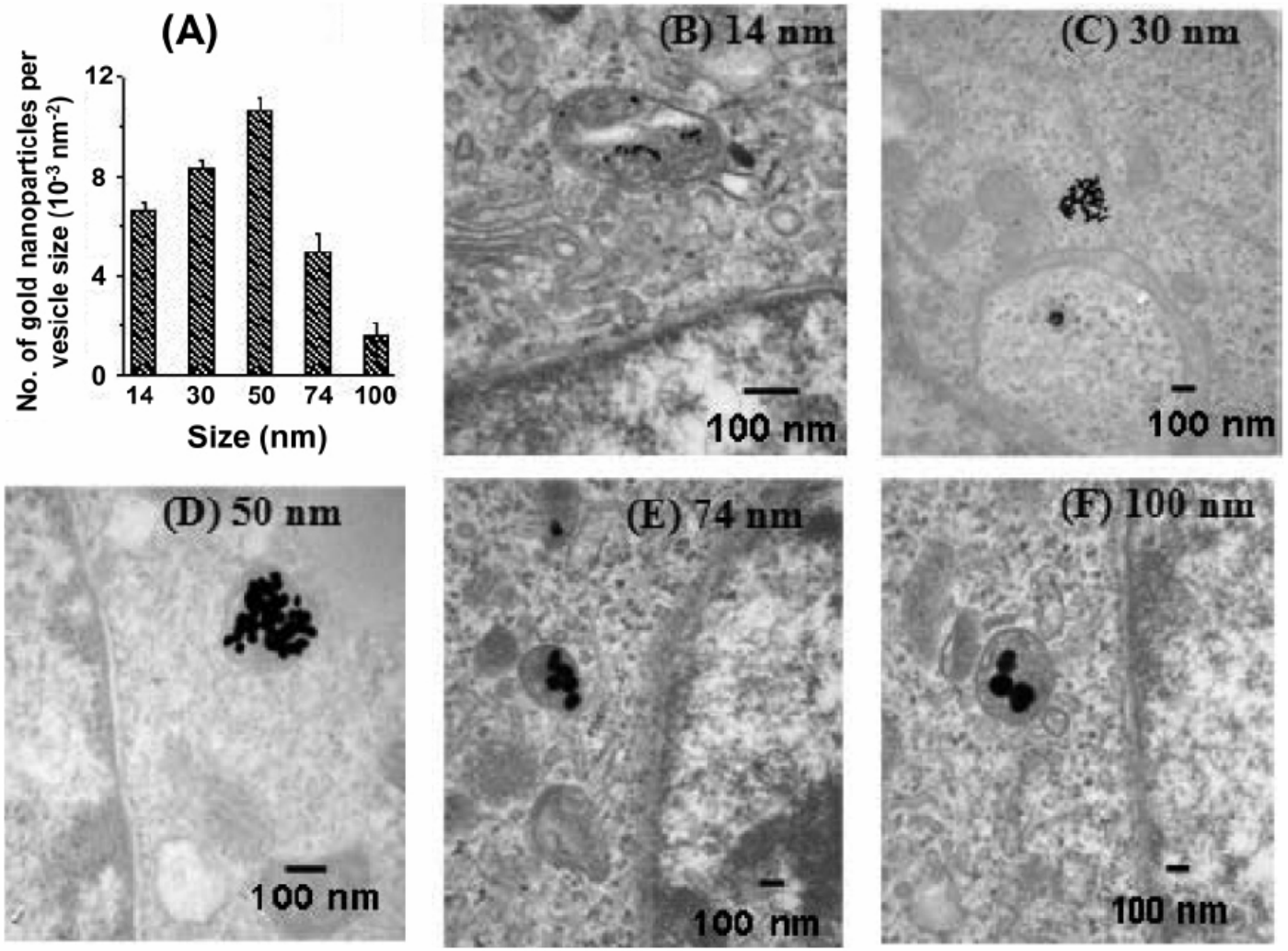

Figure 2. Transmission electron microscopy imaging and measurements of gold nanoparticles in cells. (A) The graph of number of gold nanoparticles per vesicle diameter vs nanoparticle size. (B−F) TEM images of gold nanoparticles with sizes 14, 30, 50, 74, and 100 nm trapped inside vesicles of a Hela cell, respectively. (TEM images were recorded at a voltage of 75 kV with a Hitachi H7000.)

Use of Nanobarcodes® Particles in Bioassays

R. Griffith Freeman, Paul A. Raju, Scott M. Norton,
Ian D. Walton, Patrick C. Smith, Lin He, Michael J. Natan,
Michael Y. Sha, and Sharron G. Penn

Submicrometer Metallic Barcodes

Sheila R. Nicewarner-Peña,[1] R. Griffith Freeman,[2]
Brian D. Reiss,[1] Lin He,[2] David J. Peña,[1] Ian D. Walton,[2]
Remy Cromer,[2] Christine D. Keating,[1]* Michael J. Natan[2]*

SCIENCE VOL 294 5 OCTOBER 2001

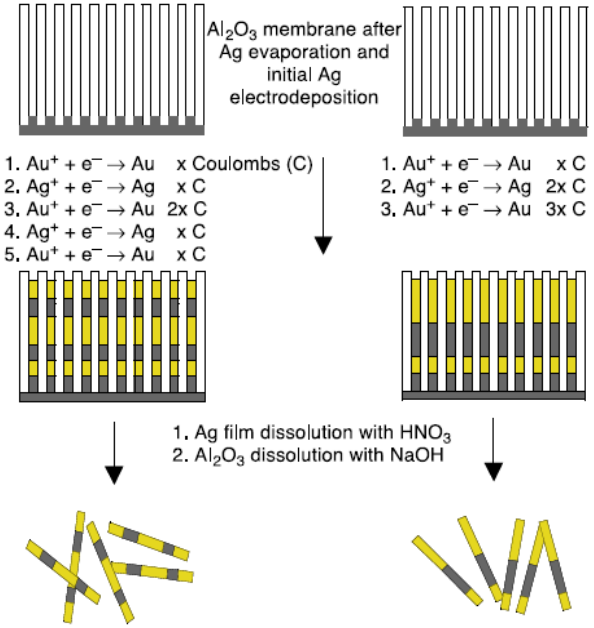

Fig. 1. Synthesis of barcoded particles.

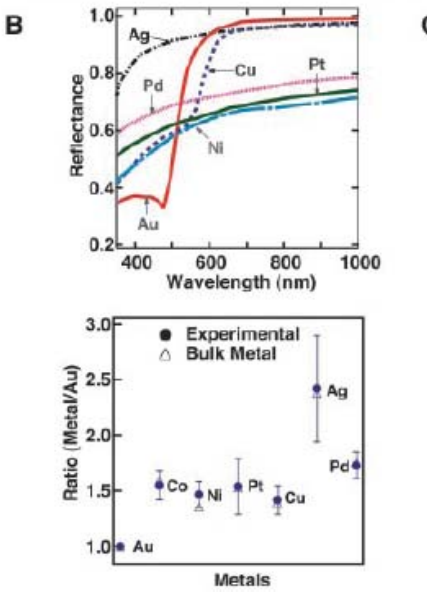

Surface Functionalization

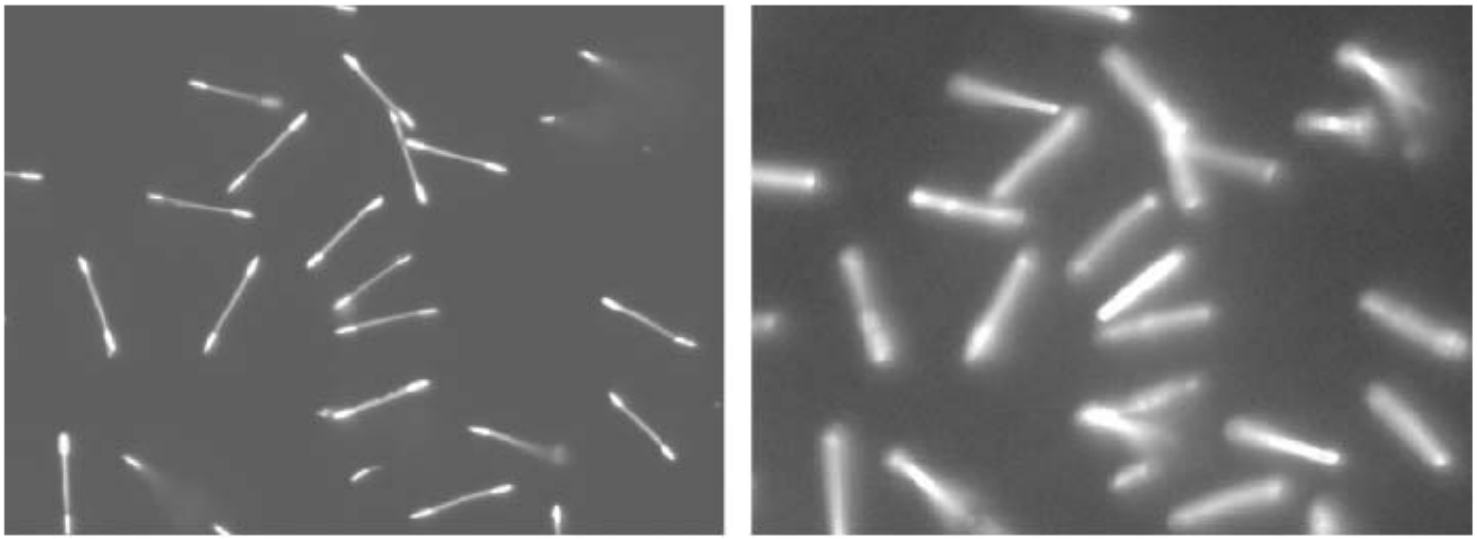

Reflectance **Fluorescence**

Fig. 2. Signal detection of oligonucleotide-derivatized NBCs hybridized with complementary Cy5 oligonucleotide.

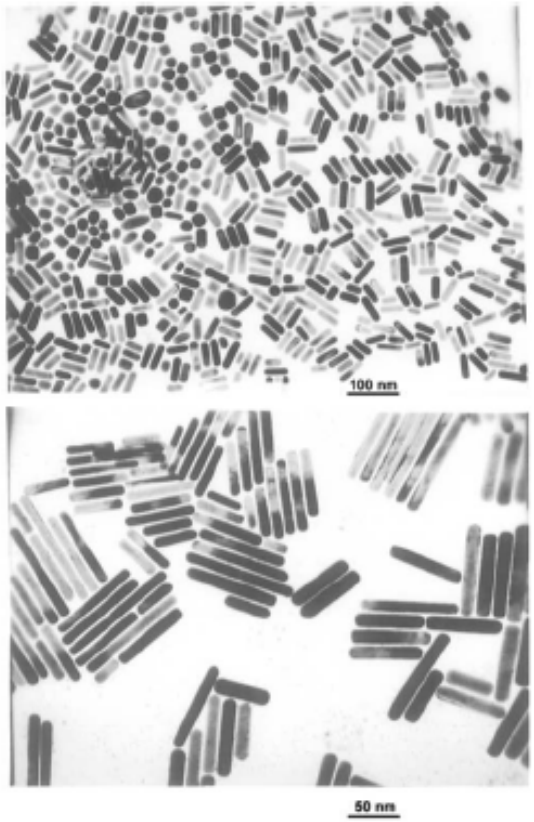

Fig. 2 TEM images of Au nanorods with different mean aspect ratios: 2.6 (top) and 7.6 (bottom). Reprinted with permission from reference 23, © 1997 American Chemical Society.

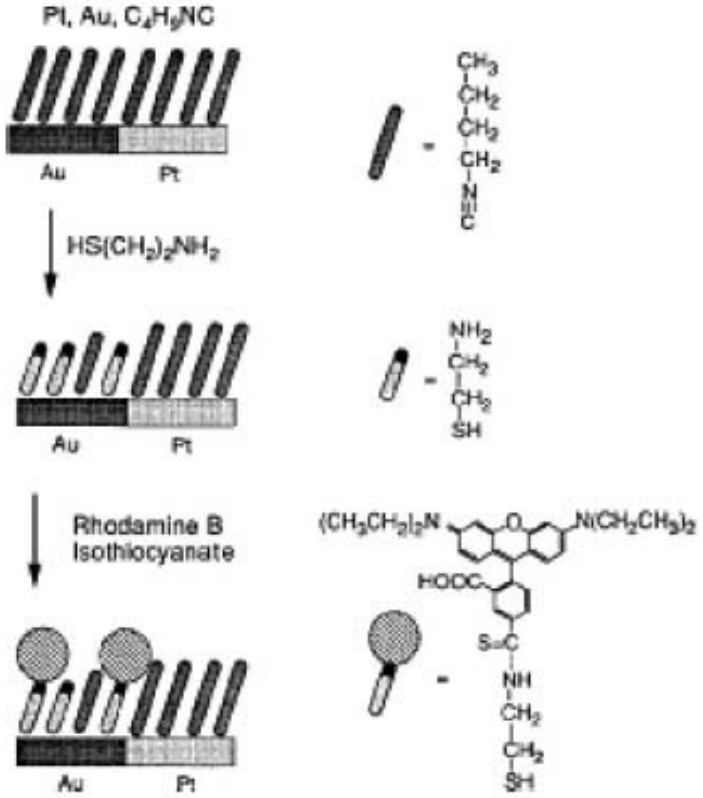

Scheme 5 Functionalization of a two-segment gold–platinum nanowire. Reprinted with permission from reference 42.

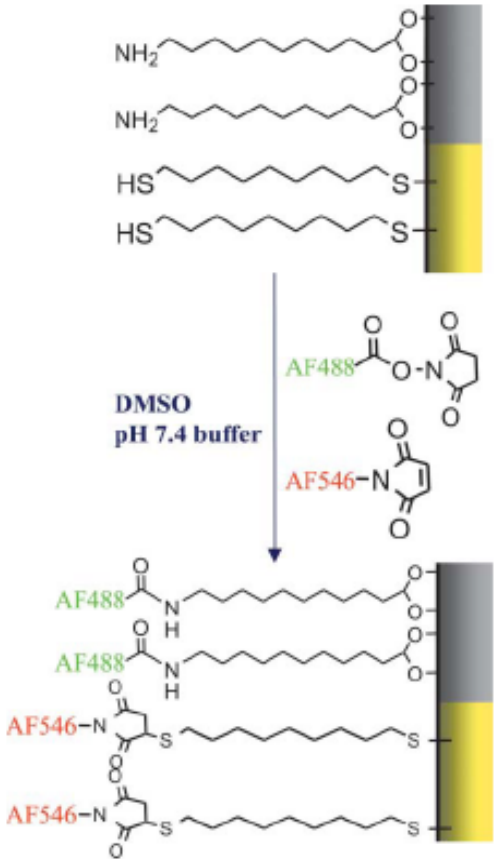

Scheme 6 Orthogonal self-assembly on gold and nickel segments of a single nanowire.

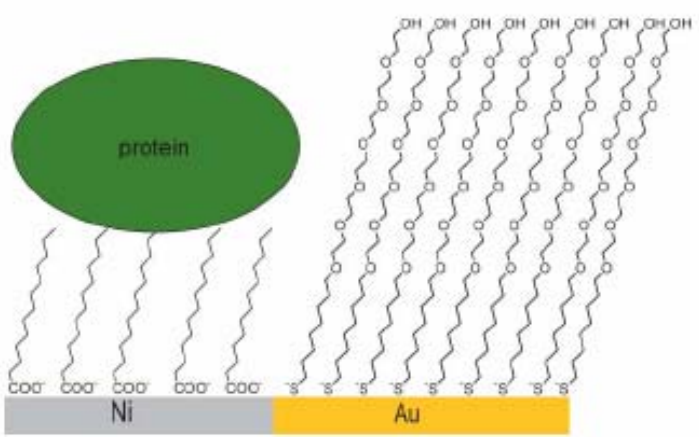

Scheme 7 Selective protein adsorption on a gold–nickel nanowire.

Multifunctional nanorods for gene delivery

ALIASGER K. SALEM[1,2], PETER C. SEARSON[2] AND KAM W. LEONG*[1]

[1]Department of Biomedical Engineering, Johns Hopkins School of Medicine, Baltimore, Maryland 21205, USA
[2]Department of Materials Science and Engineering, Johns Hopkins University, Baltimore, Maryland 21218, USA
*e-mail: kleong@bme.jhu.edu

nature materials | VOL 2 | OCTOBER 2003 |

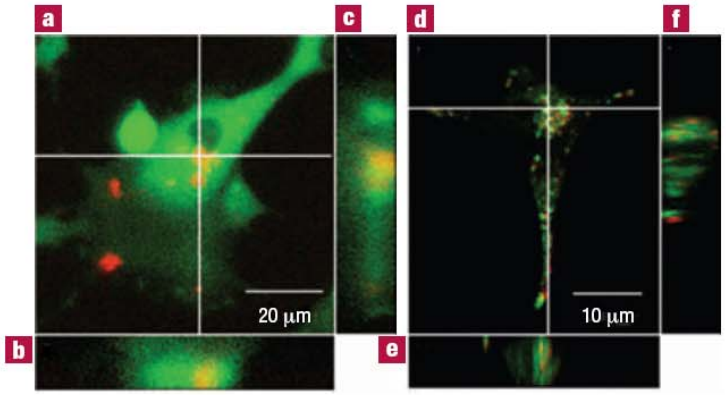

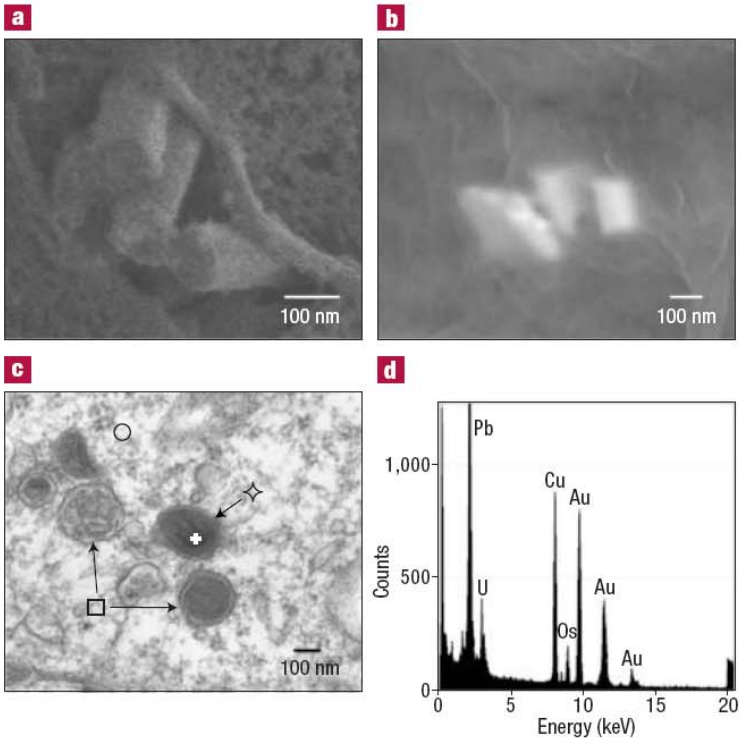

Figure 2 Stacked laser scanning confocal microscope images of transfected cells. **a**, A live HEK293 cell (red/633 nm, green/543 nm). Rhodamine (633 nm) identifies the subcellular location of the nanorods whilst GFP expression (543 nm) provides confirmation of transfection. **b**,**c**, Orthogonal sections confirm that the nanorods are within the cell. Confocal microscope stacked images **d**, of a live HEK 293 cell stained with Lysotracker Green identifying the location of the nanorods (Rhodamine) in relation to acidic organelles in both orthogonal sections **e** and **f**.

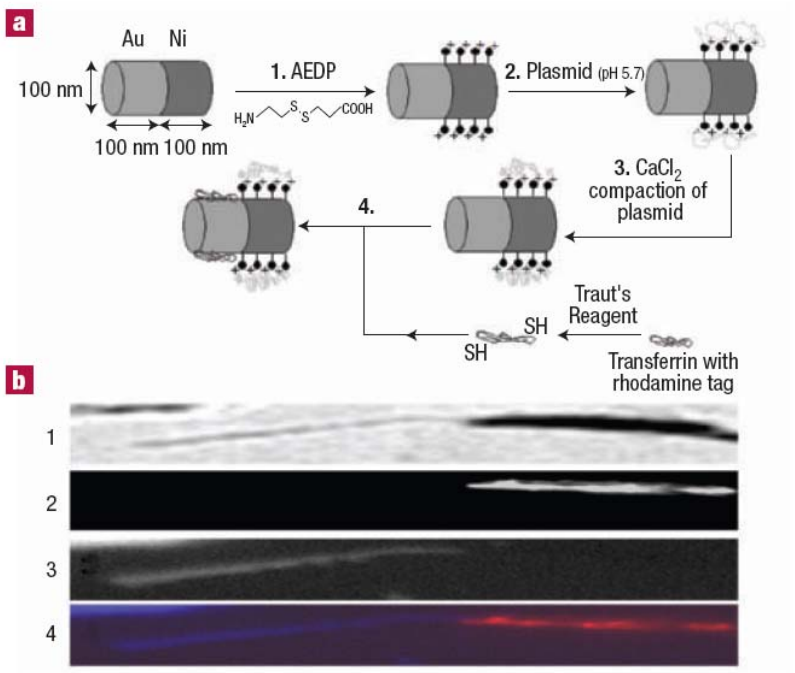

Figure 1 Spatially selective binding of DNA plasmids and transferrin to multicomponent nanorods. a, Illustration of nanorod functionalization. **1**. Nanorods are incubated with the 3-[(2-aminoethyl) dithio] propionic acid (AEDP) linker. The carboxylate end-group binds to the Ni segment. The disulphide linkage acts as a cleavable point within the spacer to promote DNA release within the reducing environment of the cell. **2**. Plasmids are bound by electrostatic interactions to the protonated amines presented on the surface of the nickel segment. **3**. $CaCl_2$ compacts the surface-immobilized plasmids. **4**. Rhodamine-conjugated transferrin is selectively bound to the gold segment of the nanorods. **b**, Confirmation of selective functionalization of nanorods is observed by light and fluorescent microscopy. **1**. Light microscope image of dual functionalized Au/Ni nanorod 20 μm long. **2.** Fluorescence image of the rhodamine-tagged (633 nm) transferrin on the Au segment. **3.** Fluorescence image of the Hoechst-stained (350/450 nm) plasmids on the Ni segment. **4.** Fluorescent overlay image combining **b2** and **b3**.

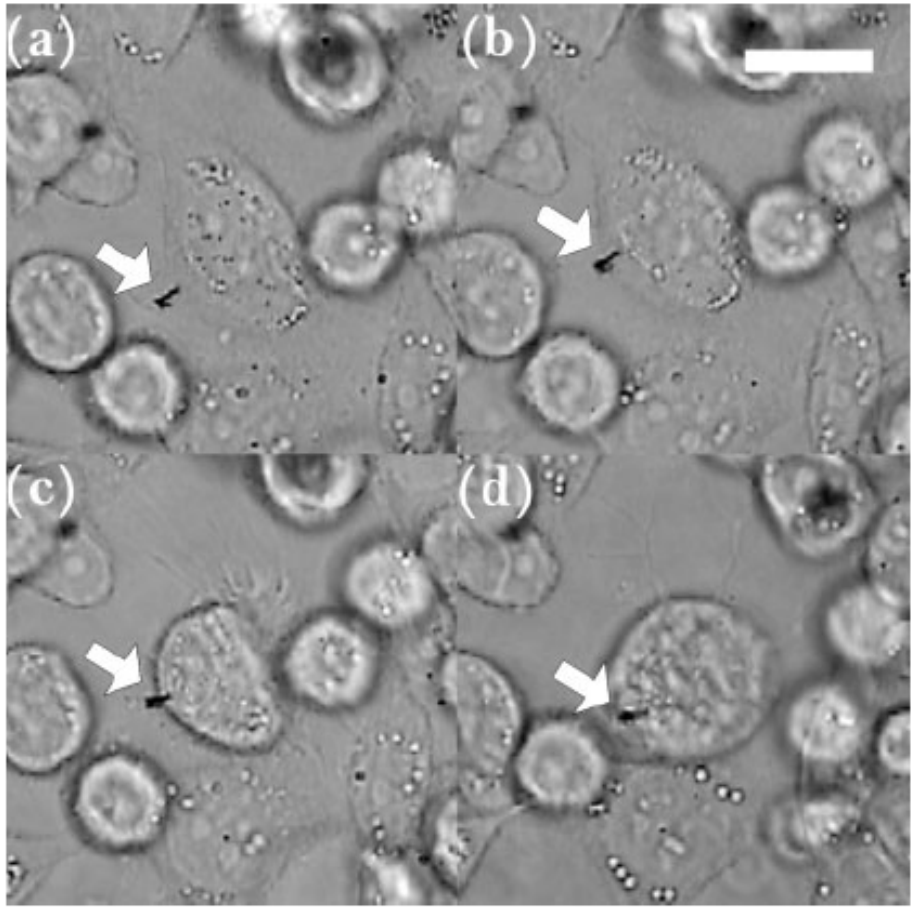

Figure 2. Phase contrast images of serum-coated gold nanowires entering a HeLa cell. The nanowire is indicated by an arrow. The scale bar represents 20 μm.

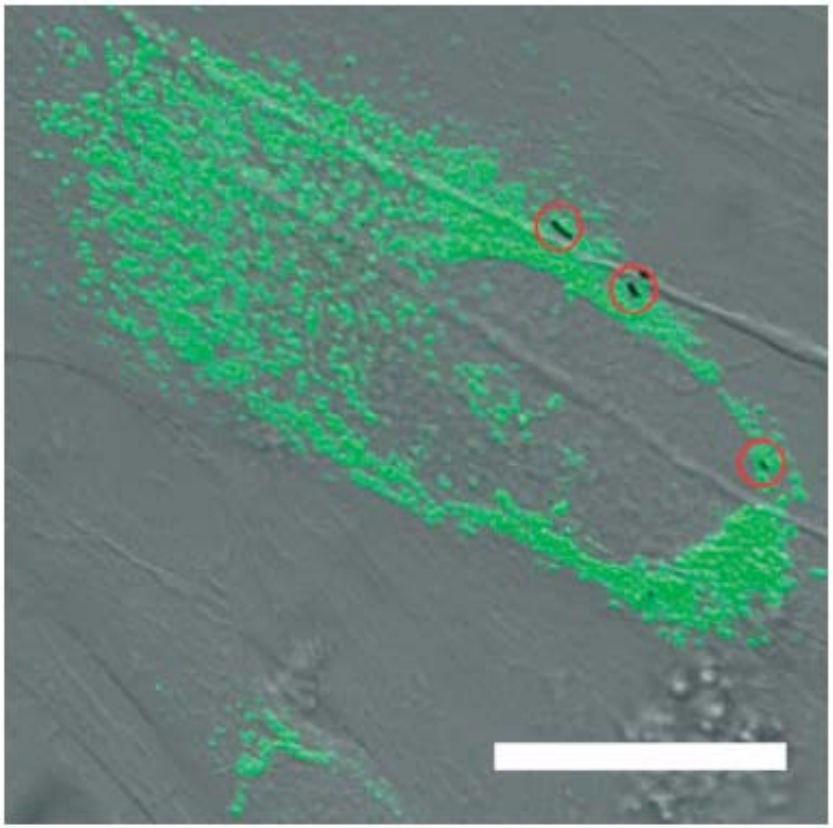

Figure 4. Combined differential interference contrast and fluorescence image of plasmid-coated nanowires and fibroblast cells expressing GFP. The nanowires are indicated by the red circles. The scale bar represents 20 μm.

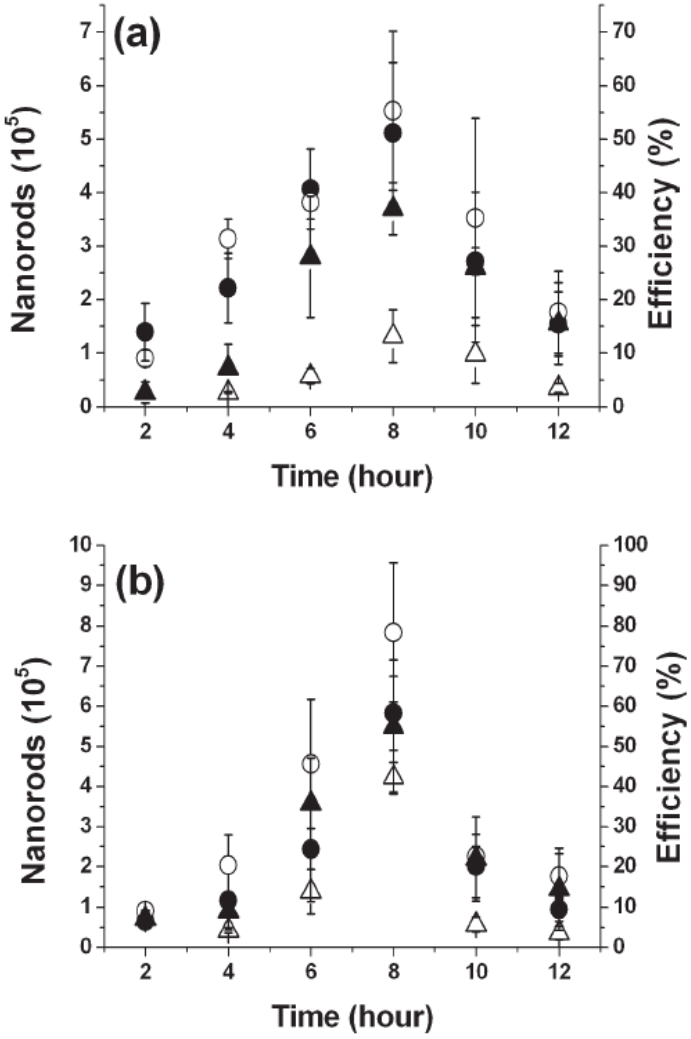
(a)
Nanorods (10^5)
Efficiency (%)
Time (hour)
(b)
Nanorods (10^5)
Efficiency (%)
Time (hour)

Applications of Quantum Dots in Biology

An Overview

Charles Z. Hotz

- Size dependent emission spectra
- Single excitation
- Higher photostability
- Narrow emission peak
- Low toxicity for coated quantum dots

Nucleation and Growth of CdSe on ZnS Quantum Crystallite Seeds, and Vice Versa, in Inverse Micelle Media

A. R. Kortan, R. Hull, R. L. Opila, M. G. Bawendi, M. L. Steigerwald, P. J. Carroll, and L. E. Brus*

Contribution from AT&T Bell Laboratories, Murray Hill, New Jersey 07974.
Received June 20, 1989

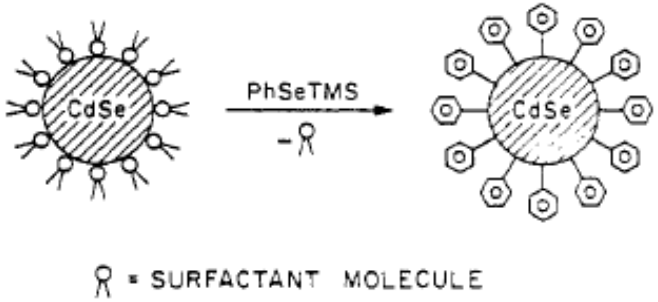

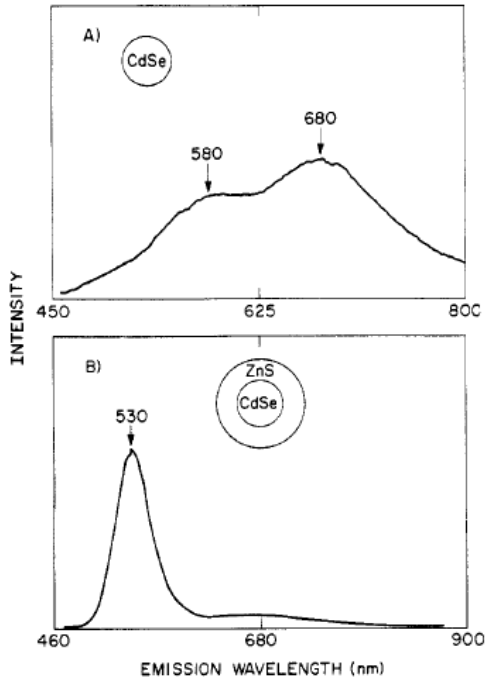

Figure 2. Room temperature luminescence spectra after annealing: (A) (CdSe)Ph, (B) $(CdSe)_1(ZnS)_4Ph$. The integrated quantum yield in B is more than an order of magnitude higher than in A.

Semiconductor Nanocrystals as Fluorescent Biological Labels

Marcel Bruchez Jr., Mario Moronne, Peter Gin, Shimon Weiss,*
A. Paul Alivisatos*

SCIENCE VOL 281 25 SEPTEMBER 1998

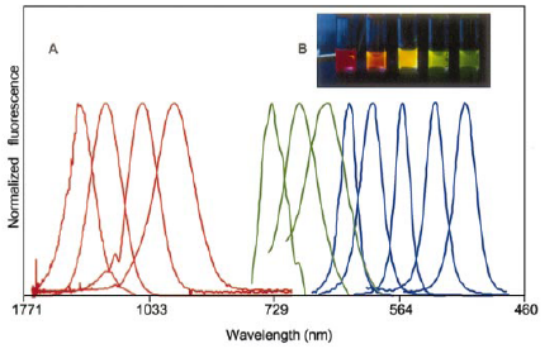

Fig. 2. (**A**) Size- and material-dependent emission spectra of several surfactant-coated semiconductor nanocrystals in a variety of sizes. The blue series represents different sizes of CdSe nanocrystals (*16*) with diameters of 2.1, 2.4, 3.1, 3.6, and 4.6 nm (from right to left). The green series is of InP nanocrystals (*26*) with diameters of 3.0, 3.5, and 4.6 nm. The red series is of InAs nanocrystals (*16*) with diameters of 2.8, 3.6, 4.6, and 6.0 nm. (**B**) A true-color image of a series of silica-coated core (CdSe)–shell (ZnS or CdS) nanocrystal probes in aqueous buffer, all illuminated simultaneously with a handheld ultraviolet lamp.

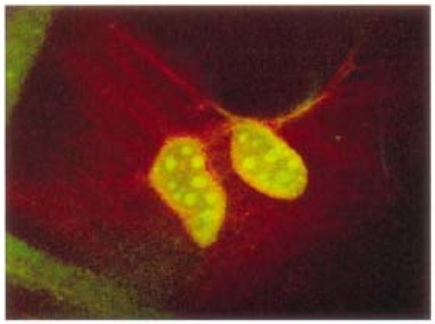

Fig. 3. Cross section of a dual-labeled sample examined with a Bio-Rad 1024 MRC laser-scanning confocal microscope with a 40× oil 1.3 numerical aperture objective. The mouse 3T3 fibroblasts were grown and prepared as described in (*27*). A false-colored image was obtained with 363-nm excitation, with simultaneous two-channel detection (522DF 35-nm FWHM narrow-pass filter for the green, and a 585-nm long-pass filter for the red). Image width: 84 μm.

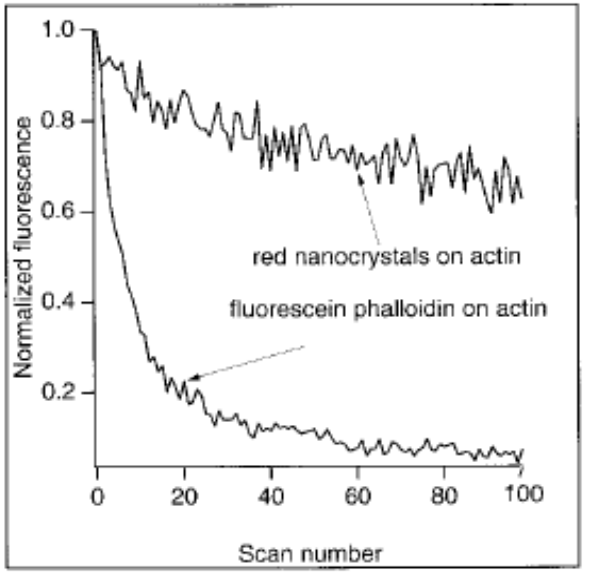

Fig. 4. Sequential scan photostability comparison of fluorescein-phalloidin–labeled actin fibers compared with nanocrystal-labeled actin fibers. Fluorescein was excited at 488 nm and the nanocrystals at 363 nm by a laser scanning confocal microscope with a 12-μs dwell time and ~20-mW power for each laser. The average intensity of four pixels was followed in each sample through 100 successive scans and normalized to its initial value. The intensity of the fluorescein drops quickly to autofluorescence levels, whereas the intensity of the nanocrystals drops only slightly.

Quantum Dot Bioconjugates for Ultrasensitive Nonisotopic Detection

Warren C. W. Chan and Shuming Nie*

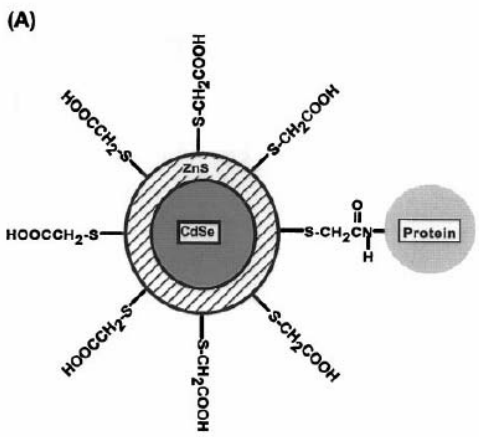

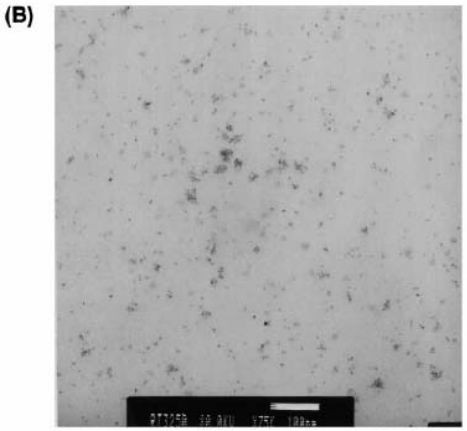

Fig. 1. (**A**) Schematic of a ZnS-capped CdSe QD that is covalently coupled to a protein by mercaptoacetic acid. (**B**) TEM of QD-transferrin (an iron-transport protein) conjugates. Scale bar, 100 nm. Clusters of closely spaced particles were mainly formed by sample spreading and drying on the carbon grid and not by chemical cross-linking. ZnS-capped QDs with a CdSe core size of 4.2 nm were prepared according to the procedure developed by Hines and Guyot-Sionnest (*7*). The colloidal QDs were dissolved in chloroform and were reacted with glacial mercaptoacetic acid (~1.0 M) for 2 hours. An aqueous phosphate-buffered saline (PBS) solution (pH 7.4) was added to this reaction mixture at a 1:1 volume ratio. After vigorous shaking and mixing, the chloroform and water layers separated spontaneously. The aqueous layer, which contained mercapto-coated QDs, was extracted. Excess mercaptoacetic acid was removed by four or more rounds of centrifugation. The purified QDs were conjugated to transferrin and IgG with the cross-linking reagent ethyl-3-(dimethylaminopropyl)carbodiimide. Standard protocols were followed (*16*), except the excess proteins were removed by repeated centrifugation. The purified conjugates were stored in PBS at room temperature.

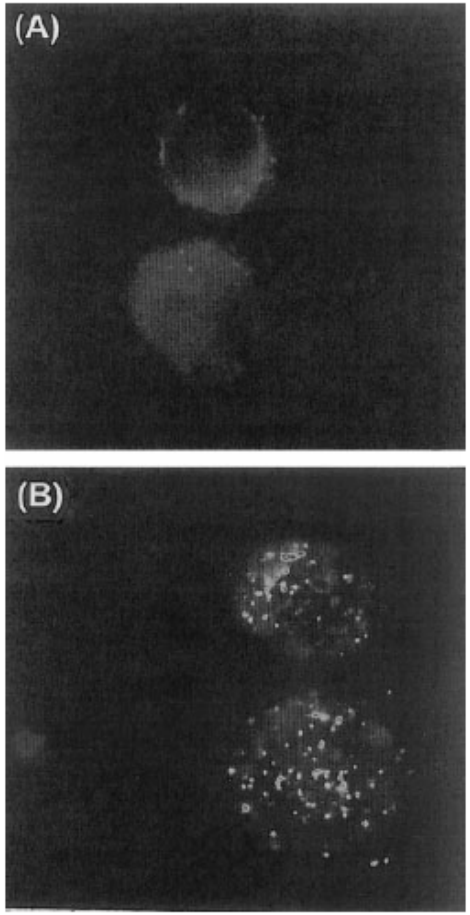

Fig. 4. Luminescence images of cultured HeLa cells that were incubated with (**A**) mercapto-QDs and (**B**) QD-transferrin conjugates. The QD bioconjugates were transported into the cell by receptor-mediated endocytosis and were detected as clusters or aggregates. Luminescence "blinking" was not observed for these clusters because of statistical averaging. The images were obtained with an epifluorescence microscope that was equipped with a high-resolution CCD camera (1.4 million pixels) (Photometrix, Tucson, Arizona) and a 100-W Hg excitation lamp. HeLa cells were grown in a minimum essential medium containing 10% fetal calf serum, 1% antibiotics (penicillin and streptomycin), and fungizone. The cultured cells were incubated overnight with either control QDs or the transferrin conjugates at 37°C. After repeated washings to eliminate excess QDs, the cells were removed from the petri dish and placed on a glass cover slip for imaging. The trypsin-treated cells had a spherical shape on the cover slip. Cell diameter, ~10 μm.

Optical Properties

- Broadband Absorption
  - Single laser excitation
- Sharp Emission
  - 20-30 nm symmetric emission
- High Quantum Yield
  - 20 x more than R6G
- Good Photostability
  - 100 x more stable for R6G (4 Hrs vs 10 mins)
- Loner fluorescent lifetime (20-40 ns vs 5 ns)

Structure

- Core quantum dot
  - CdSe, hydrophobic, not stable, lower QE (~5%)
  - Defects =>Trap state
- Core-shell quantum dot
  - ZnS/CdSe, hydrophobic, stable, higher QE (~50%)
  - Coated with higher bandgap materials or passivation reduces defects
- Water soluble quantum dot
  - Hydrophilic polymer coating
- Quantum dot bioconjugation
  - Bioconjugate to hydrophilic quantum dot

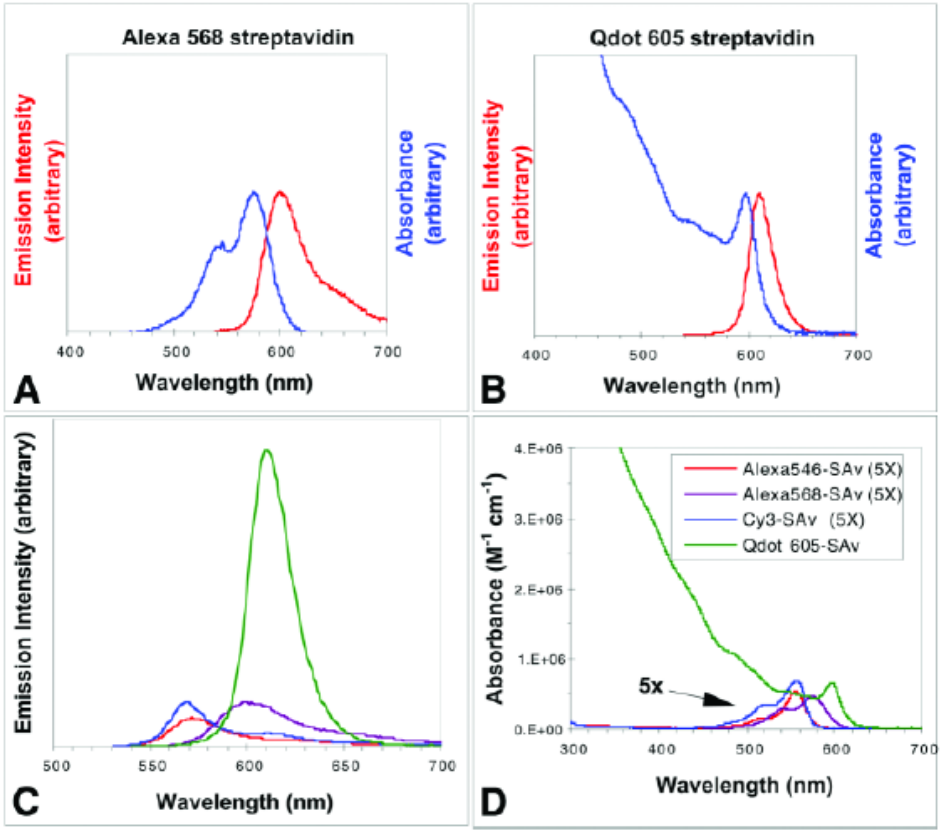

Fig. 1. Comparison of absorbance and emission spectra (normalized) of **(A)** Alexa® 568 streptavidin conjugate and **(B)** Qdot® 605 streptavidin conjugate. Note that the quantum dot conjugate can absorb light efficiently far to the blue of the emission. **(C)** Comparison of emission spectra (nonnormalized) of streptavidin conjugates of Qdot 605 (—), Alexa 546 (—), Alexa 568 (—), and Cy3® (—). The spectra were taken under conditions in which each fluorophore absorbed the same amount of excitation light. The measured quantum yields of the conjugates were 55, 8, 16, and 11%, respectively. **(D)** Comparison of absorbance spectra (nonnormalized, each 1 μ*M* flurophore) of Qdot 605 streptavidin conjugate (—), Cy3 streptavidin conjugate (—), Alexa 546 streptavidin conjugate (—), and Alexa 568 streptavidin conjugate (—). Note that all dye spectra are enhanced fivefold for clarity. Alexa, Cy3, and Qdot are registered trademarks of Molecular Probes, Amersham Biosciences, and Quantum Dot Corporation, respectively.

Table 1
Optical Properties of Quantum Dots Compared to Common Dyes[a]

Fluorescent dye	$\lambda_{excitation}$ (nm)	$\lambda_{emission}$ (nm)	$\varepsilon(mol^{-1}\text{-}cm^{-1})$
Qdot 525	400	525	280,000
Alexa 488	495	519	78,000
Fluorescein	494	518	79,000
Qdot 565	400	565	960,000
Cy3	550	570	130,000
Alexa 555	555	565	112,000
Qdot 585	400	585	1,840,000
R-Phycoerythrin	565	578	1,960,000
TMR	555	580	90,000
Qdot 605	400	605	2,320,000
Alexa 568	578	603	88,000
Texas Red	595	615	96,000
Qdot 655	400	655	4,720,000
APC	650	660	700,000
Alexa 647	650	668	250,000
Cy5	649	670	200,000
Alexa 647-PE	565	668	1,960,000

[a]The extinction coefficients (ε) are generally much larger for quantum dots than for fluorescent dyes. Furthermore, the excitation wavelength ($\lambda_{excitation}$) can be much farther from the emission ($\lambda_{emission}$).

Photo Stability

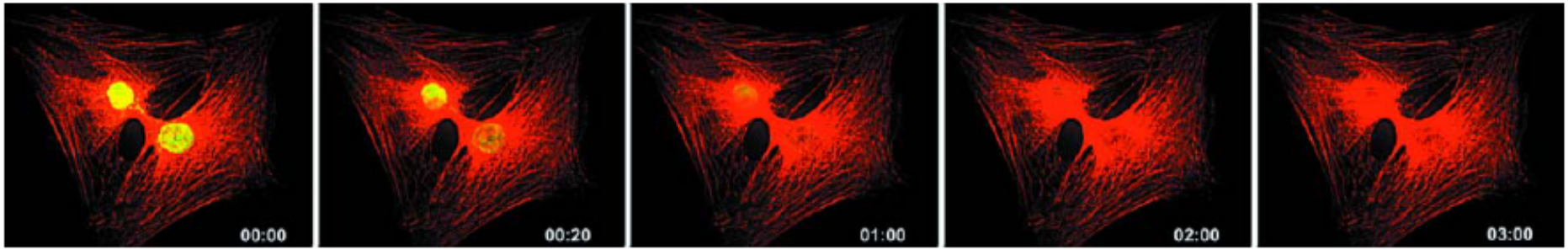

Fig. 2. Comparison of photostability between Qdot® 605 and Alexa Fluor® 488 streptavidin conjugates. Actin filaments in two 3T3 mouse fibroblast cells were labeled with Qdot 605 streptavidin conjugate (red), and the nuclei were stained with Alexa Fluor 488 streptavidin (green). The specimens were continuously illuminated for 3 min with light from a 100-W mercury lamp under a ×100 1.30 oil objective. An excitation filter (excitation: 485 ± 20 nm) was used to excite both Alexa 488 and Qdot 605. Emission filters (emission: 535 ± 10 and em 605 ± 10 nm) on a motorized filter wheel were used to collect Alexa 488 and Qdot 605 signals, respectively. Images were captured with a cooled charge-coupled device camera at 10-s intervals for each color automatically. Images at 0, 20, 60, 120, and 180 s are shown. Whereas Alexa 488 labeling signal faded quickly and became undetectable within 2 min, the Qdot 605 signal showed no obvious change for the entire 3-min illumination period.

Near-Complete Suppression of Quantum Dot Blinking in Ambient Conditions

Sungchul Hohng, and Taekjip Ha

J. Am. Chem. Soc., **2004**, 126 (5), 1324-1325• DOI: 10.1021/ja039686w • Publication Date (Web): 20 January 2004

140 mM BME

β-mercaptoethanol

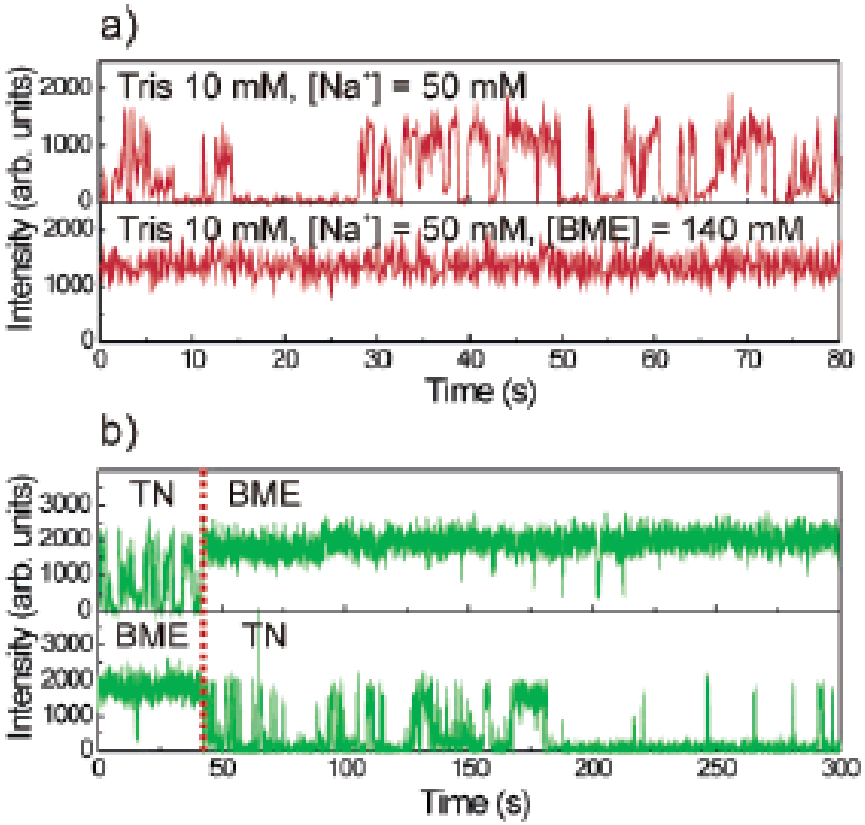

QD Blinking

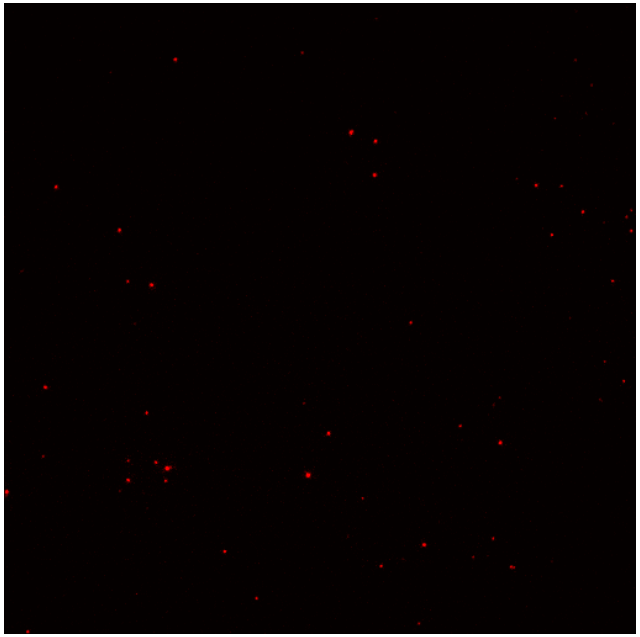

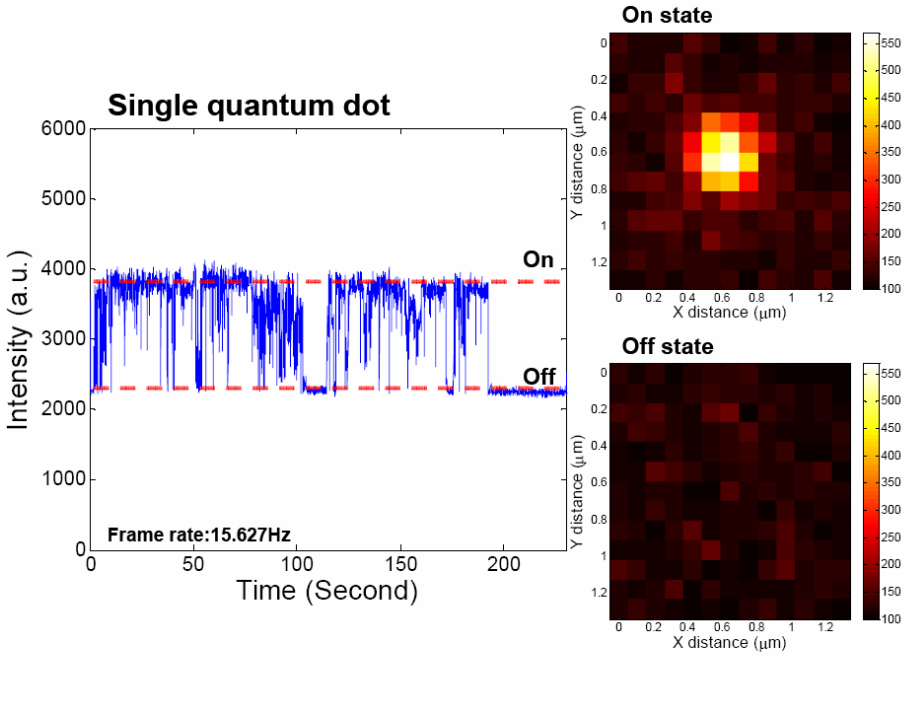
Single quantum dot
Intensity (a.u.)
Time (Second)
Frame rate:15.627Hz
On
Off
On state
Off state
Y distance (μm)
X distance (μm)

Blinking event of two Qdots

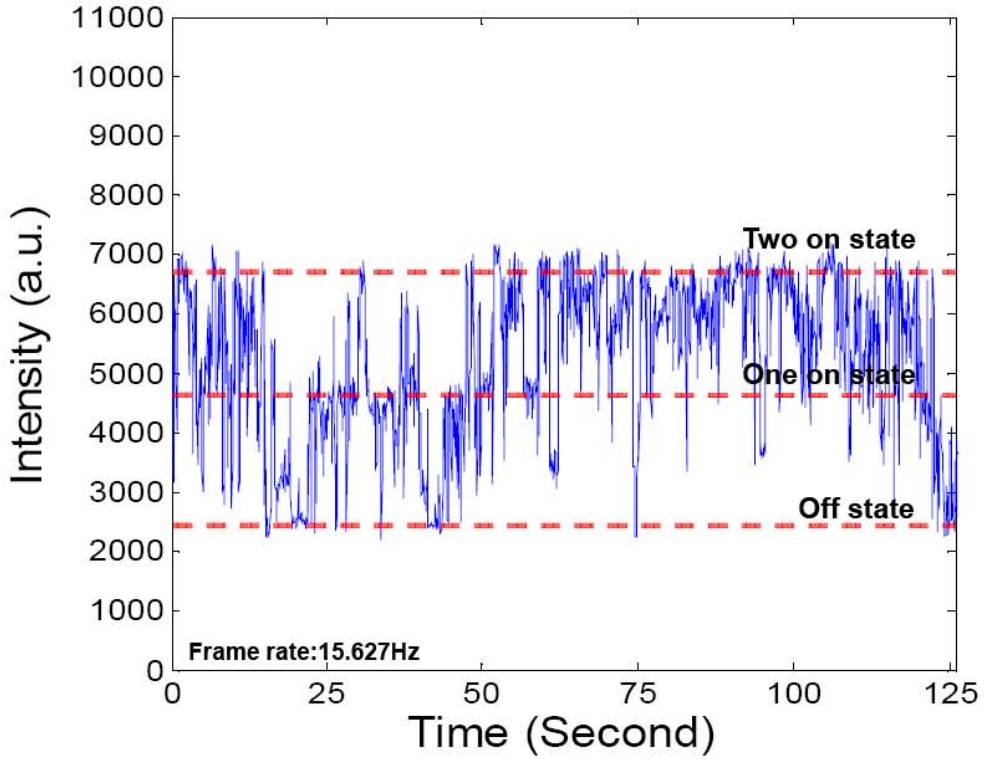

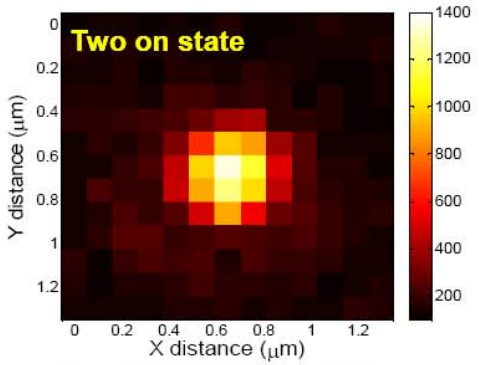

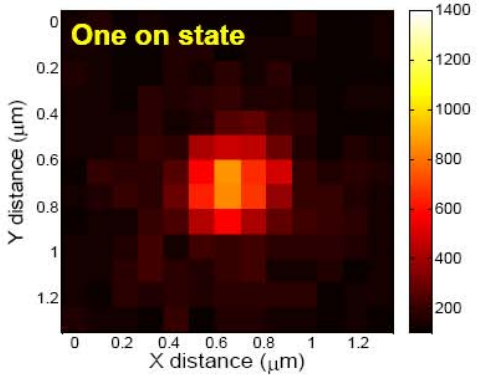

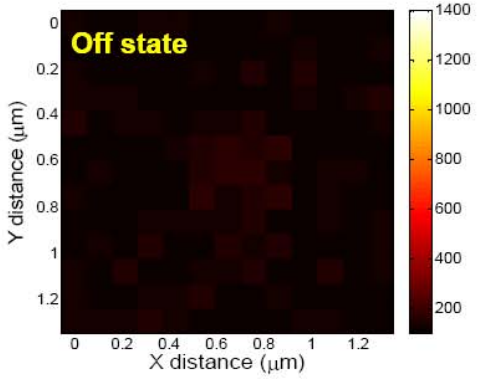

Single QDot

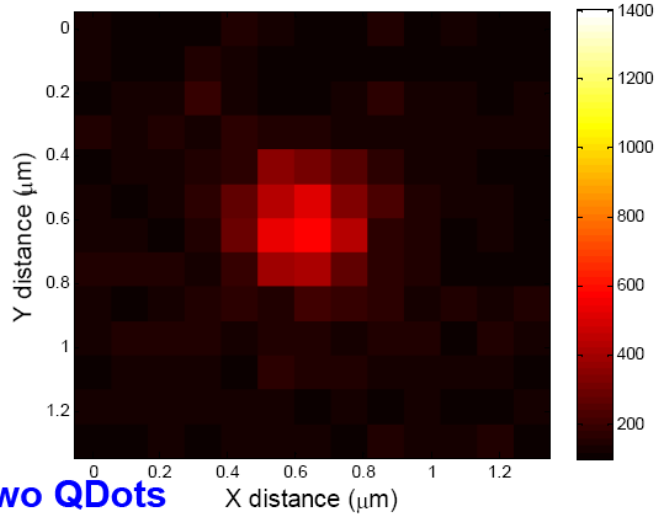

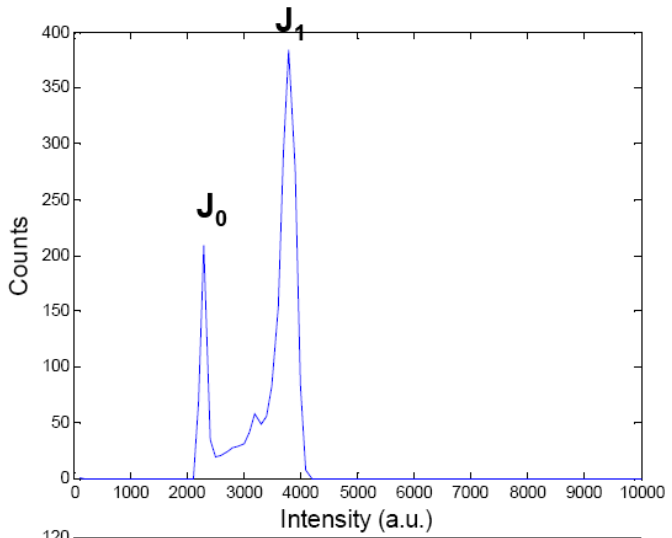

Two QDots

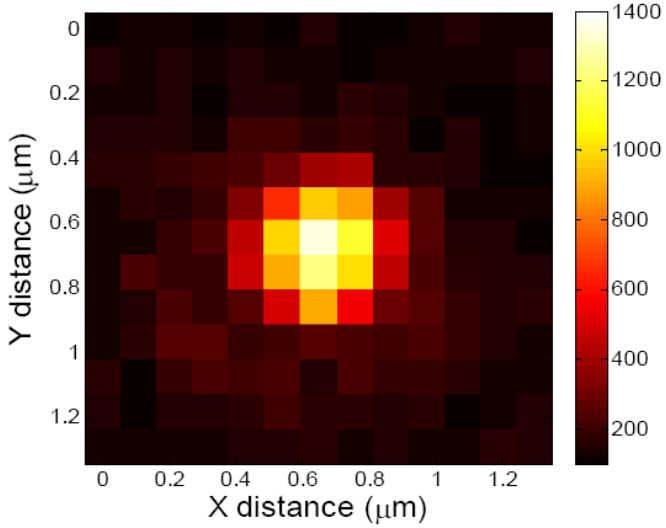

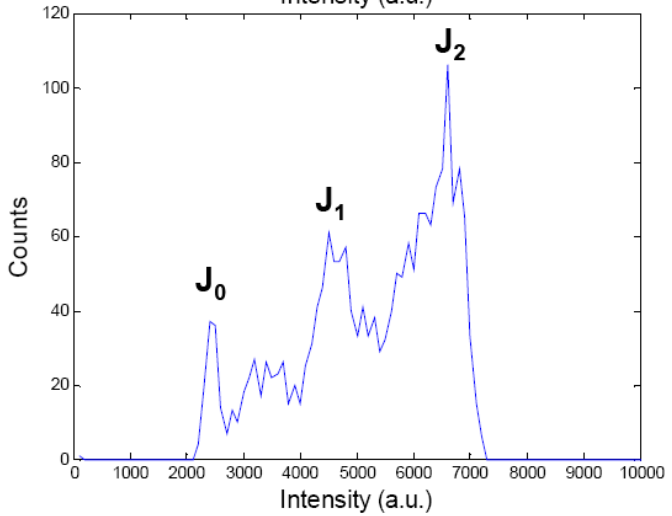

Single QDot case

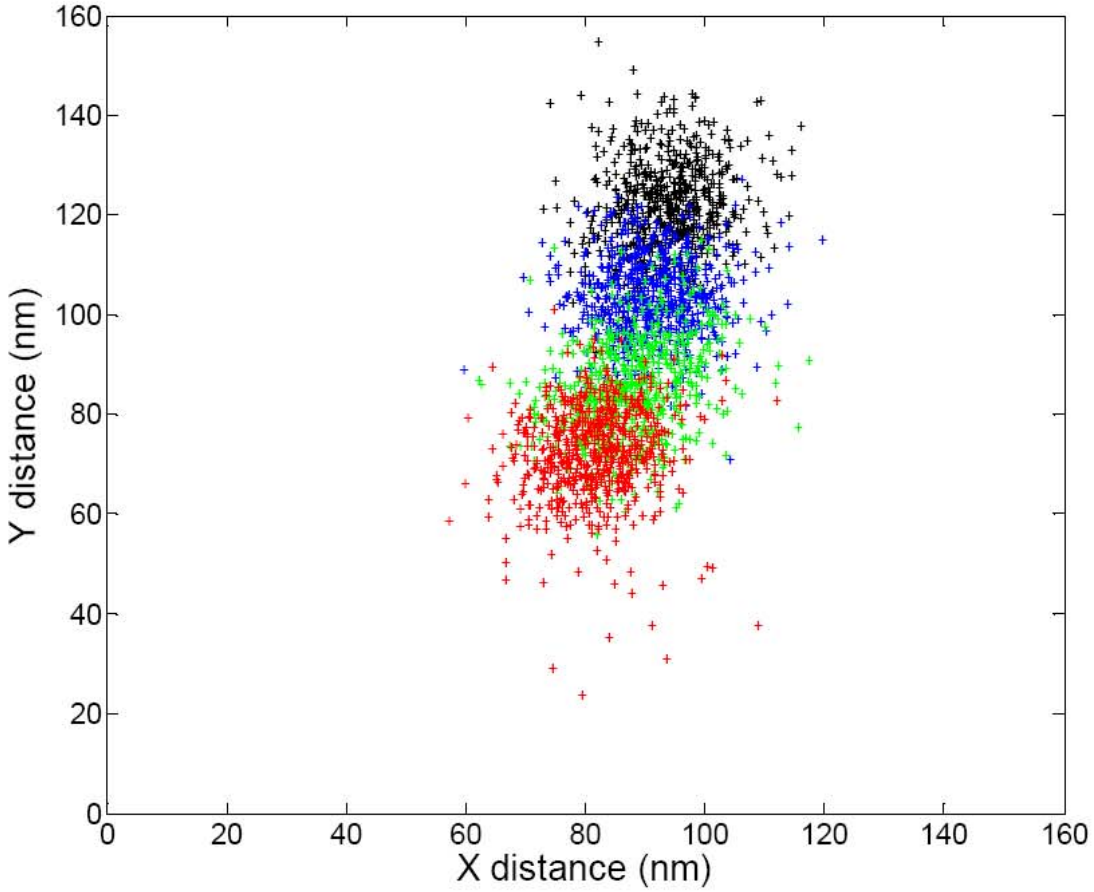

Black spot (1-636)

Standard deviation
=(σx+ σy)/2
=(6.99+9.35)/2=8.17 nm

Blue spot (637-1272)

Standard deviation
=(σx+ σy)/2
=(7.42+7.99)/2=7.70 nm

Green spot (1273-1908)

Standard deviation
=(σx+ σy)/2
=(7.86+9.66)/2=8.76 nm

Red spot (1909-2547)

Standard deviation
=(σx+ σy)/2
=(7.35+9.41)/2=8.38 nm

All spot (1-2547)

Standard deviation
=(σx+ σy)/2
=(8.70+20.80)/2=14.75 nm

Multiplexing by Q-dot

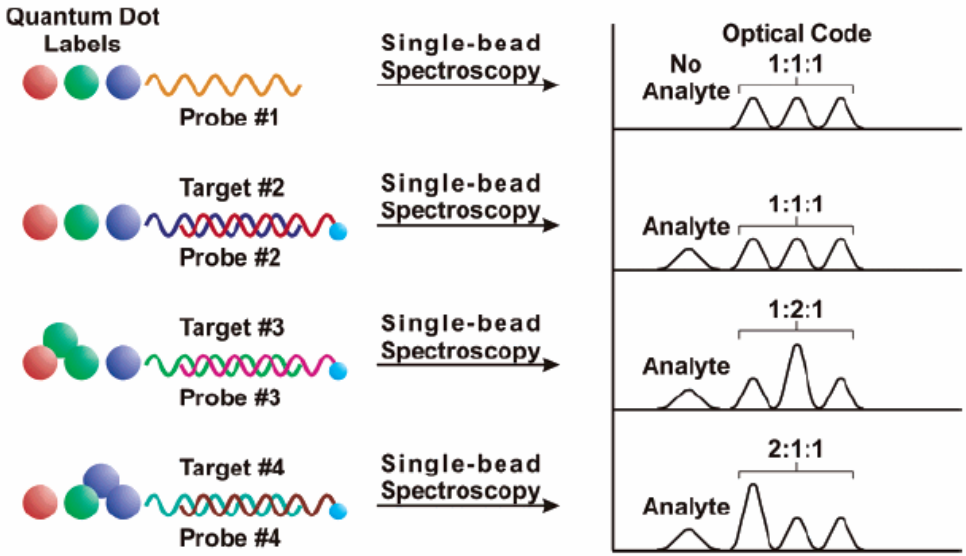

Figure 3. Quantum dots can be employed for detecting multiple targets in a single assay. Specifically, varying the numbers and ratios of different quantum dots per target results in a unique fluorescent signal for each individual target. (Reprinted with permission of Nature Publishing Group. *Nature Biotech.*, Vol. 19, 2001, by Nie, et al.)

Encoding

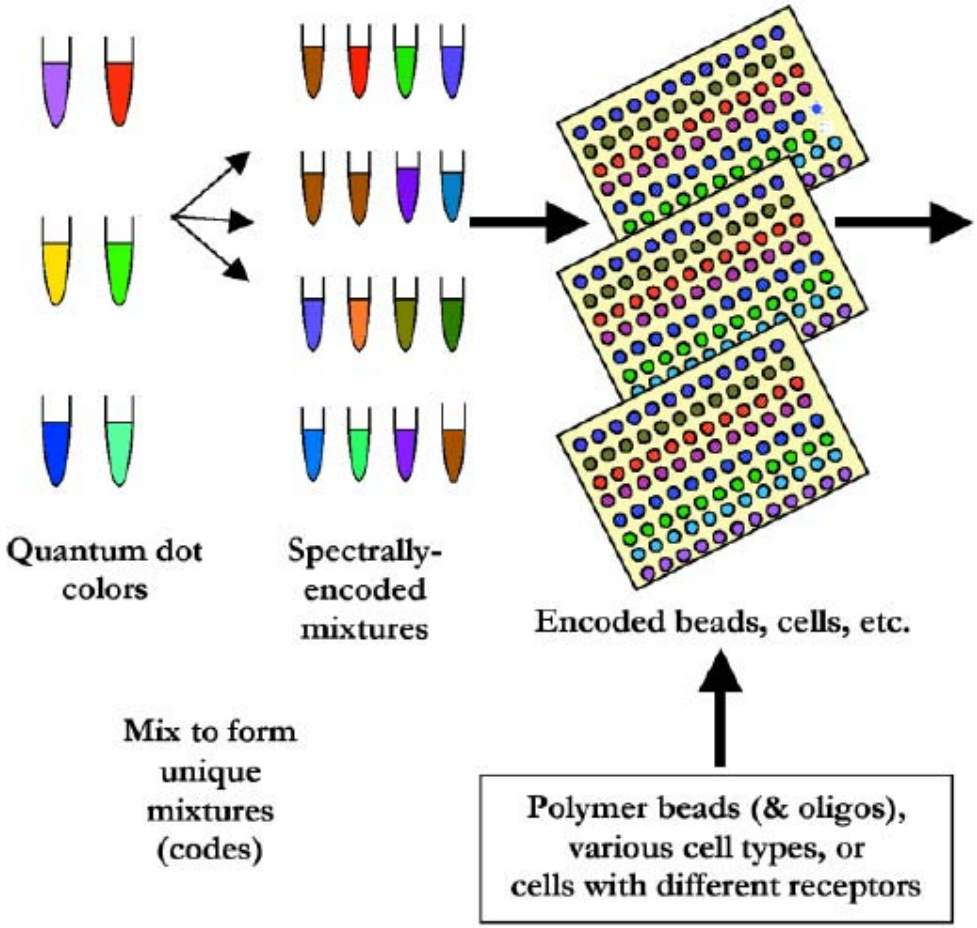

Application	Format
Multiplexed gene expression	Encoded beads each with gene-specific oligos
Multiplexed SNP genotyping	Encoded beads with allele-specific oligos
Multiplexed immunoassays	Encoded beads with antibodies
Multiplexed cell-based assays	Mixed cell types encoded with quantum dots
Multiplexed reporter assays	Encoded cell lines expressing various receptors

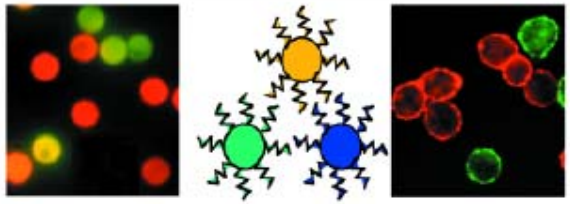

Fig. 6. Concept of encoding using quantum dots. Quantum dot colors can be mixed to produce spectral codes. These mixtures can be combined with polymer beads to produce encoded beads that can be subsequently coupled to distinct oligonucleotides or other affinity molecules. Alternatively, the quantum dot spectral codes can be used to label cells to differentiate cell lines, or cell lines bearing different receptors. SNP, single nucleotide polymorphism.

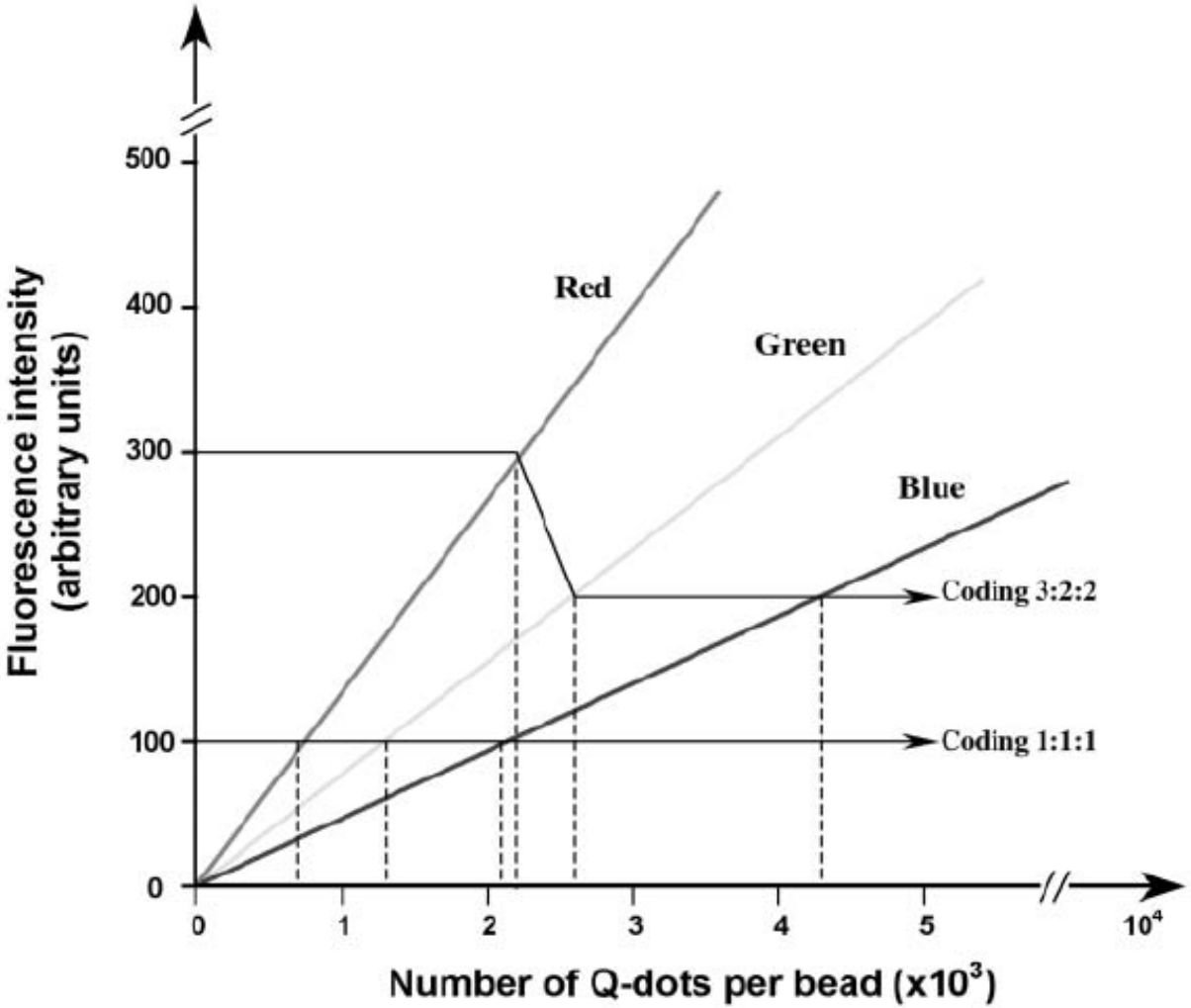

Fig. 1. Schematic drawing of working curves for preparation of multicolor quantum dot microbeads. Arrows depict two representative beads coded with intensity ratios of 1 : 1 : 1 and 3 : 2 : 2, and the number of quantum dots (or concentration) can be obtained from the x axis. Each single bead may contain quantum dots (Q-dots) ranging from several hundred to millions, depending on the bead size and surface area.

Quantum Dot Bio-conjugation

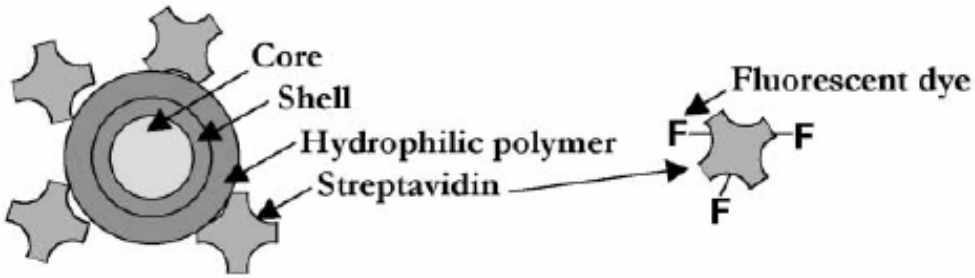

Fig. 3. Schematic of Qdot™ Nanocrystal Probe compared to a typically labeled fluorescent dye protein conjugate (see text for descriptions). Proteins generally carry several fluorescent dye labels (F). By contrast, each quantum dot is conjugated to multiple protein molecules.

Q-dot Aggregation

Clustering

Clustering

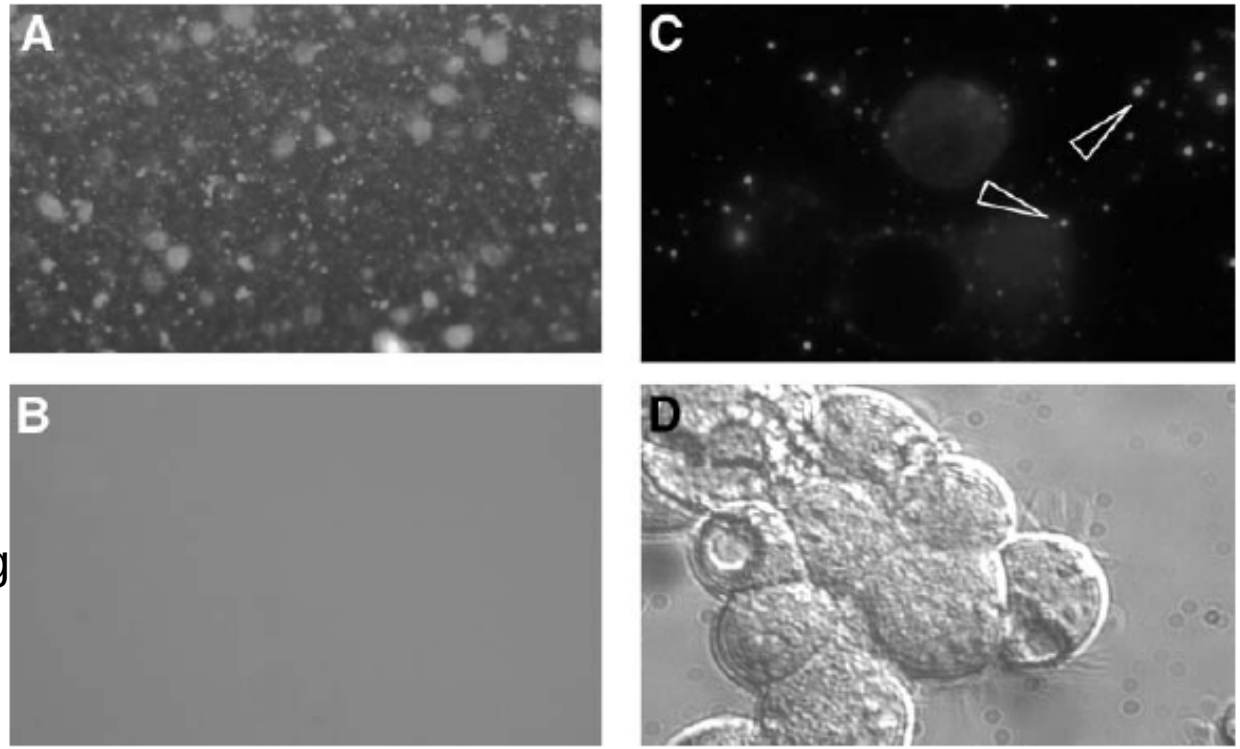

Non-Clustering

Fig. 4. Evidence for quantum dot aggregation (magnification: ×40): **(A)** fluorescent image of aggregated SA-quantum dots in absence of cells; **(B)** image of nonaggregated SA-quantum dots in absence of cells; **(C)** image of cells surrounded by aggregated SA-quantum dots (arrowheads); **(D)** bright-field image.

Biotinylated Cell

Cell + Biotin

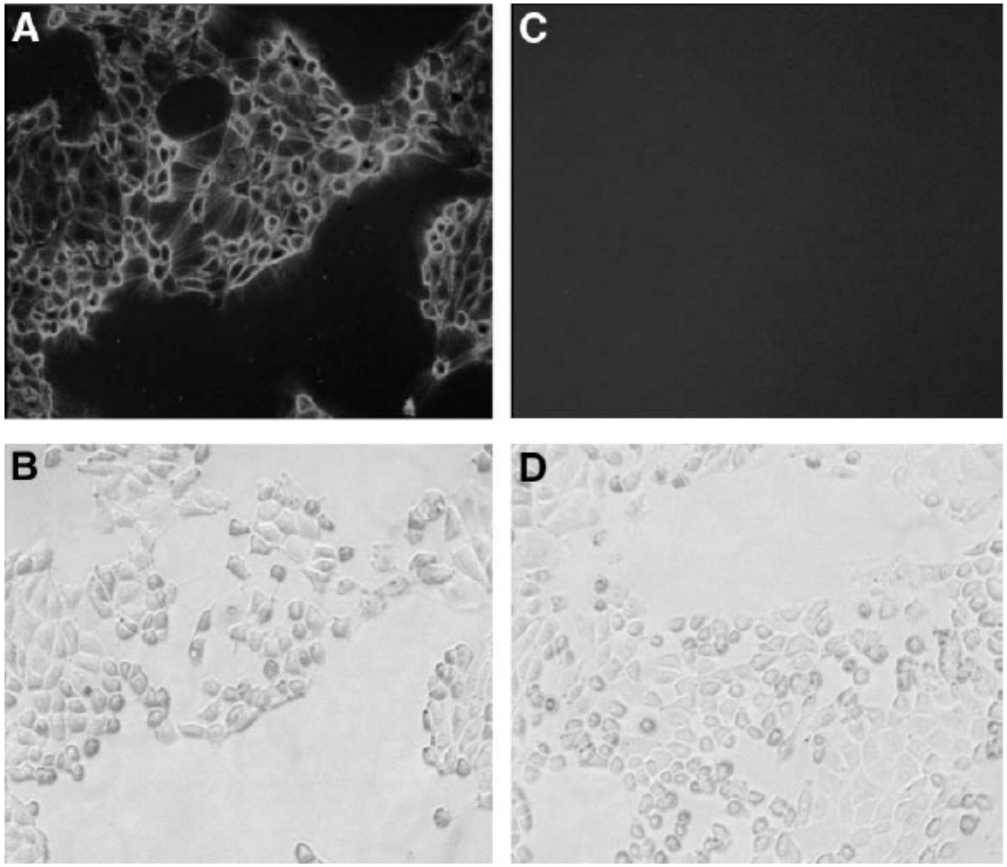

Fig. 1. Labeling of biotinylated HEK293 cells with SA-quantum dots (magnification: ×10). Three-day-old HEK293 cells cultured on poly-D-lysine glass-bottomed microwell dishes were biotinylated as described in **Subheading 3.2.1.** **(A,B)** Biotinylated HEK293 cells incubated with SA-quantum dots (50 n*M*); **(C,D)** biotinylated HEK293 cells labeled with SA-quantum dots after preincubating with 2 mg/mL of biotin.

Q-dot Antibody Labeling

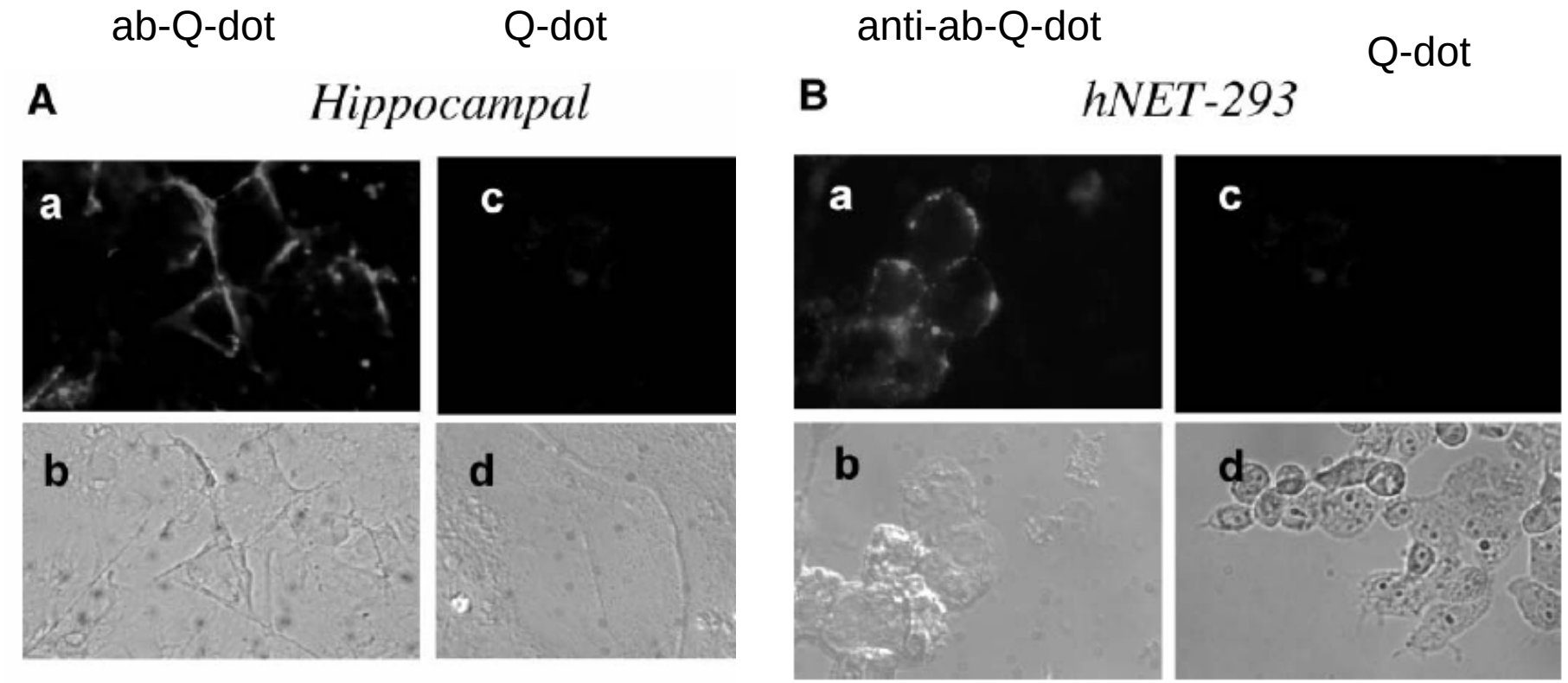

Fig. 5. SA-quantum dots and SA-Alexa Red recognize biotin-modified antibody-labeled cultures. **(A)** Eight-day-old *fixed* primary hippocampal cultures incubated with anti-LAMP followed by SA-quantum dots (a, b) or SA-quantum dots alone (c, d); **(B)** labeling of live hNET-293 cells with anti-hNET + biotinylated anti-rabbit IgG followed by SA-quantum dots (a, b) or SA-quantum dots alone (c, d).

Microbiol. Immunol., **48**(12), 985–994, 2004

Editor-Communicated Paper

Quantum Dots Targeted to the Assigned Organelle in Living Cells

QDs conjugated with (1)nuclear- and(2) mitochondria-targeting ligands.

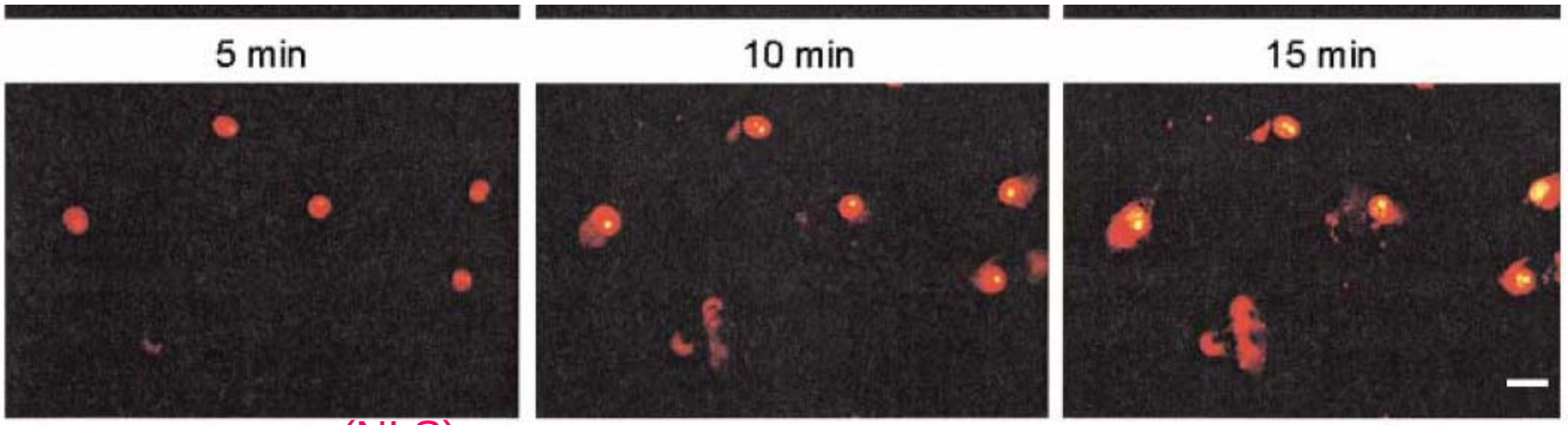

(NLS)

Fig. 3. Localization of R_{11}KC-conjugated QDs to nucleus. (a) Cells were pre-stained with Hoechst®33342, and stimulated with FITC-labeled QD-conjugated R_{11}KC peptide (1 μM final) for 3 hr at 37 C with 5% CO_2 condition. (b) Cells were pre-stained with Hoechst®33342, and stimulated with QD-R^{11}KC (1 μM final) for the indicated time at 37 C under 5% CO_2 condition with a culture fluorescence microscope (IM-310 system, Olympus). Images were taken using D1X digital camera (Nikon) equipped with IM-310 system at the indicated time by a 3 sec exposure. Bars indicated 10 μm.

1176 *Bioconjugate Chem.* **2005,** *16,* 1176–1180

Tat Peptide as an Efficient Molecule To Translocate Gold Nanoparticles into the Cell Nucleus

Jesus M. de la Fuente*,§ and Catherine C. Berry

Centre for Cell Engineering, Institute of Biomedical and Life Science, Joseph Black Building, University of Glasgow, Glasgow G12 8QQ, U.K Received February 9, 2005; Revised Manuscript Received June 10, 2005

- We report in this article the synthesis of water-soluble gold nanoparticles functionalized with a Tat protein-derived peptide sequence

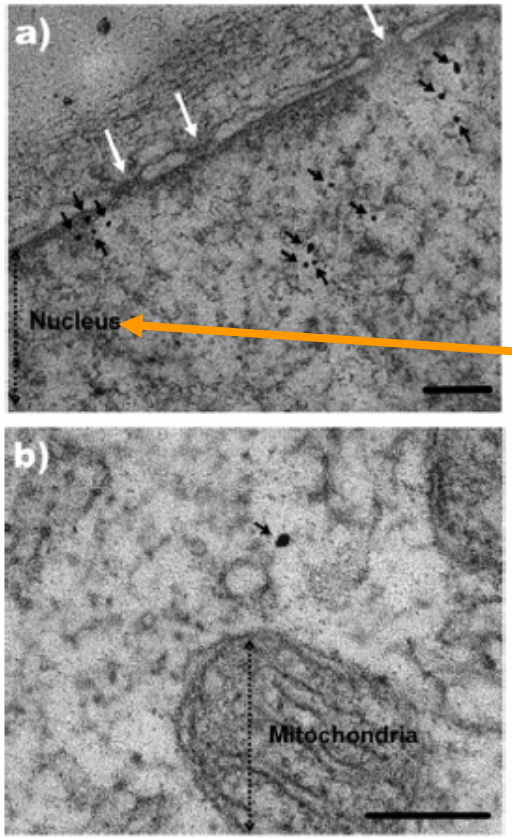

Figure 3. Transmission electron micrographs of human fibroblasts incubated with **Au@Tat** (a) and **Au@tiopronin** (b) nanoparticles. The black dots indicated with arrows are nanoparticles, and white arrows show nuclear membrane pores. (scale bars = 50 nm).

Au@tiopronin with the Tat protein-derived sequence (GRKKRRQRRR) was carried out using the reactivity of the free carboxyl group of the tiopronin (Scheme 1).

the specificity of **Au@Tat** particles to be translocated and accumulate in the cell nucleus.

Cellular Trajectories of Peptide-Modified Gold Particle Complexes: Comparison of Nuclear Localization Signals and Peptide Transduction Domains

Alexander G. Tkachenko, Huan Xie, Yanli Liu, Donna Coleman, Joseph Ryan, Wilhelm R. Glomm, Mathew K. Shipton, Stefan Franzen,* and Daniel L. Feldheim*

Table 1. Peptide Sequences Used in Nanoparticle–BSA–Peptide Complexes[a]

no.	peptide sequence	origin of peptide	nuclear localization prediction, %	cytoplasm localization prediction, %
M1	CGGGPKKKRKVGG	SV40 large T NLS	82.6	13
M2	CGGRKKRRQRRRAP	HIV-1 Tat protein NLS	73.9	21.7
M3	CGGFSTSLRARKA	adenoviral NLS	47.8	47.8
M4	CKKKKKKGGRGDMFG	integrin binding domain and oligolysine	73.9	17.4

Table 3. Location of Peptide-Coated Nanoparticles after 3-h Incubation Times with Various Cell Lines

no.	peptide sequence	HeLa	3T3/NIH	HepG2
M1	CGGGPKKKRKVGG	cytoplasm	cytoplasm	cytoplasm
M2	CGGRKKRRQRRRAP	cytoplasm	no uptake	cytoplasm
M3	CGGFSTSLRARKA	nucleus	cytoplasm	no uptake
M4	CKKKKKKGGRGDMFG	nucleus	cytoplasm	nucleus

Intracellular Delivery of Quantum Dots for Live Cell Labeling and Organelle Tracking**

By *Austin M. Derfus, Warren C. W. Chan*, and *Sangeeta N. Bhatia**

- Adv. Mater. 2004,16, no.12,961

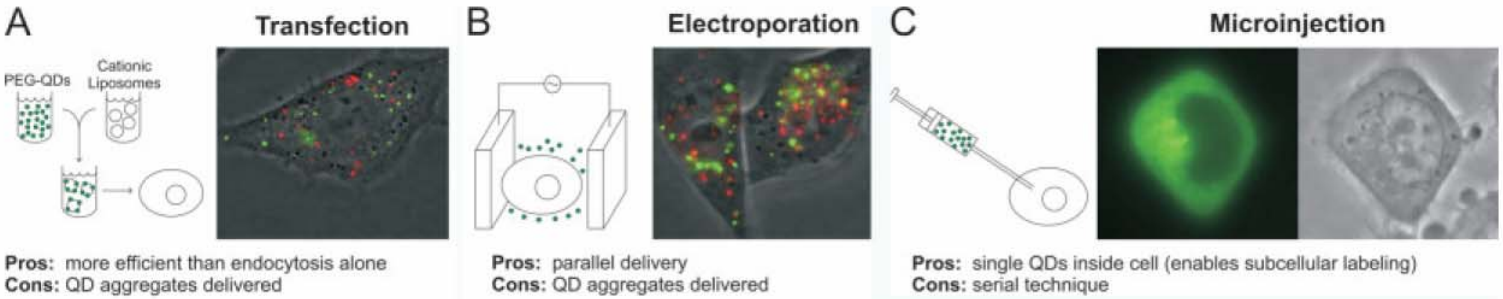

(1)23mer nuclear localization sequence peptide from SV40 T antigen plus additional residues.

(2) 28mer mitochondrial localization sequence peptide

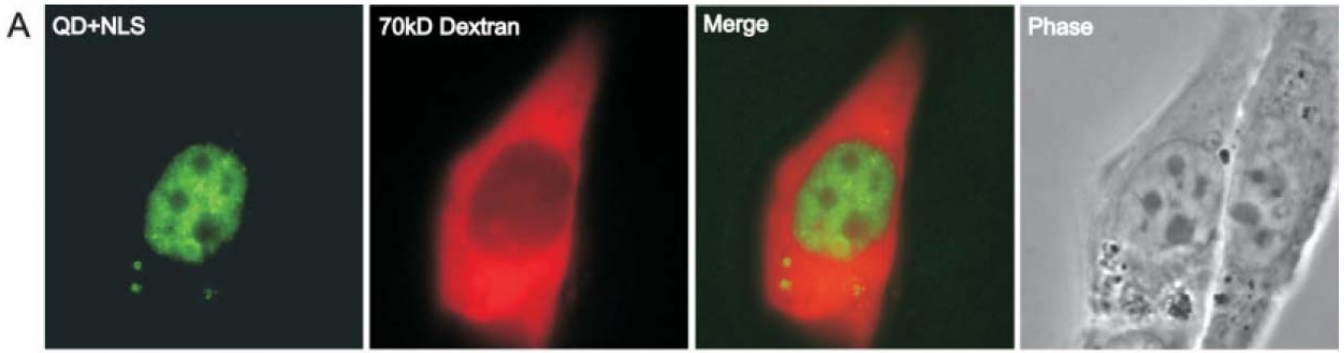

920 *Bioconjugate Chem.* **2006,** *17,* 920–927

Self-Assembled Quantum Dot–Peptide Bioconjugates for Selective Intracellular Delivery

James B. Delehanty,[†,*] Igor L. Medintz,[†] Thomas Pons,[‡,||] Florence M. Brunel,[§] Philip E. Dawson,[§] and Hedi Mattoussi[‡,*]

- The polyhistidine sequence allows the peptide to self-assemble onto the QD surface via metal-affinity interactions, -
- (2) CdSe- Zns QDs- HIV 1

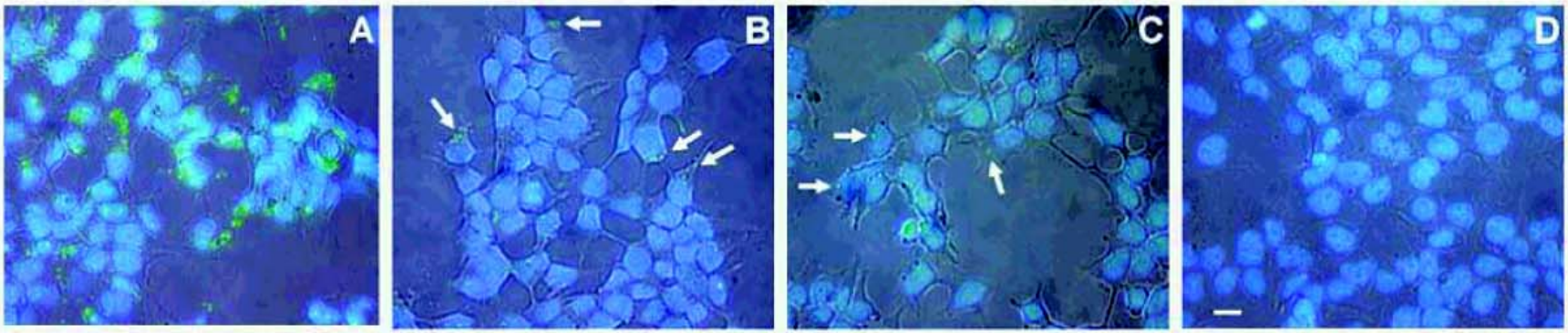

Figure 2. Dose-dependent cellular internalization of QD–CPP assemblies. HEK 293T/17 cells were incubated with 510-nm QD–CPP assemblies (QD:CPP ratio 1:50) at QD concentrations of 250 nM (A), 60 nM (B), 15 nM (C), or with 250 nM QDs without CPP (D); cells were also stained with DAPI. Overlay of phase contrast, QD fluorescence (green), and DAPI fluorescence (blue), show the dose-dependent nature of the QD–CPP delivery. Images also show that QD staining is nonnuclear, punctate fluorescence located in the cytoplasm. Negligible cell-surface associated fluorescence was observed. Arrows indicate regions of QD–CPP internalization at lower concentrations. Scale bar is 10 μm.

Figure 3. QD-CPP internalization and colocalization within endocytotic vesicles.

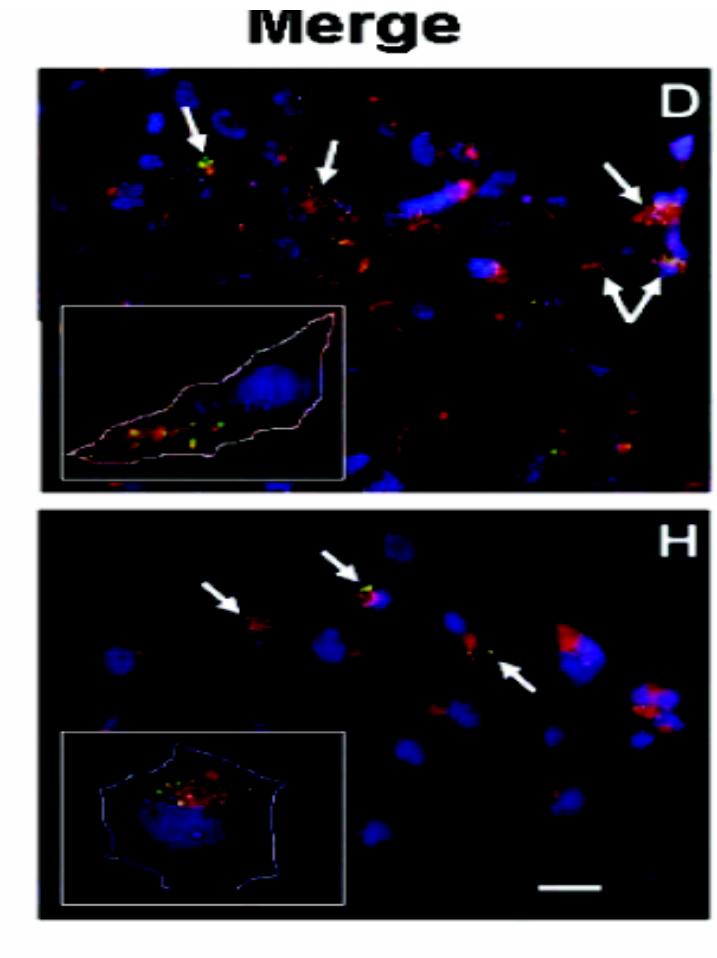

920 *Bioconjugate Chem.* **2006**, *17*, 920–927

Self-Assembled Quantum Dot−Peptide Bioconjugates for Selective Intracellular Delivery

James B. Delehanty,[†,*] Igor L. Medintz,[†] Thomas Pons,[‡,||] Florence M. Brunel,[§] Philip E. Dawson,[§] and Hedi Mattoussi[‡,*]

QDs –peptides assemlies were colocalized within endosomes.

Multifunctional Gold Nanoparticle–Peptide Complexes for Nuclear Targeting

Alexander G. Tkachenko, Huan Xie, Donna Coleman, Wilhelm Glomm, Joseph Ryan, Miles F. Anderson, Stefan Franzen,* and Daniel L. Feldheim*

- JACS,2003, 125, 4700

Table 1. Peptide Sequences Used in Nanoparticle–BSA–Peptide Complexes[a]

#	peptide sequence	origin of peptide	peptide/BSA
1	CGGGPKKKRKVGG	SV40 large T NLS	7 ± 1
2	CGGFSTSLRARKA	adenoviral NLS	8 ± 1
3	CKKKKKKSEDEYPYVPN	adenoviral RME	9 ± 2
4	CKKKKKKKSEDEYPYVP-NFSTSLRARKA	adenoviral fiber protein	6 ± 2

NLS RME

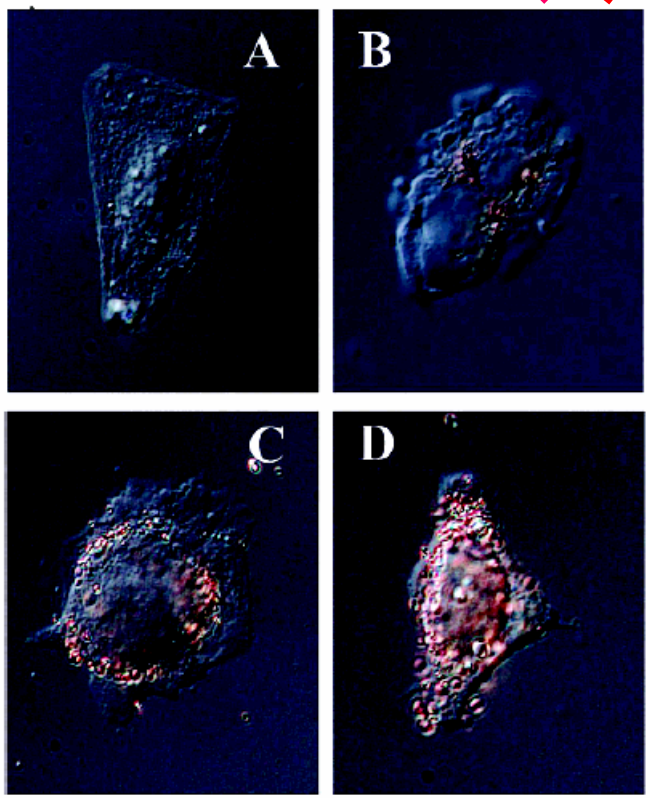

Figure 1. Nanoparticle−peptide complexes incubated with HepG2 cells for 2 h: #2 (A), #3 (B), #4 (C), and #2/#3 (D). The HepG2 cell line was

NLS+RME

Feldherr has shown that peptide #1, the NLS from SV-40 virus, is translocated to the nucleus when attached to gold nanoparticles, if the particles are injected into the cytoplasm.2e

Surprisingly, when these complexes were added to cell growth media, they were found inside the cytoplasm of HepG2 cells; however, they did not enter the nucleus.

- JACS,2003, 125, 4700

Fluorescent CdSe/ZnS Nanocrystal–Peptide Conjugates for Long-term, Nontoxic Imaging and Nuclear Targeting in Living Cells

Fanqing Chen, and Daniele Gerion

Nano Letters, **2004**, 4 (10), 1827-1832• DOI: 10.1021/nl049170q • Publication Date (Web): 09 September 2004

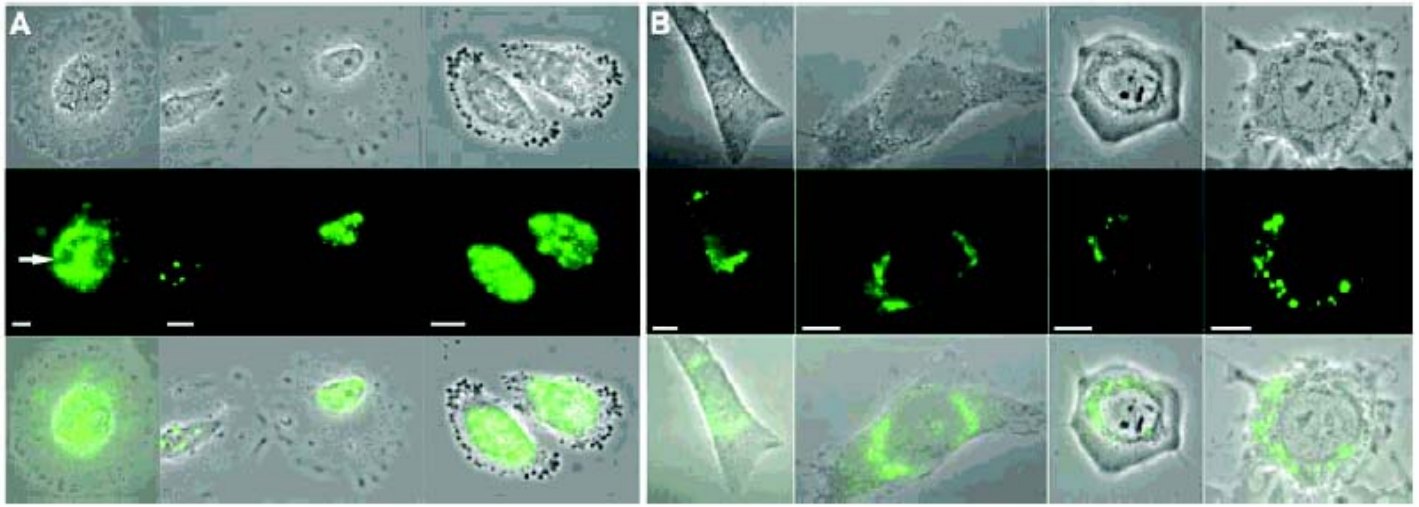

Figure 2. Localization of NLS−qdots in the nucleus (A) or in the perinuclear region (B). In both panels, the top row represents the phase

The NLS-qdot conjugates are observed either in the cell nucleus (Figure 2, panel A) or in the perinuclear region (Figure 2, panel B).

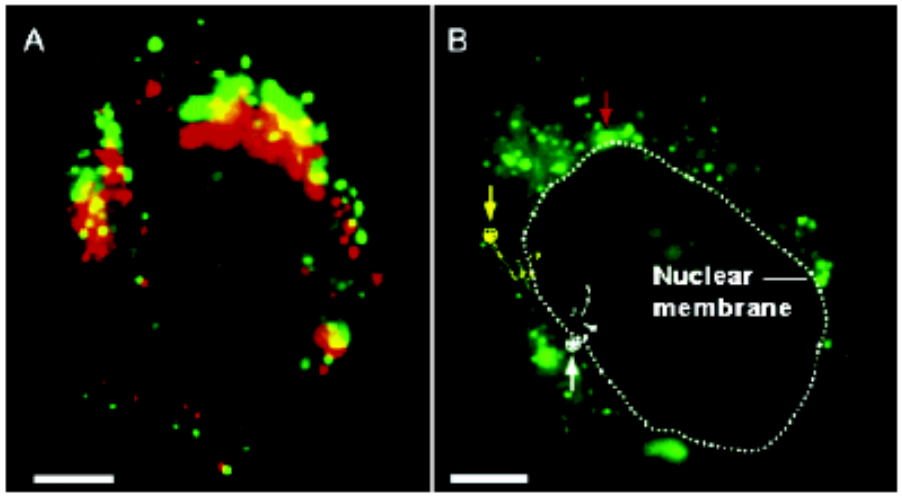

Figure 4. Movement of NLS−qdot conjugates. (A) False-color overlay of fluorescence from a cell taken at 4 min intervals, about 2 h after transfection. In 4 min, the dots moved from the green to the red position. The features at the top of the image go downward and the features on the bottom go upward. Notice the movement of the fluorescent dots at the bottom of the image toward the nucleus. Integration time: 700 ms. (B) An example of a large aggregate of NLS−qdots is indicated with the red arrow. This feature is immobile during the entire period of illumination (15 min). In contrast, smaller, weaker, blurred yet distinguishable features move continuously during the measurement. The pathways of two of these spots are shown. The positions of the spots at the beginning of the measurement are indicated by the circled stars and the arrows. Positions are determined every 15 s for a total time of 15 min. Integration time: 500 ms/frame. Scale bar: 5 μm.

The general direction of movements of the NLS-qdots goes from the periphery of the cytoplasm to the perinuclear region (Figure 4A).